TGF-β REPROGRAMS METABOLISM AND NKCC2 EXPRESSION IN RENAL TUBULE EPITHELIAL CELLS

By

Kuniko Hunter

Dissertation

Submitted to the Faculty of the

Graduate School of Vanderbilt University

in partial fulfillment of the requirements

for the degree of

DOCTOR OF PHILOSOPHY

in

Biomedical Engineering

May 12, 2023

Nashville, Tennessee

Approved:

William H. Fissell, M.D.

W. David Merryman, Ph.D.

Cynthia Reinhart-King, Ph.D.

Matthew Tyska, Ph.D.

Roy Zent, M.D., Ph.D.

To my mother,
for your unwavering love and support.

In loving memory of my father,
who always believed in me.

ACKNOWLEDGMENTS

My first thanks go to my advisor Bill. Thank you for your patience, encouragement, and knowledge that you have passed on to me. On the days when nothing seemed work, your passion for helping patients inspired me to keep going. Your mentorship has been crucial to my success.

I am grateful for the consideration and thoughtful discussions that my committee members Roy Zent, W. David Merryman, Matthew Tyska, and Cynthia Reinhart-King provided. It has been a true benefit to have your expertise. Thank you in particular to Cindy and Roy for your kindness and valuable advice over the years.

Thank you to my colleagues in the Department of Biomedical Engineering and the Division of Nephrology who I have been lucky to meet. I would like to thank everyone in MRB-IV P435 for your camaraderie and the insights you have given me over the years. Thank you to Hal and Rachel for taking me under your wings and teaching me the fundamentals of bench research, answering countless questions, and many thoughtful conversations. Thank you as well to Sylvia, Seiver, and Nina.

Thank you to all the professors and teachers who stoked my curiosity and encouraged me on the path of my education. Thank you to Mathilde, Sasi, Dean, Graznya, and Alex, who served as mentors over the years and who fueled my passion for research. Thank you to Mathilde and Sasi for your mentorship. I would also like to thank Dean for encouraging me to pursue graduate school.

I want to thank my friends for making the good days even better and for being a support in harder times. You broaden my perspectives, inspire me to be curious, and motivate me to think differently. The kindness and compassion of each of you has been invaluable throughout this dissertation. A special thanks to H.

Finally, I would like to thank my family. Thank you to my mother, who has been a source of unwavering support. Your humor and tenacity are a constant inspiration. Thank you to my father, who always believed in me.

TABLE OF CONTENTS

LIST OF TABLES

LIST OF FIGURES

CHAPTER 1

General introduction, significance & contribution

1.1 Motivation

Chronic kidney disease (CKD) is the ninth leading cause of death in the United States and affects 15% of the adult population (CDC, 2021). CKD affects an estimated 37 million Americans. Due to the asymptomatic nature of CKD progression, approximately 90% of those with it are unaware until it progresses to irreversible end-stage renal disease (ESRD), making it an under-recognized public health crisis (CDC, 2021). Most Americans with kidney failure are treated with in-center dialysis, an expensive and burdensome treatment course with high morbidity rates. In the US, hemodialysis has a total annual cost exceeding $42 billion, yet only a 35% five-year survival rate. (USRDS, 2022). Transplantation, the best and most economical treatment, is severely limited by the scarcity of donor organs. On average, over 3,000 patients are added to the kidney wait list per month and 13 people pass away each day waiting for a transplant (USRDS, 2022).

One solution to eliminating this scarcity problem and treating kidney failure is to bioengineer a mass-produced universal donor kidney. The current barrier to developing a universal donor kidney is producing fully differentiated human renal tubule epithelial cells (HREC) in vitro. HREC are highly specialized, polarized cells that consume large amounts of energy to transport solutes against concentration gradients within the kidney. Present cell culture techniques are unable to accurately reproduce HREC function. In vitro, these cells poorly recapitulate their original corresponding in vivo counterparts and exhibit a flattened morphology and loss of apical brush border phenotype. This dedifferentiation limits HREC in vitro use in a wide variety of health-related fields, including drug development, mechanistic discovery, toxicity screenings and artificial organ development. We seek to understand the molecular mechanisms underlying these changes to establish culture conditions that restore differentiated morphology to HREC in vitro.

1.2 Goal

This dissertation seeks to determine the specific mechanisms guiding renal tubule epithelial cell differentiation. Native renal epithelia are characterized by an elaborate array of sodium transporters which enable the orchestrated reabsorption and secretion of a diverse array of ions whilst maintaining normal cell homeostasis. The described studies will help clarify the role of substrate stiffness-mediated pathways and metabolic activity in governing renal tubule epithelial cell differentiation. Understanding the interplay of stiffness sensing, metabolism, and differentiation is critical to understanding kidney disease pathogenesis and for creating more accurate models of the renal tubule epithelia for application in the bioartificial kidney. Elucidation of

interactions between TGF-β dependent mechanosensing and AMPK-mediated metabolic sensing will also provide the opportunity to identify therapeutic targets for the treatment of CKD and renal fibrogenesis.

1.3 Specific Aims

1.3.1 Aim 1: Inhibition of TGF-β improves primary renal tubule cell differentiation in long-term culture

In Chapter 4, we demonstrate that control of the TGF-β signal transduction pathway is sufficient to reverse the erosion of some functional phenotypes associated with renal tubule epithelial cell culture in conventional flat inelastic scaffolds. TGF-β inhibition in vitro leads to the appearance of functions characteristic of native tubule cells, including diuretic-inhibitable fluid transport, phlorizin-inhibitable glucose uptake, probenecid-inhibitable organic anion excretion, and apical acid extrusion. We demonstrate that these interventions are sufficient to maintain renal cell differentiation for extended periods of time (more than 40 weeks).

1.3.2 Aim 2: Metformin and TGF-β inhibition direct renal tubule cell metabolism toward increased glycolysis and oxidative phosphorylation

In Chapter 5, we demonstrate that AMP-activated protein kinase (AMPK) activation and TGF-β inhibition additively increase the expression and activity of renal tubule epithelial cell glycolytic and mitochondrial metabolic machinery. AMPK activator metformin increases anaerobic glycolysis and reduces electron transport chain glucose dependency, thus decreasing coupling efficiency while increasing spare respiratory capacity. Conversely, TGF-β inhibitor SB431542 reduces glycolysis while increasing cell oxidative phosphorylation and electron transport chain dependency. When administered together, the two treatments have a synergistic effect that increases both glycolytic and oxidative phosphorylation capacities, imparting greater metabolic flexibility. In terms of substrate dependency, when administered separately metformin and SB431542 both increase fatty acid oxidation dependency, but not when administered together. In summary, metformin and SB431542 ameliorate the metabolic dysregulation brought on by cell culture stress by increasing the flux of glucose and fatty acids towards oxidative phosphorylation.

1.3.3 Aim 3: Canonical Smad-dependent TGF-β signaling governs NKCC2 expression via HNF-1α in renal tubule epithelial cells

In Chapter 6, we demonstrate that TGF-β signaling suppresses Na-K-2Cl cotransporter 2 (NKCC2) transcription through the Smad/Snail signaling axis which represses the transcription factor Hepatic Nuclear Factor 1α (HNF-1α). The role of the TGF-β receptor 1 (ALK5) is confirmed. We find that non-canonical TGF-β signaling pathways are not involved in the the transcriptional repression of NKCC2. Genetic knockout

of the canonical TGF-β intermediate Smad2 increases protein expression of NKCC2, while genetic rescue Smad2, Smad3, Smad4 and Snail1 attenuates NKCC2 expression. We find that Smad2 knockout is sufficient to increase activity of the HNF-1α promoter, while Smad2, Smad3, and Smad4 rescues suppress HNF-1α promoter activation. Finally, genetic overexpression of HNF-1α is demonstrated to be sufficient to increase NKCC2 expression. In short, the roles of Smad2, Smad3, Smad4, Snail1 and HNF-1α on renal NKCC2 expression are demonstrated.

1.4 Innovations & list of contributions

The proposed studies will establish new genetic targets for the in vitro differentiation of renal tubule epithelial cells and provide greater insight to the mechanisms of tubulointerstitial fibrosis and metabolic dysregulation driving CKD. This will provide a valuable resource for the wider scientific community to pursue the study of immunosuppression-free transplants that have not previously been possible due to the limitations of existing cell models. Hereafter are gathered the publications resulting from research conducted throughout this PhD:

- Hunter K, Love H, Fissell W. *Canonical Smad2 TGF-β signaling governs HNF-1α-dependent NKCC2 transcription and fluid transport in renal tubule epithelial cells.* In preparation.
- Hunter K, Yao N, Love H, Fissell W. *Metformin and TGF-β inhibition direct renal tubule cell metabolism toward increased glycolysis and oxidative phosphorylation.* In preparation.
- Hunter K, Love H, Evans R, Roy S, Zent R, Harris R, Wilson M, Fissell W. *Inhibition of TGF-β improves primary renal tubule cell differentiation in long-term culture.* Tissue Engineering Part A. https://doi.org/10.1089/ten.TEA.2022.0147.
- Love H, Evans R, Hunter K, Roy S, Fissell W. *Functionalizing Polyacrylamide Hydrogels for Renal Cell Culture Under Fluid Shear Stress.* Tissue Engineering Part A. Vol. 28, No. 19-20. October 2022. https://doi.org/10.1089/ten.tea.2022.0079.

1.5 Outline of the dissertation

In this Section, we provide a detailed overview of the contributions of this thesis. For each chapter, we first introduce the underlying problem of interest and present the contributions.

Chapter 2 provides relevant background material on the classification and prevalence of CKD. Approaches to preserving kidney function are described. A brief overview of existing renal replacement therapies and current advances in renal bioengineering is given.

Chapter 3 describes further background on the molecular mechanisms underlying the development of CKD. Information on the anatomy and physiology of the kidney is presented, as well as discussion on renal tubule cell metabolism. Renal metabolic reprogramming is introduced. We uncover the mechanistic roles of

energy sensor AMPK and its activator, hypoglycemic drug metformin. We follow by defining the TGF-β signaling pathway and its roles in the development of CKD and metabolic dysregulation. An overview of the canonical Smad and non-canonical TGF-β signaling pathways is given. Related work on renal Smad knockout models is presented.

Chapter 4 details the first reported study demonstrating the role of TGF-β in governing phlorizin-inhibitable glucose uptake and probenecid-inhibitable organic anion excretion in renal tubule epithelial cells, as detailed in Aim 1.3.1. The roles of canonical Smad signaling and metformin are also explored.

Chapter 5 covers the first reported study demonstrating the role of TGF-β and metformin in governing renal tubule epithelial cell anaerobic glycolysis, oxidative phosphorylation and substrate dependency, as detailed in Aim 1.3.2. Mechanisms of tubule cell metabolic reprogramming are explored.

Chapter 6 presents the first reported study demonstrating the role of Smad-dependent TGF-β signaling in governing Na-K-Cl cotransporter 2 (NKCC2) expression. This study describes the Smad/Snail/HNF-1α/NKCC2 signaling axis, as detailed in Aim 1.3.3.

Chapter 7 concludes and depicts future research directions closely related to contributions from this dissertation. We also illuminate perspectives set forth within these contributions.

CHAPTER 2

Chronic kidney disease, approaches to preserving kidney function, and renal bioengineering

2.1 Introduction to chronic kidney disease

Chronic kidney disease (CKD) is responsible for about 1.2million deaths globally each year and is estimated to become the fifth leading cause of death worldwide by 2040 (Foreman et al., 2018). CKD is estimated to affect approximately 15% of the adult population, yet due to the asymptomatic nature of CKD progression, about 90% of those with CKD are unaware until it progresses to irreversible end-stage renal disease (ESRD), making it an under-recognized public health crisis (CDC, 2021). The increasing prevalence of CKD is caused in part by an increase in the prevalence of the factors that contribute to its, including type 2 diabetes mellitus, obesity, hypertension, and cardiovascular disease. Improved longevity of the general population, a reduction in the mortality of dialysis patients, increases in CKD incidence, broadening of renal replacement therapy (RRT) acceptance criteria, and greater access to dialysis in low and middle income countries also contribute to the increasing prevalence of CKD. There are many causes of CKD, including diabetes, glomerulonephritis, and cystic kidney diseases but the causation of CKD is not yet fully elucidated.

CKD is a progressive condition characterized by the stiffening of the renal parenchyma and loss of structural and functional characteristics of renal tissue. During the progression of CKD, renal function is impaired due to the loss of nephrons and the development of renal tubulointerstitial fibroisis. Excessive accumulation of the extracellular matrix (ECM), is accompanied by a reduction in glomerular filtration rate (GFR) and abnormal albuminuria (albumin protein in the urine) (Glassock et al., 2017). CKD is typically diagnosed an estimated glomerular filtration rate of less than 60mL/min/1.73m^2 (Webster et al., 2017). Clinically CKD is characterized using markers of kidney damage, such as albuminuria, hematuria (blood in urine), or proteinuria (protein in urine) (Evans et al., 2022). The rate of loss of kidney function varies due to etiology and the presence of risk factors, but in most cases progression to kidney failure/end stage renal disease (ESRD) takes between months and decades. If left untreated, ESRD is fatal.

Impaired kidney function can result in the emergence of other health conditions. This most frequently manifests as heart failure and cardiovascular issues, due to the kidneys' role in waste and fluid management, blood pressure, vitamin D and erythropoietin production, and acid-base balance. In clinical settings, blood creatinine levels and proteinuria are used to monitor kidney function. Biomarkers like hyperkalemia (blood potassium levels), metabolic acidosis (systemic acid accumulation), hyperphosphatemia (blood phosphate accumulation), vitamin D deficiency, secondary hyperparathyroidism, and anemia are also monitored in the

development of CKD. Hypertension is one of the primary factors influencing the onset of CKD. Lifestyle management, including diet, physical activity, and weight loss, is also an important component of maintaining renal function for those with CKD. Reducing sodium intake and increasing exercise can be used to reduce hypertension. Proteinuria can be reduced by controlling protein intake. Techniques for managing CKD include cardiovascular risk reduction, avoidance of potential nephrotoxins (e.g., nonsteroidal anti-inflammatory drugs), and adjustments to drug dosing. Angiotensin-converting enzyme (ACE) inhibitors and angiotensin receptor blockers (ARBs) are used to help protect kidney function by reducing proteinuria and blood pressure.

Renal replacement therapies (RRT) provide life sustaining treatment for those with kidney failure. The vast majority of Americans with ESRD are treated with in-center hemodialysis, an expensive and burdensome treatment course with high morbidity rates. Conservative care strategies of preserving kidney function without the use of dialysis or transplantation are emerging (Brown et al., 2015; Teruel et al., 2015). The primary goals of conservative care are symptom management and maintaining patient quality of life. Globally, millions of people die annually due to a lack of access to RRT, and often without supportive or palliative care. According to estimates, RRT is not available to over 90% of ESRD patients in low- and middle-income countries. It is estimated that the number of people who die prematurely due to a lack of RRT access is three times the number of those receiving treatment (Thurlow et al., 2021).

2.2 Renal replacement therapies

ESRD can be treated by RRT. The goals of RRT include replacing renal function while improving patient survival and well-being. There are currently several modalities of RRT that are used to treat kidney disease. These include hemodialysis, peritoneal dialysis, and kidney transplantation. Hemodialysis and peritoneal dialysis are procedures that filter waste products from the blood, while kidney transplantation is the process by which a diseased kidney is surgically replaced with an allograft donor kidney. Due to the limited supply of donor kidneys and comorbidities that preclude many would-be transplant recipients from transplantation, dialysis remains the prevailing treatment option for most people with ESRD (Thurlow et al., 2021). Current advances and technical challenges of each RRT modality are described in this section.

2.2.1 Hemodialysis

Hemodialysis is the most common form of dialysis, accounting for approximately 90% of dialysis patients. Approximately 2.6 million people are estimated to have received hemodialysis in 2010, and this number is expected to double by 2030 (Liyanage et al., 2015). During hemodialysis, a machine called a dialyzer is used to filter wastes and water from the blood. In this machine, blood passes through hollow fibers surrounded by dialysis solution, creating an osmotic gradient for the dilution of solutes. Hemodialysis is a burdensome

treatment course that is typically administered three times per week for four hours at a time. Night and home dialysis are lesser implemented alternatives that offer increased flexibility.

Patient experiences and outcomes can be strongly impacted by the circumstances surrounding the start of dialysis and the modality and access choices taken. Compared to the general population, hemodialysis patients experience poorer health-related quality of life (Yang et al., 2015; Chuasuwan et al., 2020). Urgently initiated dialysis and less preparation are also linked to lower survival and increased morbity (Hasegawa et al., 2009; Tennankore et al., 2012). Surgery is typically conducted prior to commencing treatment to create vascular access, but catheters may be used in cases where this is not possible. Patients and clinicians may have divergent and conflicting goals for hemodialysis treatment which present an additional challenge in its implementation. Clinicians often focus on outcomes such as mortality and biochemical markers, while patients prioritize well-being and lifestyle (Evangelidis et al., 2017). Small solute clearance has traditionally been used to assess the efficacy of dialysis, but there is growing evidence that small solute clearance reflects only one of many factors that influence the outcomes of dialysis (Vanholder et al., 2015). The significance of considering patient preferences and satisfaction when making decisions and assessing dialysis as a treatment option is becoming more widely acknowledged (Walker et al., 2015; Perl et al., 2016).

Although hemodialysis is the most prevalent RRT, it has its own limitations. In high-income countries, 25% of patients die within a year of starting hemodialysis.This figure is even higher in low- and middle-income countries, which underscores the importance of preserving renal function in patients with, or at high risk of developing CKD (Kalantar-Zadeh et al., 2021). The low patient survival rates is underscored by the high cost of hemodialysis. In the US, hemodialysis has a total annual cost exceeding $42 billion, yet only a 35% five-year survival rate (USRDS, 2022) demonstrating the need to develop more economical and life-preserving solutions to ESRD.

2.2.2 Peritoneal dialysis

Peritoneal dialysis (PD) is an alternative to hemodialysis, that consists of using the peritoneum to dialyze wastes from the body rather than an external apparatus. A catheter is surgically placed in the abdomen. This catheter is then used to fill the peritoneum with liquid, composed of electrolytes (e.g. sodium, chloride, calcium, and magnesium), an osmotic agent (e.g. glucose), and lactate. Osmotic forces drive wastes from the blood to this liquid, which is later removed (Crabtree et al., 2019). Due to its continuous nature, PD offers much more flexibility than hemodialysis, and has improved tolerability for those with heart disease. Due to the need for abdominal access, PD, however, is not suitable for patients with prior abdominal surgery or inflammatory bowel disease.

Issues may arise because PD requires some technical expertise. PD-related peritonitis (infection of the

peritoneum) may result from touch contamination of the access port. To avoid an excessive fluid loss, the volume of the dialysis must be closely monitored. Large volume gains can lead to edema and hypertension, while large volume losses can result in hypovolemic shock or hypotension. Long-term use of peritoneal dialysis is associated with fibrosis of the peritoneum and can lead to peritoneal sclerosis. Peritoneal sclerosis is a potentially fatal complication wherein the bowels become obstructed due to fibrotic deposition. The high volume of glucose in PD liquid can also lead to hypertriglyceridemia and weight gain (Lo, 2016).

2.2.3 Kidney transplantation

Kidney transplantation is the best option for patients with ESRD to increase survival and quality of life (Abecassis et al., 2008). The number of kidney transplants being performed in the US is increasing year over year. In 2019, 23,401 kidney transplants were performed (Sawinski and Poggio, 2021). Recent advances in surgical, immunosuppressive, and postoperative protocols have led to a one-year kidney allograft survival rate of over 95% (Poggio et al., 2020). Despite these advances, achieving long-term graft viability is still a challenge, with the median kidney transplant survival in the US being only 11.2 years (Merion et al., 2018).

Kidney transplantation is severely limited by the scarcity of donor organs. On average, over 3,000 patients are added to the kidney wait list per month and 13 people pass away each day waiting for a transplant (USRDS, 2022). Mismatch in organ supply and increasing transplant demand has led to greater use of more "marginal" kidneys for transplantation, which negatively contributes to national allograft survival rates (Munagala and Phancao, 2016). Donor kidneys can come from either deceased or living donors. Living donor candidates undergo medical, surgical, and psychological evaluation by a transplant assessment team to ensure suitability for organ donation. Living donor transplants have better long-term graft survival and reduced risks of rejection and delayed graft function in comparison to deceased donor transplants (Hilbrands, 2020). Living donor transplants are also better from a pragmatic standpoint as recipients do not have to wait on the transplant list and transplant surgery can be planned. Studies have demonstrated that living donors are unlikely to develop serious long-term complication (Caliskan et al., 2022; Lentine and Segev, 2017). Deceased donor transplants, however, remain the predominant transplant organ supply accounting for approximately 64% of donor kidneys (Poggio et al., 2020).

Transplantation is a rigorous process that requires donor match, major surgery and a lifetime regiment of post-transplantation immunosuppression to prevent rejection. Prior to beginning the transplant process, patients are screened to ensure they are physically and psychologically suitable for the process. Tests are conducted to match recipients to donors and prevent ABO (i.e. blood type) and human leukocyte antigen (i.e. HLA) mismatches. Once a donor match is made, surgery is scheduled. During transplantation surgery, the recipient is placed under general anesthesia and the donor kidney is placed in the iliac fossa. The donor

kidney renal blood vessels are connected to the recipient's blood vessels and bladder. The removal of the old kidneys has been shown to increase surgical morbidity, so they are typically left in place, unless they are cancerous, infectious or cause high blood pressure as removal has been shown to increase surgical morbidity. After transplantation, immunosuppressive medications are required for the rest of the patient's life because the donor kidney is treated as a foreign object.

There are numerous challenges in kidney transplantation that contribute to poor long-term allograft and patient survival. The kidney transplant recipient population is getting older and has more co-morbidities which increases medical complexity and diminishes graft survival. The number of recipients over age 65 has doubled since 2001 and there is an inverse relationship between donor age and 10-year patient survival rates (Ghelichi-Ghojogh et al., 2021). Following national health trends, body mass index has also risen in transplant recipients, as has the number of patients with long dialysis. Although kidney transplant recipients are rigorously screened, cardiovascular disease is the primary cause of mortality among transplant recipients (Rangaswami et al., 2019). Hypertension is also common in kidney transplant recipients (Ponticelli et al., 2011). Chronic and acute antibody-mediated rejection can also cause kidney allograft failures. Non-immunological complications, such as the recurrence of primary kidney disease, cardiovascular diseases, infections, and malignancy also contribute to transplant failure. Solid organ infection is the second highest cause of mortality for donor kidney recipients, most commonly due to viruses. Late graft loss is usually multifactorial, caused by immunologic and nonimmune-mediated mechanisms. Transplant failure presents itself as slow, progressive kidney dysfunction characterized by the accumulation of interstitial fibrosis and tubular atrophy. After graft failure, patients may either transition back to dialysis or be evaluated for re-transplantation.

Posttransplant use of immunosuppressive medications is often associated with the incidence of metabolic complications. Transplant patients are often given corticosteroids, calcineurin inhibitors (CNIs), and mTOR inhibitors to reduce the likelihood of posttransplant rejection. CNIs directly damage pancreatic islet cells, which impairs insulin sensitivity and secretion and can lead to metabolic issues. Additionally, weight gain is common in kidney transplant recipients as immunosuppressive agents, surgical stress and inflammation increase the risk of hyperglycemia (Cannon et al., 2013). Immunosuppression, proteinuria, and post-transplant diabetes can lead to the development of posttransplant dyslipidemia (Holdaas et al., 2005). These issues underscore the need to further study mechanisms of metabolic dysregulation in the kidney.

2.3 Renal bioengineering

In this section, four major fields of renal bioengineering are described. First Section 2.3.1 explores the use of Decellularized kidney scaffolds, Section 2.3.2 presents kidney organoids, and Section 2.3.3 introduces the concept of Kidney-on-a-chip platforms. Finally, Section 2.3.4 closes on the development of the bioartificial

implantable kidney.

2.3.1 Decellularized kidney scaffolds

Decellularized organ scaffolds are a promising solution to certain types of end-stage organ failure that could be used to meet the donor supply shortage. Unlike allogeneic donor organs, which necessitate the life-long use of immunosuppressants to prevent donor organ rejection, decellularized organ scaffolds would utilize patient-derived cells and may enable the use of donor organs that would otherwise be ineligible for transplantation (Orlando et al., 2013). Research in the field of decellularized organ scaffolds has been applied to the heart, lungs, liver, pancreas and kidney. Here we will focus on advances in decellularized kidney scaffolds.

One of the primary challenges to the development of decellularized kidney scaffolds is to remove cells while preserving the extracellular matrix (ECM), the three-dimensional network of extracellular macromolecules that provide structural support to cells. There are several methods used for decellularization, including perfusing detergents or enzymes through the renal vascular network, and mechanical or physical separation. Decellularized kidney scaffolds maintain the complex anatomical macro- and micro-structures, such as the glomeruli and peritubular capillaries, which is advantageous in facilitating cell differentiation toward kidney-specific functions of filtration, secretion, and reabsorption. Retention of cell membrane epitopes or DNA, however, can cause adverse immune responses upon implantation, so scaffolds are often disinfected and dehydrated or lyophilized and sterilized after decellularization.

Once the cellular components have been removed from the scaffold, it must be recellularized to enable the organ to recapitulate its in vivo functionality. The kidney scaffold can be repopulated with cells through perfusion of the renal artery, renal vein, and the ureter. Vascular perfusion, however, is limited by the vascular basement membrane which prevents the perfusion of cells to the interstitial compartment (Ciampi et al., 2019). Methods are being developed to encourage the extravasation of cells to the perivascular and peritubular space to increase cell seeding efficiency. It has been demonstrated that when the renal artery is reperfused with high pressures after cell seeding, cells translocate from the microcirculation into the perivascular space (Caralt et al., 2015). Cell extravasation can also be improved when cells are infused under a vacuum (Leuning et al., 2019).

Rudimentary solid organs that utilize decellularized whole organ scaffolds as a substrate have been demonstrated in vitro and in small animal models. Fedecostante et al. (2018) developed a three-dimensional nephrotoxicity platform based on decellularized rat kidney scaffolds that was repopulated with conditionally immortalized human renal proximal tubule epithelial cells. Compared to two dimensional cultures, these recellularized scaffolds showed increased sensitivity to nephrotoxic agents cisplatin and tenofovir. Song et al. (2013) created a recellularized rat kidney that produced urine when implanted orthotopically. The functionality of decellularized kidney scaffolds has been further explored using a variety of cells. Hsu et al. (2022) produced

a decellularized kidney scaffold that was recellularized with renal progenitor and differentiated cells. When cultured in a whole-organ bioreactor, the organ was able to produce urine, and reabsorb albumin, glucose, and calcium.

Although there has been significant advancement in the creation of decellularized kidney scaffolds, there are challenges that limit their functional fidelity and clinical utility. Due to the complexity of the renal anatomy, high cell seeding efficiency has not yet been accomplished. Current methods of kidney decellularization have low throughput and techniques for decellularization have not yet been scaled up to the size of a human kidney. Another problem that has not been fully resolved is the harm that decellularization and sterilization cause to ECM proteins. To achieve translational viability, methods to reduce graft immunogenicity must also be improved. Importantly, transport properties do not yet correspond to those required to achieve clinical viability.

2.3.2 Kidney organoids

Organoids are three-dimensional, self-patterning cell cultures that can model the basic structure and function of organs. Compared to conventional two-dimensional cell culture methods, organoids better represent the in vivo cell microenvironment. In terms of physiological modeling, organoids are multicellular systems with a high degree of organization. The development of kidney organoids has been driven by increases in understanding of the processes underlying renal organogenesis. Kidney organoids have potential uses in vitro drug screening and as therapeutic regenerative organs. They are currently used to study kidney tubular damage and model the genetics underlying various kidney diseases.

In vivo renal organogenesis requires the coordinated migration of and spatiotemporal signaling of several distinct cell populations (Rad et al., 2020). A variety of cell types has been explored for the development of kidney organoids. Embryonic stem cells, undifferentiated nephron progenitor cells and human induced pluripotent stem cells (iPSCs) are all commonly used for the development of renal organoids (Nishinakamura, 2019). Adult differentiated cells have also been used to create three-dimensional organoid models without the use of genetic editing (Ding et al., 2020). This is a promising advance for potential therapeutic applications as cells are proliferated and differentiated without the use of foreign DNA.

Chimeric renal organoids derived from cells of multiple species are currently being explored. Saito et al. (2022) explored the differentiation and maturation of chimeric renal organoids using mouse- and rat-derived cells. When implanted in immunodeficient mice, these multi-species derived organoids showed milder rejection after implantation than fully xenograft organoids. Xinaris et al. (2016) generated functional podocytes from a combination of murine embryonic stem cells and human stem cells. These podocytes developed complex three-dimensional filtering structures resembling native glomerular slits and accomplished selective glomerular filtration and tubular reabsorption. When these organoids were mixed with human amniotic fluid stem cells,

the resulting organoids formed vascularized glomeruli and tubules.

Complex structures that mimic different aspects of native renal anatomy and function have been achieved in kidney organoid development. Branching three-dimensional ureteric buds (UB) have been generated from primary UB progenitor cells and human fetal kidneys (Zeng et al., 2021). These UB organoids generate structures that mimic the native collecting duct with differentiated principal and intercalated cells. Zeng et al. (2021) demonstrated that genetic modification of these UB organoids can be used to model congenital disorders of the kidney and urinary tract. Shankar et al. (2021) used iPSCs to create kidney organoids that produce renin, an enzyme critical to blood pressure regulation secreted by the kidneys in vivo, when implanted in a murine model. This model will enable researchers to study the role of the renin-angiotensin system (RAS) during kidney development and evaluate new RAS-targeting therapeutics.

Kidney organoids are being increasingly used to study renal disease pathogenesis. Freedman et al. (2015) developed nephron-like organoids capable of modeling nephrotoxic renal epithelial injury. These organoids were later used to study polycystic kidney disease (PKD) via genetic knockout of the podocalyxin-like protein 1 (PODXL) and PKD1/2 genes, which are responsible for the occurrence of PKD (Cruz et al., 2017). It was later found that the deletion of PODXL lead to defects in cell attachment and adhesion, indicating that PODXL is important to junctional migration of developing podocytes (Kim et al., 2017). Low et al. (2019) developed a model of autosomal recessive PKD, an early-onset form of PKD that manifests during childhood, using iPSC of an autosomal recessive PKD patient. CRISPR-Cas9 gene editing was effective in preventing the cystic phenotype. Hale et al. (2018) used hiPSCs have been used to model nephrotic syndrome. Calandrini et al. (2020) developed tubuloids from Wilms tumors, which has enabled the creation of a biobank for childhood renal cancers for use in identifying patient-specific dug sensitivities. Organoids have also been used to study glomerulopathies (Harder et al., 2019).

Although kidney organoids are increasingly used as tools in basic research, clinical application of these tools is still in its infancy. Currently, kidney organoids are unable to fully recapitulate native tissue structures that are necessary for use as transplantable organs. Kidney organoids lack vascularization, which limits their growth capacity. Single-cell RNA sequencing studies also reveal that organoids to not mature further than an embryonic kidney, even with prolonged cell culture (Wu et al., 2018). The cell composition of lab-grown organoids is an emerging problem. Using RNA sequencing Wu et al. (2018) found that renal organoids are comprised of up to 10 to 20% off-target cells, which presents a problem to their long term use. Technical developments to overcome these limitations will require attention to cellular composition, appropriate incorporation and vascularization to host tissues, and improved functionality. Nonetheless, kidney organoids offer great potential for new directions in the field of renal regenerative therapies.

2.3.3 Kidney-on-a-chip

The tissue engineering approach of culturing cells in microchannels and microfluidic systems has been applied to renal bioengineering to create kidney-on-a-chip platforms that recapitulate important tissue- and organ-level renal functions. Kidney-on-a-chip platforms are typically made from inert, biocompatible materials to avoid chemical leaching, and have a pump or syringe apparatus to apply constant flow to the apical compartment (Wilmer et al., 2016). In comparison to conventional static cultures, this approach promotes cell differentiation in terms of tight junction formation, biomarker expression and cellular transport function. It also enables the integration of sensors for precise analysis of cellular metabolites.

Microfluidic systems enable the co-culture of different cells types, and the ability to integrate sensors for continuous measurement of cellular behavior. iPSC-derived podocytes have been used to develop a glomerulus-on-a-chip (Musah et al., 2017). Sciancalepore et al. (2014) developed a multi-layered renal microdevice embedded with adult renal stem/progenitor cells. Kidney-on-a-chip models circumvent the limitations of two-dimensional cell culture and animal models. Increased cell function and ability to closely monitor metabolite excretion/formation. Schutgens et al. (2019) combined kidney organoids with microfluidic organ-on-a-chip plates to create "tubuloids" with a tubuloid structure and active transport function. Kidney-on-a-chips with circulatory cells and non-epithelial renal cells are being developed for disease modeling. Weinberg et al. (2008) developed a nephron-on-a-chip with an inlet for blood, an outlet for blood, and an outlet for urine.Mu et al. (2013) created a three-dimensional vascular network for in vitro modeling of mass transfer.

Kidney-on-a-chip has many potential applications in drug development and testing. Nephrotoxicity is often not discovered until testing is initiated in humans in phase III and phase IV clinical trials (Tiong et al., 2014). Preliminary nephrotoxicity testing is typically performed in animal models, which is expensive and slow. Further, animal models may fail to predict human nephrotoxicity due to species-specific physiology. Yin et al. (2020) developed a multi-layer microfluidic chip comprised of a microfluidic device for generating drug concentration gradients and a platform for renal cell culture for nephrotoxicity screening. The in vitro use of cell lines offers a less expensive alternative that circumvents the ethical concerns of animal models. Although many cell lines do not fully recapitulate the structure and function of the native renal epithelia, kidney-on-a-chip platforms may be able to leverage novel bioengineering techniques to enhance cell differentiation in vitro.

While current kidney-on-a-chip models are useful for disease modeling and nephrotoxicity screening in comparison to conventional static culture, there are still limitations that limit their utility. Species-dependent variations may limit the utility of animal-derived cell lines in human disease models and nephrotoxicity screening. While human-derived primary cells and cell lines are commonly used in kidney-on-a-chip studies, current models only partially reproduce normal physiology and inadequately model tubular drug transporters

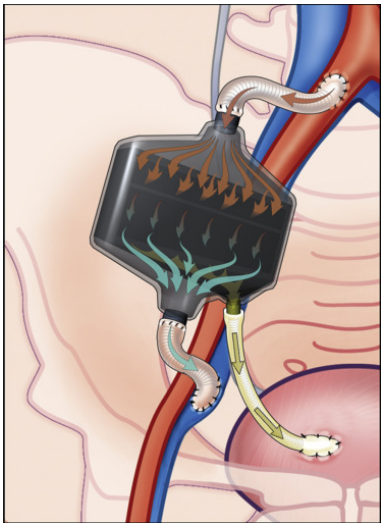

Figure 2.1: **A representation drawing of the implantable bioartificial kidney** The device is implanted in the iliac fossa and connected the patient's blood supply. A hemofilter with silicon nanoporous membranes mimic the slit-shaped pores of podocytes filters the blood. The ultrafiltrate then flows through the cellular bioreactor which contains living renal tubule epithelial cells, which resorb solutes from the ultrafiltrate, much like the native kidney. Wastes in the concentrated ultrafiltrate are routed from the cell bioreactor to the bladder. *Adapted from (Salani et al., 2018)*

and metabolic enzymes.

2.3.4 Bioartificial kidney

Dialysis and kidney transplantation are currently the only viable RRT options for patients with ESRD. Both treatment modalities, however, have limited long-term efficacy. A bioartificial kidney seeks to create a fully functional kidney by utilizing a cell-based bioengineering approach. The bioartificial kidney is designed to mimic many functions of the natural kidney by linking a hemofilter and bioreactor in series, much like the glomerulus and the nephron in the native organ. The bioartificial kidney would be surgically implanted in the iliac fossa to establish a permanent connection to the blood supply. The hemofilter, which is based on silicon nanopore membranes (SNM), will function like the glomerulus of the native kidney by selectively filtering solutes from the blood based on molecular size. The second component of the bioartificial kidney will consist of a cellular bioreactor of renal tubule epithelial cells seeded onto the SNM scaffold. This portion of the bioreactor would mimic the native tubules by reabsorbing water and solutes from the filtrate and excreting waste. This configuration enables the bioartificial kidney to perform ultrafiltration using the body's blood pressure, thereby negating the need for pumps or an external power supply (Groth et al., 2022).

The SNM will provide mechanical support for the cells and isolate them from the host immune system. The SNM will have a uniform slit pore design that increases hydraulic permeability and selectivity compared to the circular pores in standard hollow-fiber membranes (Kanani et al., 2010). SNM have several characteristics

which make them a well-suited hemofilter. SNM pores can be as small as 5 nanometers, and selectivity has been demonstrated in vitro using various globular proteins (Fissell et al., 2009). SNM membranes have high hydraulic permeability that can achieve a rate of 30mL/min using only the arterial-venous pressure differential, which negates the need for an internal or external pump to drive filtration (Fissell et al., 2009). filters blood continuously, which mitigates the inconveniences and morbidities associated with hemodialysis.

Cell sources for the bioartificial kidney are still being explored. While immortalized cell lines are commonly used to study renal biology and in renal bioengineering models, cell lines do not fully recapitulate native cell phenotypes or display full functional differentiation (Jenkinson et al., 2012; Jang et al., 2013). Immortalized cell lines exhibit continued growth, which while useful in populating platforms, may lead to poor long-term viability due to overgrowth (Ozgen et al., 2004). Additionally, species-dependent variations in tubular function may cause adverse zoonotic reactions. Primary cells achieve better in vitro differentiation than immortalized cell lines but are limited by the number of population doublings they can achieve (Sanechika et al., 2011). Induced pluripotent stem cells (iPSCs) have been explored, but there are ethical concerns over using human embryos and fetal cells for organ development.

Development of the bioartificial kidney has the potential to increase access to donor organs and increase global healthcare equity. Despite this, challenges remain in its development, including improvement of chip-level filtration efficiency, cell sourcing and maintenance of cell phenotype in vitro. Functional studies, such as water reabsorption assays, must be completed to demonstrate intracorporeal viability. Nonetheless, success in creating a bioengineered kidney could change the paradigm of renal replacement therapy and improve access to treatment and quality of life for those experiencing ESRD.

CHAPTER 3

Metabolic reprogramming and renal fibrosis in chronic kidney disease

3.1 Introduction to renal tubule epithelial cell metabolism

The kidneys are the primary regulators of body fluid and electrolyte homeostasis. An individual kidney filters about 180 liters of plasma and reabsorbs more than 99% of filtered sodium (over one kilogram) each day, through a diverse number of transporters, channels, and pumps (Moe, 2012). The kidney is comprised of two main compartments, the glomerulus, and the nephron. The glomerulus filters blood to produce a primary filtrate of water and solutes (e.g., Na^+, K^+, HCO_3^-, urea). Filtrate from the glomerulus flows into the lumen of the nephron, a gland-like structure surrounded by capillaries. Along the nephron, renal tubule epithelial cells perform absorption, resorption and excretion, to modify the ultrafiltrate produced by the glomeruli.

The nephron is comprised of 14 functionally and anatomically discrete segments containing at least 16 distinct epithelial cell types (Georgas et al., 2008; Lee, 2015; Harding et al., 2003). Each cell type has its own characteristic set of cellular functions which depends highly on gene expression (Lee, 2015). Deep RNA sequencing of micro-dissected renal tubules has achieved quantitative transcriptomic profiling of each tubule segment. This data revealed that there are unique patterns of the distribution of region-specific transcription factors, metabolic enzymes, transporters, and G protein-coupled receptors along the nephron (Lee, 2015).

The renal tubule segments are summarized in Figure 3.1. The proximal tubules reabsorb the majority of H_2O and electrolytes, while solutes are secreted into the filtrate (Zhuo and Li, 2013). The Loop of Henle, which is comprised of the thin descending, thin ascending, thick ascending, and cortical thick ascending limbs, is responsible for solute concentration. Here the "thick" and "thin" terminology denote the size of the epithelial cells in each section, rather than the size of the lumen. The distal tubule and collection duct perform highly regulated solute transport. The proximal tubule and thick ascending limb, which perform most water reabsorption, have the highest mitochondrial density of any nephron segment (Soltoff, 1986).

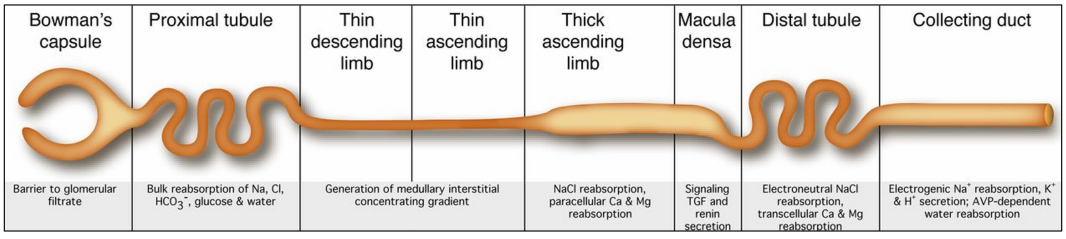

Figure 3.1: **Major renal tubule segments.** *Adapted from (Yu et al., 2015b)*

In the renal tubule, active transport is coupled to the electrochemical gradient generated by sodium-

potassium ATPase (Na^+-K^+ ATPase) (Palmer, 2015). Na^+-K^+ ATPase is a basolateral transmembrane pump that generates electrochemical gradients that directly and indirectly drive other cell transport activities (Mandel and Balaban, 1981). A vast amount of ATP is required to accomplish this transcellular transport. This high ATP requirement necessitates high mitochondrial density, making renal tubule epithelial cells the second most metabolically active cells in the body, second only to cardiac myocytes.

In a healthy kidney, dynamic mitochondrial turn over through fission and fusion reactions maintain a healthy mitochondrial pool. β-oxidation of fatty acids provides fuel substrate for oxidative phosphorylation and mitochondria have sufficient NAD co-factors to create abundant ATP. As shown in Figure 3.2, a variety of substrates, including free fatty acids, pyruvate, lactate, glutamine, and citrate, are broken down into metabolites that feed the tricarboxylic acid (TCA) cycle, to produce NADH and $FADH_2$ for OXPHOS.

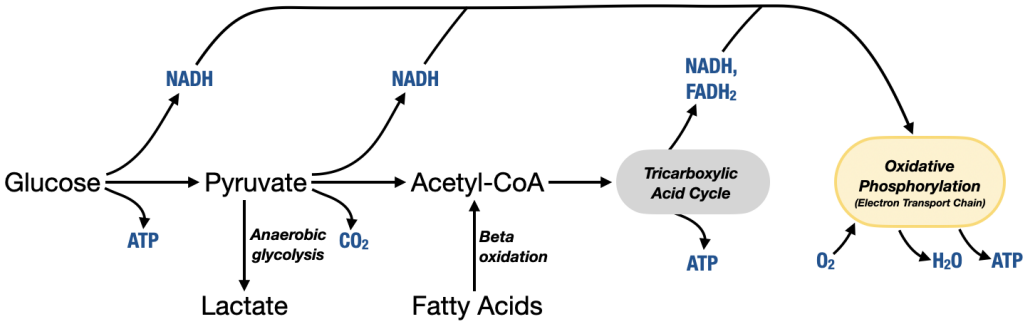

Figure 3.2: **Primary metabolic pathways in the renal tubule**

The kidneys contribute to glucose homeostasis via reabsorption, production, and utilization. In the healthy kidney, about 95% of ATP production occurs via oxidative phosphorylation (OXPHOS), while anaerobic metabolism is more prevalent in the hypoxic renal medulla (Soltoff, 1986). In both cases, cytosolic glucose undergoes glycolysis to produce pyruvate. In healthy renal tubule cells, pyruvate is then imported to the mitochondria and converted to acetyl-CoA. Acetyl-CoA then enters the tricarboxylic acid (TCA) cycle to produce reducing agents, NADH and $FADH_2$, for OXPHOS in the electron transport chain (ETC). A dysfunctional ETC increases glycolysis, which causes an increase in lactate and pyruvate as glucose is no longer directed toward full oxidative metabolism. Most ATP is produced via fatty acid β-oxidation (FAO) by RPTEC in vivo because it generates more ATP per molecule than glucose oxidation, which is advantageous given the high energy demands of these cells.

3.1.1 Fatty acid oxidation

Human renal tubule epithelial cells (HREC) produce much of their ATP in the mitochondrial and peroxisomal compartments via fatty acid β-oxidation (FAO). Fatty acid (FA) uptake occurs through membrane diffusion

or facilitated transport by membrane proteins. Transport rates depend on FA size and number of saturations, membrane lipid composition, and protein composition. Long chain fatty acid (LCFA) uptake is facilitated by LCFA transporter cluster of differentiation 36 (CD36). Lipids are usually transported by associating with hydrosoluble lipoprotein particles, which enables controlled recognition and delivery in vivo. Non-esterified FAs are mainly transported with serum albumin, a protein abundant in plasma and interstitial fluids that can bind FA and other lipophilic molecules. In in vitro systems, albumin-promoted FA delivery follows the "pseudofacilitation model" in which FAs are delivered as a function of their unbound concentration in the media at physiological concentrations of albumin (200μM) (Alsabeeh et al., 2018). At lower concentrations ($<150\mu$M) delivery depends on albumin concentration. In addition to acting as an energy source, FA also act as signaling molecules and are incorporated into membranes as triacylglycerols. De novo lipid synthesis is regulated by fatty acid synthase (FAS), and its upstream effectors ATP citrate lyase (ACLY) and acetyl-coenzyme A carboxylase alpha (ACACA).

Fatty acid metabolism requires mitochondrial import, which is mediated by carnitine palmitoyl-transferase 1 (CPT1). CPT1 is considered the rate-limiting enzyme in FAO. The peroxisome proliferator-activated receptors (PPAR) and PPAR-γ coactivator-1α (PGC1α) are key transcription factors that regulate the expression of proteins involved in FA uptake and oxidation. Normally, FA uptake, oxidation and synthesis are tightly balanced to avoid intracellular lipid accumulation. Tubular accumulation of triglycerides may induce cellular lipotoxicity that contributes to fibrosis development (Herman-Edelstein et al., 2014; Declèves and Sharma, 2015).

When cells are placed under biological stress (e.g. transient hypoxia) FAO is shut down for a period of time that outlasts injury. In these situations carbohydrate oxidation does not take over (Kang et al., 2015). Facing these metabolic constraints, surviving tubular epithelial cells exhibit a phenotypic switch that includes increased glycolysis, cytoskeletal rearrangement and increased production of extracellular matrix (ECM) proteins. In vitro experiments indicate that inhibition of FAO causes ATP depletion, cell death, dedifferentiation and intracellular lipid accumulation. In vivo, dysregulation of FAO profoundly affects the fate of tubular epithelial cells, promoting epithelial-mesenchymal transition (EMT), inflammation, and eventually interstitial fibrosis.

3.1.2 Renal metabolic reprogramming

In vitro and in diseased kidneys, mitochondrial biogenesis decreases and metabolic pathways become dysregulated. As shown in Figure 3.3, damaged mitochondria release cytotoxic components, β-oxidation decreases, fatty acids accumulate and become peroxidation products that cause inflammation. Diseased mitochondria have insufficient NAD co-factors to produce adequate ATP.

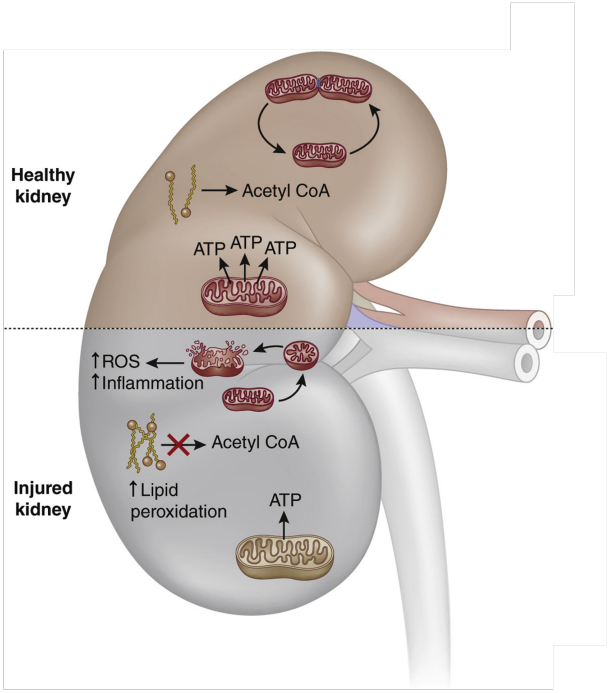

Figure 3.3: **Kidney injury leads to dysregulation of metabolic pathways.** Adapted from (Kang et al., 2015)

Mammalian cells primarily utilize two distinct catabolic pathways for generating cellular energy, glycolysis and oxidative phosphorylation (OXPHOS). Anaerobic glycolysis produces 2 ATP per glucose molecule, while the oxidation of glucose by OXPHOS can produce up to 36 ATP per glucose molecule. Differentiated cells primarily rely on mitochondrial OXPHOS to metabolize glucose into carbon dioxide through the oxidation of pyruvate in the tricarboxylic acid (TCA) cycle. In the absence of oxygen, differentiated cells utilize anaerobic glycolysis to produce ATP from glucose. In contrast, proliferative cells rely on glycolytic metabolism even in the presence of oxygen, even though OXPHOS is about fifteen times more effective at producing ATP than glycolysis, because it allows for the accumulation of intermediary metabolites while producing a modest amount of ATP.

Metabolic reprogramming is a common phenotype in cancer that allows cancer cells to exhibit high growth rates and sustain cell proliferation. It was originally hypothesized that cancer cells develop a mitochondrial defect that impairs normal respiration (Heiden et al., 2009; Warburg, 1956). It has, however, since been shown that mitochondrial function is not impaired in most cancer cells. The metabolic reprogramming of cancer cells is primarily driven by the deregulation of growth factors and nutrient-sensing signaling pathways.

Metabolic status is emerging as a dynamic regulator of cell phenotype rather than a static process involved in cellular homeostasis. In normal proliferating tissues, such as the developing embryo or during wound healing, growth factor signals stimulate cells to utilize metabolic intermediates for anabolic growth processes,

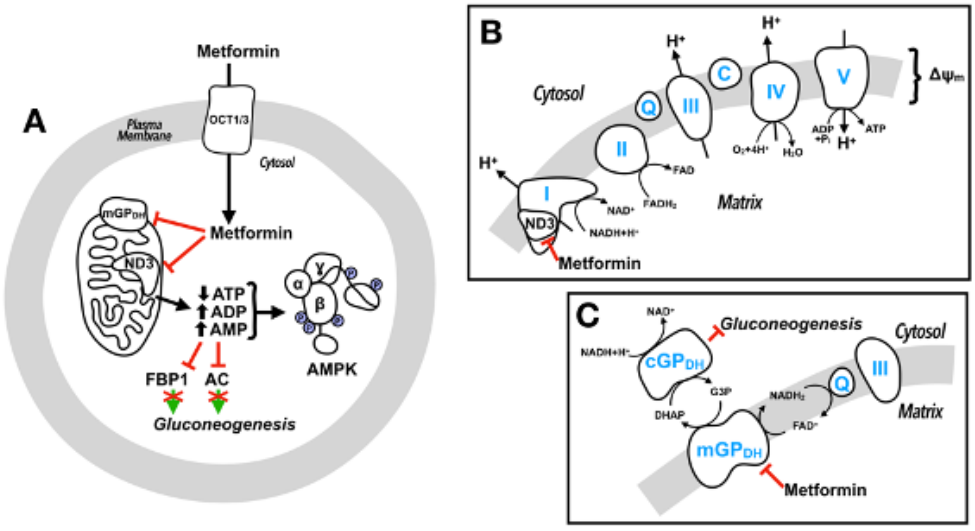

Figure 3.4: **Diagram of metformin's mechanism of action A.** Metformin enters the cell through OCT1/3 transporters. **B.** Metformin inhibits electron transport chain (ETC) Complex I ND3 subunit to suppress ETC ATP generation and reduce mitochondrial transmembrane potential ($\Delta\Psi$). **C.** Metformin also inhibits mitochondrial glycerophosphate dehydrogenase (mGPDH), thus reducing NADH oxidation.

whereas differentiated cells direct nutrients towards full metabolic extraction. Metabolite fluctuation can both, directly and indirectly, influence differentiation by influencing epigenetic states and the expression of metabolic pathways. Metabolites such as acetyl-CoA, α-ketoglutarate, 2-hydroxyglutarate, and butyrate are donors, substrates, cofactors, and agonists for epigenetic modification and the activities of epigenetic modifying complexes (Chisolm and Weinmann, 2018). Epigenetic regulatory events provide a mechanistic link between metabolism and differentiation programs.

3.1.3 Metformin

Renal metabolic dysregulation is commonly treated with the drug metformin. Metformin (*N*-*N*-dimethylbiguanide hydrochloride) is a first-line, standard clinical hypoglycemic drug that is used for the treatment of type II diabetes mellitus (T2DM) and polycystic ovary syndrome (PCOS). Metformin is a biguanide extracted from the herb *Galega officinalis* (a.k.a. French lilac, Italian fitch, goat's rue). Metformin modulates cell metabolic activity by inhibiting mitochondrial respiratory chain Complex I (a.k.a. NADH: ubiquinone oxidoreductase) and mitochondrial glycerophosphate dehydrogenase (mGPDH) as shown in Figure 3.4A. Metformin's ability to inhibit NADH oxidation by ETC Complex I is highly conserved, occurring in *C. elegans*, the bacterium *E. coli*, the yeast *Pichia pastoris*, and isolated cardiomyocyte mitochondria (Bridges et al., 2014; Wu et al., 2016).

Metformin is imported to the cell by Organic cation transporters 1 and 3 (OCT-1 and OCT-3). Once in the cell, metformin inhibits Complex I by binding its ND3 core subunit. As shown in Figure 3.4B, this inhibition

of Complex I decreases NADH oxidation and proton pumping across the inner mitochondrial membrane, resulting in a lowered proton gradient ($\Delta\Psi$), reduced oxygen consumption, and reduction of proton-driven ATP synthesis (Foretz et al., 2014). The exact molecular interactions between metformin and Complex I have yet to be elucidated, but metformin does not alter the structure of the whole complex (Hirst et al., 2012). Metformin is a reversible non-competitive inhibitor that likely binds to some amphipathic regions of Complex I.

Metformin's second main target mGPDH connects glycolysis, fatty acid metabolism, and OXPHOS and is an integral part of the mammalian respiratory chain and the glycerol phosphate (GP)-shuttle. mGPDH expression is primarily regulated at the transcriptional level, while its activity is regulated by redox state and allosteric binding with various metabolites and ions (Mráček et al., 2013). Its metabolic role is not yet fully understood but it plays an important role in contributing to cellular redox balance as a component of the GP-shuttle, as shown in Figure 3.4C. The GP-shuttle is comprised of the mitochondrial membrane-bound mGPDH and the cytosolic GPDH (cGPDH). The two GPDH isoforms catalyze the oxidation of cytosolic glycerol-3-phosphate (G3P) to dihydroxyacetone phosphate (DAP) with concurrent reduction of flavin adenine dinucleotide (FAD) to $FADH_2$ and electron transfer to CoQ10 (Mráček et al., 2013). This enables cytosolic NADH oxidation to bypass Complex I, which is suggested to be important for maintaining redox intermediates in glycolytic cells. The inhibition of mGPDH results in increased cytosolic NADH through modulation of cytosolic and mitochondrial redox state. In this way, the GP-shuttle enables sustained cytosolic ATP production without the accumulation of an intermediate by-product, such as lactic acid.

Metformin exhibits a dose-dependent response. High concentrations of metformin (20-100mM) directly inhibit Complex I activity in isolated mitochondria, while clinically relevant concentrations ($<100\mu$M) do not. Micromolar concentrations, however, are sufficient to achieve a dose- and time-dependent inhibition of Complex I in situ and in vivo in skeletal muscle from both healthy and diabetic rats (El-Mir et al., 2000; Detaille et al., 2002; Guigas et al., 2004; Wessels et al., 2014). It is suspected that the transmembrane electrochemical potential ($\Delta\Psi$) of energized cells enables the slow accumulation of metformin, which is positively charged (Owen et al., 2000; Bridges et al., 2014). It is hypothesized that micromolar concentrations of metformin in the cytoplasm could accumulate to reach millimolar concentrations in the mitochondria, due to the Nernst potential of a positively charged molecule across the energized mitochondrial membrane (Fontaine, 2014). This mechanism may partially explain metformin's low toxicity. If mitochondrial import is $\Delta\Psi$-driven, reduced mitochondrial potential induced by the drug would prevent its accumulation.

3.1.4 AMP-activated protein kinase

Metformin's beneficial effects on modulating cell metabolism are mainly attributed to its role in activating AMP-activated protein kinase (AMPK). Inhibition of Complex I prevents mitochondrial ATP production,

increasing cytoplasmic ADP:ATP and AMP:ATP ratios which leads to AMPK activation. AMPK plays a critical role in metabolic regulation by inhibiting anabolic activities to minimize cellular ATP consumption and by stimulating catabolic activities to stimulate ATP production.

AMPK is a heterotrimeric protein complex that is comprised of α-, β-, and γ-subunits. Cystathionine β-synthase (CBS) domains in the γ-subunit enable AMPK to detect changes in cytosolic AMP:ATP ratios. Therefore, when AMP binds both domains, the γ-subunit undergoes a conformational change that exposes the catalytic domain in the α-subunit. AMPK binding is dynamic as the binding of AMP to a CBS domain increases the binding affinity of the second domain. Finally, AMPK is activated when phosphorylation takes place at Thr172 in this catalytic domain. Calcium/calmodulin-dependent protein kinase II (CaMKK2), liver kinase B1 (LKB1), and TGF-β-activated kinase 1 (TAK1) phosphorylate AMPK while and protein phosphatase 2A (PP2A), protein phosphatase 2C (PP2C), and magnesium-manganese-dependent protein phosphatase 1E (PPM1E) dephosphorylate AMPK.

AMPK enables cells to adapt to low-energy conditions by reprogramming cell metabolism through transcriptional modulation of biosynthetic pathways. AMPK inhibits gluconeogenesis by phosphorylating class IIA histone deacetylases (HDACs) and CREB Regulated Transcriptional Coactivator 2 (CRTC2), which activate the forkhead box protein O (FOXO) and cAMP response element-binding protein (CREB) pathways, respectively (Mihaylova et al., 2011; Koo et al., 2005). AMPK inhibits lipid and sterol synthesis by phosphorylating the acetyl-CoA carboxylases (ACCs), which catalyze the first step of lipid synthesis (Lee et al., 2018). Similarly, AMPK also inhibits cholesterol synthesis by inhibiting the phosphorylation of HMG-CoA reductase (HMGCR) (Motoshima et al., 2006; Jeon, 2016). Lastly, AMPK prevents glycogen storage by phosphorylating glycogen synthases GYS1/2 (Janzen et al., 2018).

AMPK stimulates cell energy generation by enhancing glucose utilization via increased cell glucose import and glycolytic flux. TXNIP (thioredoxin-interacting protein) and TBC1D1 (Tre-2/Bub2/Cdc16 domain family member 1) are phosphorylated by AMPK to increase membrane localization of glucose transporters GLUT1 and GLUT4 (Wu et al., 2013; Chavez et al., 2008). AMPK also stimulates glycolysis by phosphorylating PFKFB3 (6-phosphofructo-2-kinase/fructose-2,6-bisphosphatase 3), which mediates the activity of PFK1 (phosphofructo-kinase), a rate-limiting enzyme in glycolysis (Domenech et al., 2015; Wu and Wei, 2012).

In addition to its role in modulating cell metabolism, AMPK regulates cell physiological processes related to cell growth, polarity, transcription, mitosis, and autophagy. AMPK is involved in the regulation of cell motility, adhesion, and invasion through its interactions with cytoskeletal proteins and adhesion molecules (Schaffer et al., 2015; Bays et al., 2017). AMPK stimulation leads to Na^+-K^+-ATPase α1-subunit dephosphorylation at Ser18, which may prevent endocytosis of the sodium pump (Benziane et al., 2012). AMPK also inhibits O-GlcNAc (O-linked β-N-acetylglucosamine) epigenetic modifications by phosphorylating GFAT1 (Ruan

et al., 2013; Gélinas et al., 2018).

AMPK has become a therapeutic target in several diseases, including diabetes, obesity, and cancer. Metformin is currently used as a complementary therapeutic agent for radiotherapy and chemotherapy for the treatment and prevention of cancer due to its ability to reduce the incidence of cancers, reduce cancer mortality, and increase response to treatment (Zi et al., 2018).

3.2 The role of TGF-β in renal mechanotransduction and CKD

Cells can sense the surrounding microenvironment and modulate their behavior based on mechanical cues. Mechanical properties of the microenvironment, such as substratum stiffness, apical shear stress, and contact-mediated cell-cell interactions are critical mediators of HREC fate, but the interactions of these factors is yet to be fully understood. In addition to substrate stiffness, cells respond to confinement, porosity, and density. A stiff extracellular matrix (ECM) promotes cell spreading, while a soft ECM promotes confined adhesion (e.g. cell rounding). The role of mechanotransduction in guiding renal tubule epithelial cell differentiation and dysregulation remains obscure, despite its importance in nephrogenesis and disease progression. Mechanical properties of the microenvironment, such as substratum stiffness.

3.2.1 Transforming Growth Factor-β

Transforming Growth Factor-β (TGF-β) is a classic mechanotransductive cell signaling pathway. TGF-β is a pluripotent cytokine involved in the regulation of epithelial cell fate and plasticity, but can also promote tumorigenesis and is a well-identified mediator of renal fibrosis and CKD (Batlle and Massagué, 2019). Overexpression of TGF-β1 in the liver causes renal fibrosis in mice (Bottinger et al., 1996). The ability to halt renal fibrosis by inhibiting TGF-β has been demonstrated using neutralizing antibodies, inhibitors of the TGF-β receptor II, and TGF-β antisense oligonucleotides (Voelker et al., 2017; Border et al., 1990; Liu et al., 2018; Cordeiro et al., 2003).

TGF-β signaling is initiated when stiffness-mediated traction forces cause a conformational change in the TGF-β Latency Complex which allows the release of the TGF-β1 ligand. Induction of the TGF-β signaling pathway occurs when biologically active TGF-β1 ligand binds to the TGF-β receptor II (TβRII), which then activates the TGF-β receptor I (TβRI) to induce the formation of a heterotetrameric complex of two TβRIs and two TβRIIs and recruitment of the receptor-associated Smad (r-Smad) proteins. In the receptor complex, the constitutively active TβRI phosphorylates the recruited r-Smad (e.g. Smad2 or Smad3) at its C-terminal serine residues. Upon phosphorylation, the active r-Smad forms a complex with the co-Smad (Smad4) as shown in Figure 3.5A. This complex translocates to the nucleus where it acts as a transcription factor (TF) to regulate target gene expression in cooperation with other TFs and co-factors. TGF-β initiates canonical and

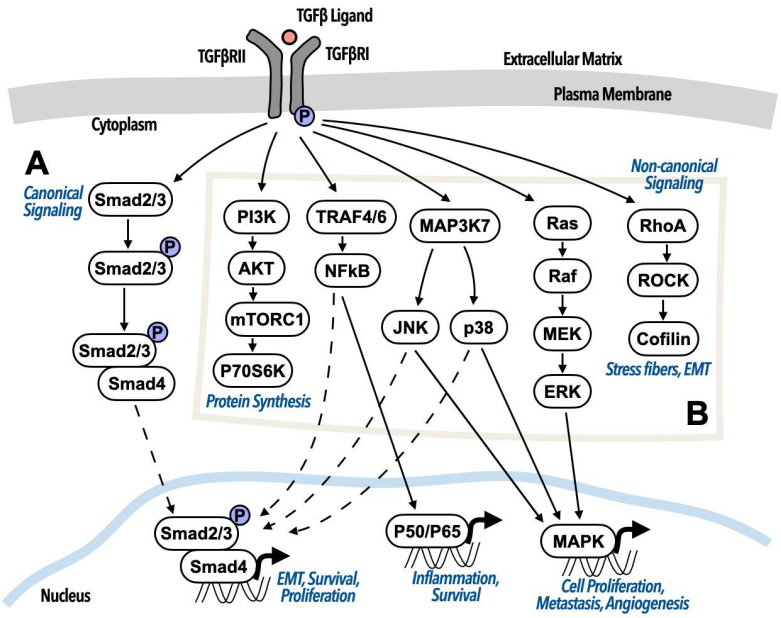

Figure 3.5: **Overview of the major TGF-β signaling pathways. A.**Canonical TGF-β signaling pathway. **B.** In non-canonical signaling, the TGF-β receptor complex transmits its signal through a number of non-Smad factors, including the mitogen-activated protein kinases (MAPKs), tumor necrosis factor (TNF) receptor-associated factor 4/6 (TRAF4/6), phosphatidylinositide 3-kinase (PI3K), and Rho family small GTPases.

non-canonical pathways to exert multiple signaling cascades, as shown in Figure 3.5.

3.2.2 Smad protein signaling

The Smad proteins were the first identified intermediates of TGF-β signaling in Drosophila MAD and C. *elegans* SMA genes. Smads are divided into three distinct classes based on their role in TGF-β signal transduction: receptor-associated (r-Smads) which transduce TGF-β receptor activation, the common Smad (co-Smad), which binds the activated r-Smads, and the inhibitory Smads (i-Smads) which attenuate TGF-β signaling through inhibitory binding with the r-Smads. TGF-β nuclear transduction can activate transcription of genes encoding the i-Smads (e.g., Smad6 and Smad7) to initiate a negative feedback loop that inhibits canonical Smad-dependent TGF-β signaling. The i-Smads inhibit r-Smad activity by blocking interaction with TβRI or by competing with co-Smads to prevent the formation of an r-Smad/co-Smad complex. Conversely, during fibrogenesis, r-Smads can attenuate i-Smad activity to perpetuate canonical TGF-β signaling. In CKD, Smad3 is highly activated, which is associated with the attenuation of inhibitory Smad7 through ubiquitin-dependent degradation (Meng et al., 2015). Smad3 is associated with many fibrogenic genes, including various collagen isoforms (e.g., Col1A1, Col1A2, Col3A1, Col6A1, Col6A3), and overexpression can enhance TGF-β mediated cell apoptosis in acute kidney injury by upregulating pro-apoptotic genes. The

increased Smad3:Smad7 ratio leads to the accumulation and activation of myofibroblasts, overproduction of ECM, and reduction in ECM degradation (Meng et al., 2015). Inhibition of Smad3 has been shown to block TGF-β induced epithelial cell dedifferentiation and attenuate diabetic glomerulosclerosis (Li et al., 2010). Contrarily, overexpression of Smad7 is a therapeutic agent for renal fibrosis in various models of kidney disease (Sureshbabu et al., 2016). Smad7 negatively regulates canonical Smad signaling by competing with Smad2/3 binding to the TGF-βRII receptor. Smad7 can attenuate TGF-β-mediated fibrosis, carcinogenesis, and inflammation in various diseases. In addition to its role in nuclear shuttling, Smad4 is critical for regulating the ability of Smad3 and Smad7 to initiate the transcription of target genes (ichi Tsuchida et al., 2003).

Several posttranslational modifications have been shown to regulate Smad binding activity. The R-Smads and Smad4 have two highly conserved domains, the Mad homology 1 (MH1) domain in the amino terminus and the Mad homology 2 (MH2) domain in the carboxyl terminus. The MH1 domain is responsible for DNA binding (Shi et al., 1998), while the MH2 domain is required for Smad-receptor, Smad-Smad, and many Smad-transcription factor interactions (Feng and Derynck, 2005). Smad2 does not directly bind DNA because of an insert encoded by exon 3 just upstream of the DNA-binding beta-hairpin (Shi et al., 1998). An isoform lacking exon 3 (Smad2$_{\Delta exon3}$), however, binds DNA equivalently to Smad3 (Yagi et al., 1999). Acetylation of Smad3 and Smad2$_{\Delta exon3}$ on Lys19 by p300 and the highly related histone deacetylase CREB-binding protein (CREBBP) promote DNA binding and subsequent transcriptional activation (Simonsson et al., 2006). It is proposed that acetylation of Lys19 in Smad2$_{\Delta exon3}$ promotes DNA binding by releasing the MH1 domain from its inhibitory interaction. The Smad3-Smad4 complex can undergo poly-ADP-ribosylation (PARylation), which is induced by poly(ADP-ribose)polymerase-1 (PARP1) (Lonn et al., 2010). Monoubiquitylation induces disruption of DNA-bound Smad complexes. R-Smads are monoubiquitinated in their DNA-binding domains which attenuates their affinity for DNA. This is opposed by the DUB USP15. Monoubiquitylation at Lys519/507 in the MH2 domain of Smad4 disrupts the formation of Smad2/3-Smad4 complexes and thus their ability to bind DNA (Dupont et al., 2009).

3.2.3 Non-canonical TGF-β signaling

Non-canonical, non-Smad signaling pathways that are activated by TGF-β receptors have emerged. These include the mitogen-activated protein kinases (MAPKs), tumor necrosis factor (TNF) receptor-associated factor 4/6 (TRAF4/6), phosphatidylinositide 3-kinase (PI3K), and Rho family small GTPases as summarized in Figure 3.5B (Zhang, 2009). Activated MAPKs can exert transcriptional control through direct interaction with the nuclear Smad transcriptional complex or other downstream proteins. Activated MAPKs, Jun N-terminal kinase (JNK), p38, and extracellular signal regulated kinases (ERK), can act with the Smads to regulate cellular apoptosis and proliferation, or metastasis, angiogenesis, and cellular growth factors when acting through

other transcription factors, such as c-JUN and ATF. The RhoA-ROCK pathway can be activated to induce stress fiber formation non-transcriptionally. TGF-β can activate the RING E3 ligase tumor necrosis factor receptor-associated factor (TRAF) proteins to initiation nuclear factor-κB (NF-κB) signaling, which leads to the inflammatory response among other cellular processes.

TGF-β can activate the PI3K/AKT pathway through several direct and indirect posttranslational mechanisms. Most directly, the binding of TGF-β1 to TβRI triggers the recruitment of PI3K and the ubiquitin ligase TRAF6. TRAF6 then polyubiquitylates the PI3K's p85a regulatory subunit, thus enabling the phosphorylation of the PI3K p110 catalytic subunit, although only in the presence of Smad7 (Hamidi et al., 2017). Overexpression of Smad7 potently induces PI3K activity (Yi et al., 2005). TGF-β can activate PI3K indirectly by inducing the expression of secreted growth factors and several inhibitory microRNAs (miRNAs). TGF-β can induce expression of miRNA 216a and 217 (miR216a/217), which are negative regulators of PI3K inhibitors Smad7 and PTEN, thus alleviating their inhibitory suppression of PI3K.

3.2.4 TGF-β in CKD

TGF-β is key mediator of the development of CKD due to its role in renal fibrosis. TGF-β, however, has the dual purpose of being an anti-inflammatory cytokine that also negatively regulates renal inflammation. TGF-β governs several key pathological events during the development of CKD, including excessive ECM deposition in the glomeruli and tubulointerstitium, fibroblast proliferation, and glomerular and tubular epithelial-to-mesenchymal transition (EMT) (Fan et al., 1999).

3.2.5 Smad knockout models in the kidney

As discussed in Section 3.2.2, Smad2 and Smad3 are two key signaling proteins in the canonical TGF-β pathway. Although Smad2 and Smad3 share 92% amino acid homology, the two proteins have been shown to demonstrate nonoverlapped target gene binding specificity, and thus differential transcriptional activity (Brown et al., 2007; Liu et al., 2016). This effect is clearly demonstrated in the context of renal fibrosis, where Smad3 is pathogenic while Smad2 is renoprotective. Smad3 is induces excessive ECM deposition by directly binding the promoter region of collagen-producing genes and tissue inhibitor of matrix metalloproteinases (TIMP) (Hall et al., 2003). Enhancement of TIMP expression thus causes a reduction in ECM turnover by inhibition of matrix metalloproteinase (MMP) activity. In contrast, it is hypothesized that Smad2 binds to Smad3 to competitively inhibit Smad3 activation (Lan et al., 2012). In the presence of profibrotic factors (e.g. advanced glycation end-products, angiotensin II) Smad3-mediated ECM deposition is enhanced by loss of Smad2 (Chung et al., 2010; Wang et al., 2006).

Study of Smad2 is limited in part by the fact that Smad2 knockout in mice is embryonic lethal (Ju et al.,

2006). Smad2 knockout in mice causes a failure of primitive streak formation and in germ layer patterning during embryotic development (Waldrip et al., 1998; Tremblay et al., 2000). In contrast, Smad3 knockout mice are viable and can produce offspring (Zhu et al., 1998; Datto et al., 1999). Conditional deletion of Smad2 in tubule epithelial cells accelerates renal fibrosis in a mouse model of unilateral ureteral obstruction (UUO), suggesting that Smad2 has a renoprotective role (Meng et al., 2010). In comparison to wild-type diabetic mice, diabetic Smad2 knockout mice demonstrated reduced expression of fibrotic markers Snail1, E-cadherin, and MMP2, as well as myofibroblast marker α-smooth muscle actin. Contrarily, however, Smad2 knockout in renal tubule epithelial, endothelial, and interstitial cells has been reported to reduce fibrosis and EMT in a murine streptozotocin (STZ)-induced diabetic nephropathy (Loeffler et al., 2018). This discrepancy may have arisen due to subtle differences in the disease models between the two studies. UUO is a tubular injury model caused by the obstruction of urine flow that leads to tubular injury, whereas in the latter study renal injury occurs secondarily to hyperglycemia (Martínez-Klimova et al., 2019). Closer analysis also reveals that only renal tubule epithelial cells were affected by the Smad2 deletion in the UUO model, whereas numerous cell types were affected in the STZ-induced diabetic nephropathy model. These studies illuminate the highly context-dependent nature of Smad signaling dynamics in the kidney.

CHAPTER 4

Inhibition of TGF-β improves primary renal tubule cell differentiation in long-term culture

Text adapted from:

Hunter K, Larsen JA, Love HD, Evans RC, Roy S, Zent R, Harris R, Wilson MH, Fissell WH. Inhibition of TGF-β improves primary renal tubule cell differentiation in long-term culture. Tissue Engineering Part A. 2022; *with permission from Mary Ann Liebert, Inc.*

Chapter abstract

Patient-oriented applications of cell culture include cell therapy of organ failure like chronic renal failure. Clinical deployment of a cell-based device for artificial renal replacement requires qualitative and quantitative fidelity of a cultured cell to its in vivo counterpart. Active specific apicobasal ion transport reabsorbs 90–99% of the filtered load of salt and water in the kidney. In a bioengineered kidney, tubular transport concentrates wastes and eliminates the need for hemodialysis, but renal tubule cells in culture transport little or no salt and water due to dedifferentiation that mammalian cells undergo in vitro thereby losing important cell-type specific functions. We previously identified transforming growth factor-β as a signaling pathway necessary for in vitro differentiation of renal tubule cells. Inhibition of TGF-β receptor-1 led to active and inhibitable electrolyte and water transport by primary human renal tubule epithelial cells in vitro. Addition of metformin increased transport, in the context of a transient effect on 5'-AMP-activated kinase phosphorylation. These data motivated us to examine whether increased transport was an idiosyncratic effect of SB431542, probe pathways downstream of TGF-β receptors possibly responsible for the improved differentiation, evaluate whether TGF-β inhibition induced a range of differentiated tubule functions, and to explore crosstalk between the effects of SB431542 and metformin. Herein, we use multiple small-molecule inhibitors of canonical and noncanonical pathways to confirm that inhibition of canonical TGF-β signaling caused the increased apicobasal transport. Hallmarks of proximal tubule cell function including sodium reabsorption, para-amino hippurate excretion, and glucose uptake all increased with TGF-β inhibition, and the specificity of the response was shown using inhibitors of each transport protein. We did not find any evidence of crosstalk between metformin and SB431542. These data suggest that the TGF-β signaling pathway governs multiple features of differentiation in renal proximal tubule cells in vitro. Inhibition of TGF-β by pharmacologic or genome engineering approaches may be a viable approach to enhancing differentiated function of tubule cells in vitro.

4.1 Impact statement

Cell therapy of renal failure requires qualitative and quantitative fidelity between in vitro and in vivo phenotypes, which has been elusive. We show that control of TGF-β signaling can promote differentiation of renal tubule cells grown in artificial environments. This is a key enabling step for cell therapy of renal failure.

4.2 Introduction

Cell and tissue culture holds great promise for medicine far beyond its origin in viral culture. Our area of interest, artificial and biohybrid vital organs, is vitally dependent on the function of cultured cells. Unfortunately, progress has been hampered by the dedifferentiation of epithelial cells in ex vivo culture, a phenomenon described as cell culture stress. In the body, renal tubule epithelial cells are essential for homeostasis of fluid volume, electrolyte concentrations, endogenous organic solutes, and xenobiotics. Renal proximal tubule cells selectively and actively transport solutes bidirectionally between luminal filtrate and basolateral capillaries. Tubule cells cultured in laboratory conditions rapidly lose transporter expression, apical brush border microvilli, and revert to glycolytic energy generation. The importance of the renal proximal tubule in removal of protein-bound uremic toxins (PBUTs), reabsorption or excretion of drugs, and as an important site of dose-limiting toxicity for new molecular entities has led to a variety of efforts to improve the fidelity of in vitrocell culture to the in vivo counterpart. Our group has been working to develop cells and culture techniques that will allow a bioreactor of epithelial cells to perform concentration and excretion functions in an artificial kidney (Ferrell et al., 2018, 2010, 2012; Fissell, 2006; Jayagopal et al., 2019; Love et al., 2019, 2020; Wilson et al., 2020). We showed that cultured renal tubule cells exposed to an inhibitor of TGF-β signaling in combination with metformin increased transporter expression and inhibitable apicobasal transport (Love et al., 2020). That work was encouraging as it showed that tubule cells could be induced to transport salt water in vitro. We wanted to gain further insight into the mechanisms and effects of TGF-β inhibition. Proximal tubule cells primarily reabsorb salt via the sodium-proton exchanger 3 (NHE3) and also reabsorb glucose via the sodium-glucose cotransporter 2 (SGLT2). The proximal tubule excretes organic anions, including uremic toxins, through basolateral organic anion transporters.

TGF-β is representative of a superfamily of cytokines involved in regulation of cell proliferation and apoptosis across multiple organs, including the kidney 9. Ligand binding to the TGF-β receptor 2, a transmembrane serine-threonine kinase, phosphorylates TGF-β receptor 1 (TGF-βR1), triggering a series of downstream events that are grouped into "canonical" pathways involving phosphorylation of receptor-regulated Smads, and a wide range of "non-canonical" pathways. The end consequences of TGF-β signaling are both tissue and context-specific. In order to confirm that the effect of SB431542 on apicobasal transport was indeed due to TGF-R1 inhibition rather than an idiosyncratic off-target of SB431542, we tested two inhibitors

of TGF-βR1, also known as Activin-like Kinase 5 (ALK5), SB431542 and A8301. In order to evaluate whether canonical (SMAD) or non-canonical effects of TGF-β inhibition underlie the differentiation response we previously observed (Love et al., 2020), we subsequently tested an inhibitor of SMAD3 and inhibitors of phosphoinositide-3 kinase, the mammalian target of rapamycin, p38 mitogen-activated protein kinase MAPK, and TGF-β activated kinase 1. We assessed two other functions of tubule cells, glucose uptake and organic anion excretion, to test whether the effects of TGF-β inhibition were limited to sodium transport or included additional measures of proximal tubule function. Finally, as the beneficial effect of metformin was unanticipated, we examined whether SB431542 also affected an effect of metformin AMPK phosphorylation. Conversely, we tested whether metformin affected canonical TGF-β signaling by measuring the effect of metformin on SMAD phosphorylation.

In this work, we show that canonical TGF-β inhibition is necessary and sufficient for renal proximal tubule cells to actively transport fluid volume, reabsorb glucose and excrete organic anions in vitro. Thus, we demonstrate that there may be comparatively simple approaches to fostering differentiation of tubule cells on conventional cell culture substrates that are commercially available, simple to handle, and integrate well with microscopy and cell culture tools.

4.3 Results

The following section focuses on results presented. Section 4.3.1 focuses on the role of TGF-β in regulating volume transport, Section 4.3.2 provides the results on the effects of TGF-β inhibition on glucose reabsorption, and Section 4.3.3 details the effect of TGF-β on organic ion excretion. Finally, Section 4.3.4 closes on the role of metformin in these processes.

4.3.1 Volume transport

Sodium reabsorption is an essential function of the renal tubule cell. We previously showed that treatment of renal tubule cells with SB431542, a TGF-β receptor 1 inhibitor, increased apicobasal transport. We wished to determine if this was related to changes in gene expression of the predominant apical sodium-proton exchanger of the proximal tubule, NHE3. Further, we also examined whether the increased transport was an idiosyncratic response to SB431542 or was mediated by inhibition of TGF-β R1/ALK5 by other agents as well. We therefore tested a different TGF-β inhibitor, A8301, or SIS3, an inhibitor of the canonical TGF-β pathway protein Smad3. Cells expressed claudin-2 mRNA at a 1570 ± 350 -fold higher level than claudin-7. Cells also expressed mRNA for aquaporin-1 and megalin. Together, along with high-level expression of NHE3, OAT1, and SGLT2, these expression profiles suggest that the isolates we used were primarily proximal tubule cells. Cells grew to confluence in 10 days to 2 weeks. Cells formed confluent monolayers as measured by

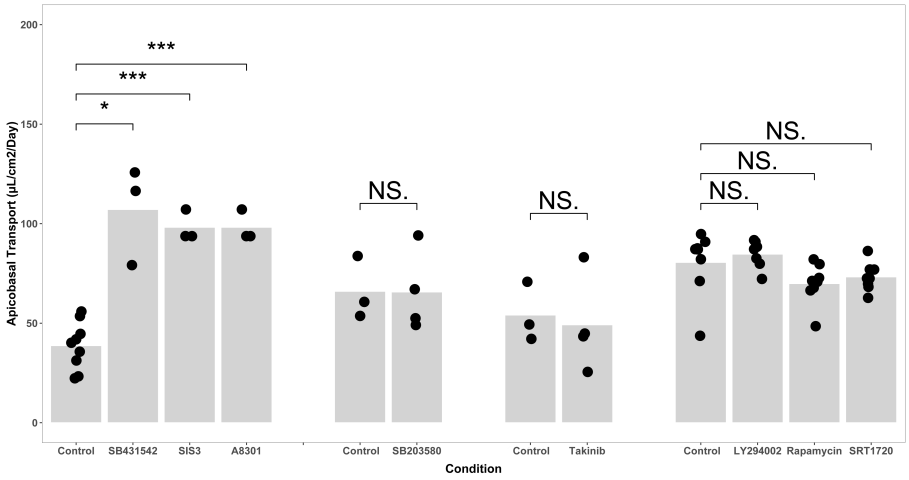

Figure 4.1: **Inhibition of canonical TGF-β signaling increases fluid transport by renal tubule cells in culture.** The results of four separate experiments are depicted in four groups above as the absolute transport values in the control groups vary from isolate to isolate. Primary renal tubule cells increased their fluid transport when either of two inhibitors of the TGF-βreceptor or an inhibitor of Smad3 phosphorylation were added to media (left, * : $p < 0.05$, ***: $p < 0.0001$ by Welch's t-test). There were no significant differences in transport between cells cultured with inhibitors of non-canonical TGF-β and cells cultured in control media, which is 50:50 DMEM:F12 with hydrocortisone, triiodothyronine, ascorbic acid, insulin, transferrin, and selenium, with 5% fetal bovine serum in the basolateral media only (rightmost three groups). Data points indicate the number of biological replicates for each condition.

TRITC-conjugated dextran concentrations in the basolateral compartment less than two percent of apical concentrations after 24 hours. We compared apicobasal fluid volume transport (μL/cm2/day) as the indicator of phenotype between control cells, cells treated with the TGF-βR1 inhibitor SB432542, the TGF-βR1 inhibitor A8301, or with an inhibitor of Smad3 phosphorylation, SIS3 (Figure 4.1). Cells cultured with SB431542 (107.1 $\pm$ 14.2 vs 38.8 $\pm$ 11.9, p = 0.033), or SIS3 (98.2 $\pm$ 4.5 vs 38.8 $\pm$ 11.9; $p < 0.0001$). or A8301 (98.2 $\pm$ 4.5 vs 38.8 $\pm$ 11.9; $p < 0.0001$; Figure 4.1 for all), all transported more fluid than corresponding control cells. We further probed TGF-β signaling by measuring transport in primary renal tubule cells incubated with inhibitors of non-canonical TGF-β signaling, LY294002 (1μM, inhibitor of phosphoinositide 3-kinase), rapamycin (40nM, inhibitor ofthe mammalian target of rapamycin, or mTOR), SB203580 (1μM, inhibitor of p38 mitogen-activated protein kinase or p38 MAPK), and takinib (2nM, inhibitor of TGF-β activated kinase 1 or TAK1). Cells retained barrier function as measured by inulin leak rates, but none of the non-canonical pathway inhibitors increased transport (Figure 4.1). These data confirm that indeed canonical TGF-β signaling mediates the change in phenotype we observe.

We previously observed that metformin-induced AMPK activation enhances the effects of SB431542 in vitro (Love et al., 2020). To develop insight regarding the mechanisms of increased transport, we compared NHE3 expression between control cells and cells incubated with a combination of metformin and SB431542

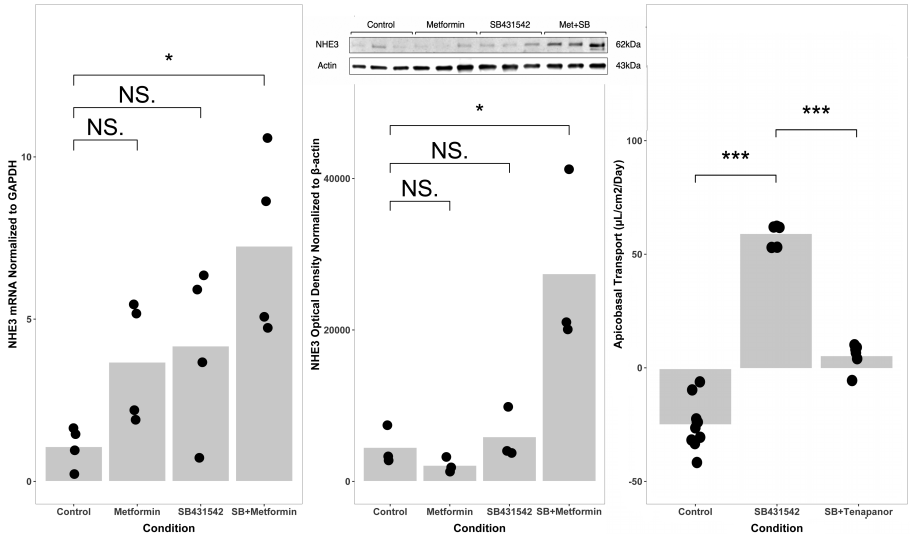

Figure 4.2: **TGF-β inhibition increases NHE3-mediated apicobasal active transport.** The results of four separate experiments are depicted in four groups above as the absolute transport values in the control groups vary from isolate to isolate. Primary renal tubule cells increased their fluid transport when either of two inhibitors of the TGF-β receptor or an inhibitor of Smad3 phosphorylation were added to media (left, * :$p < 0.05$, ***: $p < 0.0001$ by Welch's t-test). There were no significant differences in transport between cells cultured with inhibitors of non-canonical TGF-β and cells cultured in control media, which is 50:50 DMEM:F12 with hydrocortisone, triiodothyronine, ascorbic acid, insulin, transferrin, and selenium, with 5% fetal bovine serum in the basolateral media only (rightmost three groups). Data points indicate the number of biological replicates for each condition.

("M+SB") at the mRNA and protein level. While SB431542 alone did not significantly change NHE3 mRNA or protein expression, cells cultured with M+SB expressed NHE3 mRNA at a 3.8-fold higher level compared to control (p = 0.027, Figure 4.2), and expressed NHE3 protein by western blot at an approximately six-fold higher level than cells grown in control media (p = 0.032, Figure 4.2). We compared apicobasal transport between renal proximal tubule cells grown in control media, media with added M+SB, and media with M+SB and the NHE3 inhibitor, tenapanor (Markham, 2019). TGF-β bockade by SB431542 increased apicobasal transport (-24.8 $\pm$ 10.7 μL/cm2/day vs to 59.5 $\pm$ 4.6 μL/cm2/day ; $p < 0.001$, Figure 4.2) and transport was reduced to 5.7 $\pm$ 5.7 μ L/cm2/day by addition of tenapanor to the media ($p < 0.001$, Figure 4.2). NHE3 reabsorbs sodium by exchanging one sodium ion for one proton, so we were curious whether the proximal tubule cells altered the acidity of the apical media. Indeed, SB431542-treated cells acidified the apical media (pH 7.13 vs pH 7.45, p = 0.010). These data show that the effect of TGF-β inhibition on transport in proximal tubule cells is specifically mediated by expression and activity of NHE3.

4.3.2 Glucose reabsorption

We wanted to further examine the phenotypic effects of TGF-β inhibition, testing whether other features of proximal tubule cells were enhanced in vitro by blockade of the TGF-β pathway. Proximal tubule cells reabsorb filtered glucose from the glomerular filtrate through the apical sodium-glucose cotransporter SGLT2. We compared SGLT2 expression between inhibitor and control media and measured whether tubule cells in culture depleted glucose from the apical, basolateral, or both compartments. Finally, we used an inhibitor of sodium-glucose cotransport, phlorizin, to confirm that the effect we observed was specifically mediated by the SGLT2 transporter. Sodium-glucose cotransporter 2 (SGLT2) mRNA was expressed at a 2.3 fold higher level in cells cultured with the TGF-β inhibitor A8301 (p = 0.042, Figure 4.3), and SGLT2 protein was higher by western blot (p = 0.037, Figure 4.3). Cells cultured continuously for 42 weeks with the TGF-β inhibitor SB431542 reabsorbed glucose from apical media more than did control cells (apicobasal glucose concentration gradient after 24 hour incubation: -126 $\pm$ 63 μg/mL vs -352 $\pm$ 66 μg/mL; p =0.012), and addition of the SGLT inhibitor phlorizin in a second series of experiments at 47 weeks in culture prevented the reabsorption (-352 $\pm$ 66 μg/mL vs 77 $\pm$ 59 μg/mL p = 0.001, Figure 4.3). The observation that active, specifically inhibitable glucose transport is increased by TGF-β inhibition supports the hypothesis that the effects of TGF-β inhibition are more widespread than NHE3-mediated sodium transport alone.

4.3.3 Organic ion excretion

Proximal tubule cells contribute to excretion of endogenous and xenobiotic compounds from blood through high affinity active transporters indirectly coupled to sodium gradients. Proximal tubule cells in conventional culture do not express organic anion transporters such as OAT1, so we examined whether OAT1 expression and organic anion excretion changed with TGF-β inhibition. OAT1 expression by PCR showed no trend toward increased expression with addition of SB431542. OAT1 expression by western blot, however, was significantly different between control and TGF-β inhibited cells (p = 0.0031 SB431542 vs control, Figure 4.4). To examine function, we chose a classic OAT substrate widely used in renal physiology, para-amino hippurate (PAH) as an indicator of functional phenotype. We also evaluated a pharmacologic inhibitor of organic anion transport, the drug probenecid, to test the specificity of the response. Primary renal tubule cells cultured with SB431542 for 42 weeks transported PAH from basolateral to apical compartments, whereas control cells did not (apicobasal PAH gradient 493 $\pm$ 96 μg/mL in SB431542-treated wells vs -8.5 $\pm$ 7.7 μg/mL in control wells, p = 0.00086). PAH transport was inhibited by the addition of probenecid to media (apicobasal PAH gradient 493 $\pm$ 96 μg/mL in SB431542-treated wells vs 125 $\pm$ 35 μg/mL in SB431542 + probenecid wells, p = 0.0034). As with glucose transport, TGF-β inhibition increased organic anion transporter expression and specifically inhibitable active transport. confirming the specificity of the response to organic anion transport pathways.

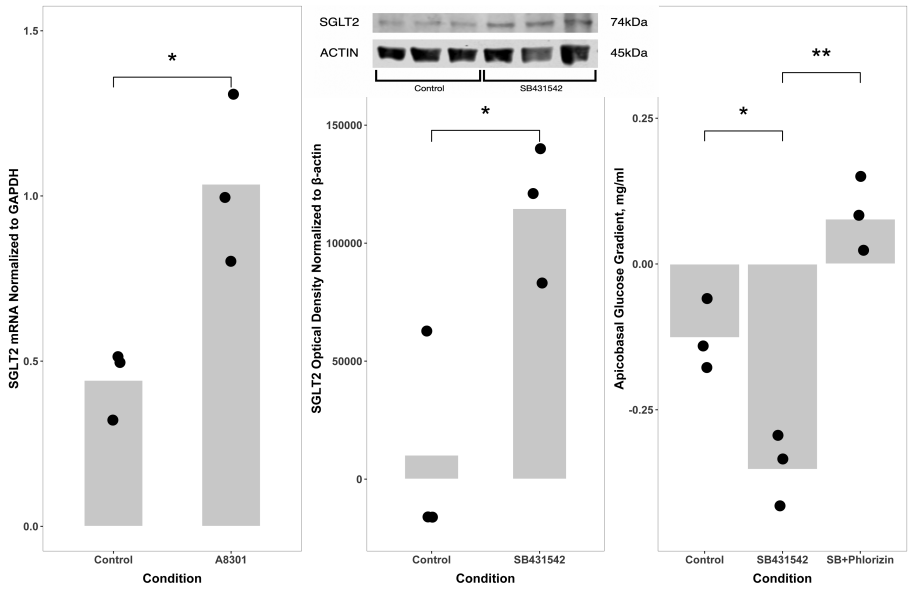

Figure 4.3: **TGF-β inhibition increases glucose reabsorption by renal proximal tubule cells in vitro.** Messenger RNA for the sodium-glucose cotransporter 2 (SGLT2) was expressed at a 2.3 fold higher level in cells cultured with A8301, a TGF-β receptor inhibitor, than in control cells (left panel; *, p = 0.042). SGLT2 protein expression by western blot (insert, middle panel) revealed that cells cultured with SB431542, a TGF-βR1 inhibitor, expressed SGLT2 at a higher level than cells cultured in control media (50:50 DMEM:F12 with hydrocortisone, triiodothyronine, ascorbic acid, insulin, transferrin, and selenium, with 5% fetal bovine serum in the basolateral media only) (middle panel; *: $p < 0.05$). Glucose concentrations in apical and basolateral media were measured 24 hours after a media change. Cells cultured with the TGF-βinhibitor SB431542 reabsorbed glucose from apical media more than did control cells (apicobasal glucose concentration gradient after 24 hour incubation: -352 $\pm$ 66 μg/mL vs -126 $\pm$ 63 μg/mL;*: p ¡ 0.05), and addition of the SGLT inhibitor phlorizin prevented the reabsorption (-352 $\pm$ 66 μg/mL vs 77 $\pm$ 59 μg/mL, **:$p < 0.01$). Data points indicate the number of biological replicates for each condition.

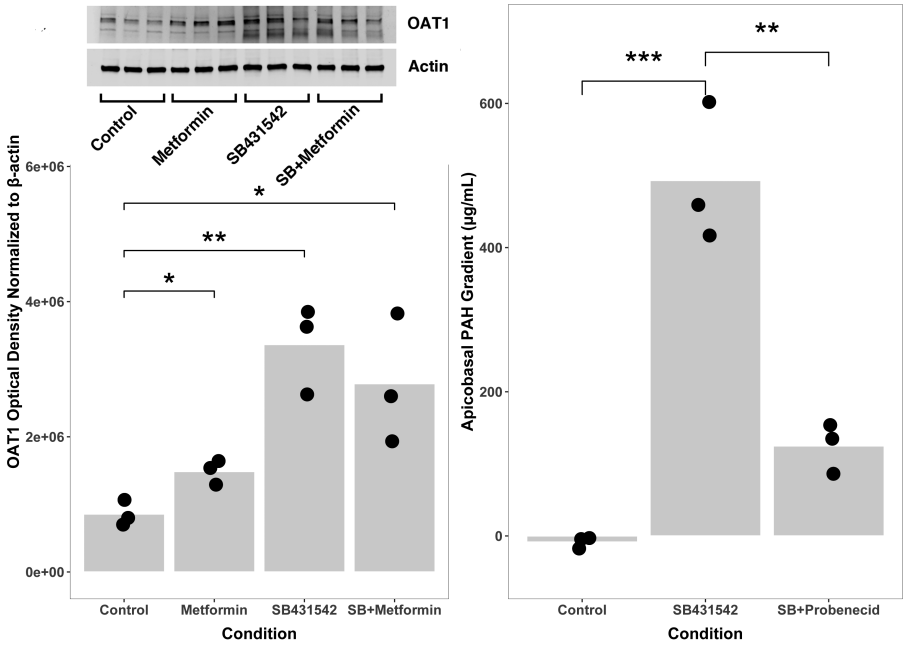

Figure 4.4: **TGF-β inhibition increases OAT1 expression and function in primary renal tubule cells.** Cells cultured with metformin, SB431542, a TGF-βinhibitor, or both, expressed OAT1 protein as measured by by western blot (left panel inset) more than cells cultured in control media (50:50 DMEM:F12 with hydrocortisone, triiodothyronine, ascorbic acid, insulin, transferrin, and selenium, with 5% fetal bovine serum in the basolateral media only)(left panel, *: < 0.05; ** $p < 0.01$). Cells cultured with SB431542 transported PAH from basolateralto apical compartments, whereas control cells did not (apicobasal PAH gradient 493 $\pm$ 96 μg/mL in SB431542-treated wells vs -8.5 $\pm$ 7.7 μg/mL in control wells, *** $p < 0.001$, right panel). PAH transport was inhibited by the addition of probenecid to media(apicobasal PAH gradient 493 $\pm$ 96 μg/mL in SB431542-treated wells vs 125 $\pm$ 35 μg/mL in SB431542 + probenecid wells, **: $p < 0.01$, right panel). Data points indicate the number of biological replicates for each condition.

4.3.4 Role of metformin

In our prior work, we noticed that metformin independently and additively increased active fluid transport by primary human cortical thick ascending limb cells (Love et al., 2020). The additive effect of the biguanide hypoglycemic agent metformin on differentiation is incompletely understood. Metformin has a mitochondrial role inhibiting Complex I, which at least transiently reduces ATP generation. Decreased ATP/ADP ratio allosterically alters AMP-activated protein kinase (AMPK) to permit liver kinase B1 (LKB1), the predominant kinase responsible for AMPK phosphorylation, to phosphorylate AMPK. Several groups have reported the influence of metformin on canonical TGF-β signaling, so we probed metformin's effects on TGF-β in these cells by comparing Smad2 phosphorylation in cells with and without metformin (Li et al., 2016; Wahdan-Alaswad et al., 2016). We confirmed that metformin increased AMPK phosphorylation as predicted, while TGF-β inhibition had no effect on AMPK phosphorylation (Figure 4.5). We found that for renal proximal tubule cells in vitro, metformin did not significantly affect a measure of canonical TGF-β signaling, Smad2 phosphorylation (Figure 4.5). These data suggest that direct crosstalk between canonical TGF-β signaling and metformin's impact on AMPK do not explain the additive effects we observed.

4.4 Discussion

4.4.1 Cell culture stress

To place the current work in context, these data follow on decades of work by multiple teams defining the roles of soluble factors, genetic manipulations, and the physical microenvironment in the etiology of cell culture stress. Primary cultures of cortical epithelial cells derived from transplant discards maintain ammoniagenesis, Vitamin D hydroxylation, and glucose transport when cultured under flow in the lumens of hollow-fiber bioreactors (Humes et al., 1999). Culturing tubule cells on an orbital shaker improves aerobic metabolism and gluconeogenesis compared to static culture (Nowak and Schnellmann, 1995; Park et al., 2020; Ren et al., 2019; Long et al., 2017). In two-dimensional culture, albumin uptake by primary renal tubule cells increased with addition of apical fluid shear stress (Ferrell et al., 2010, 2012; Long et al., 2017). Indeed, fluid shear stress affects multiple differentiation pathways, including some involved in non-canonical TGF-βsignaling (Park et al., 2020; Ren et al., 2019; Long et al., 2017). Pharmacologic and genomic interventions can improve differentiation. Small molecule beta-adrenergic stimulation increases mitochondrial number, morphology, and oxygen consumption of cultured proximal tubule cells (Wills et al., 2012). A conditionally immortalized renal tubule cell line (ciPTEC) created with temperature-sensitive SV40 large antigen could support genetic overexpression of organic anion transporters (OATs) (Nieskens et al., 2016). Such cells showed greater sensitivity to nephrotoxins and increased excretion of classic PBUTs compared to cells without overexpression of OATs. Co-culture of tubule cells with endothelial cells in a 3D-printed convoluted channel seeded with

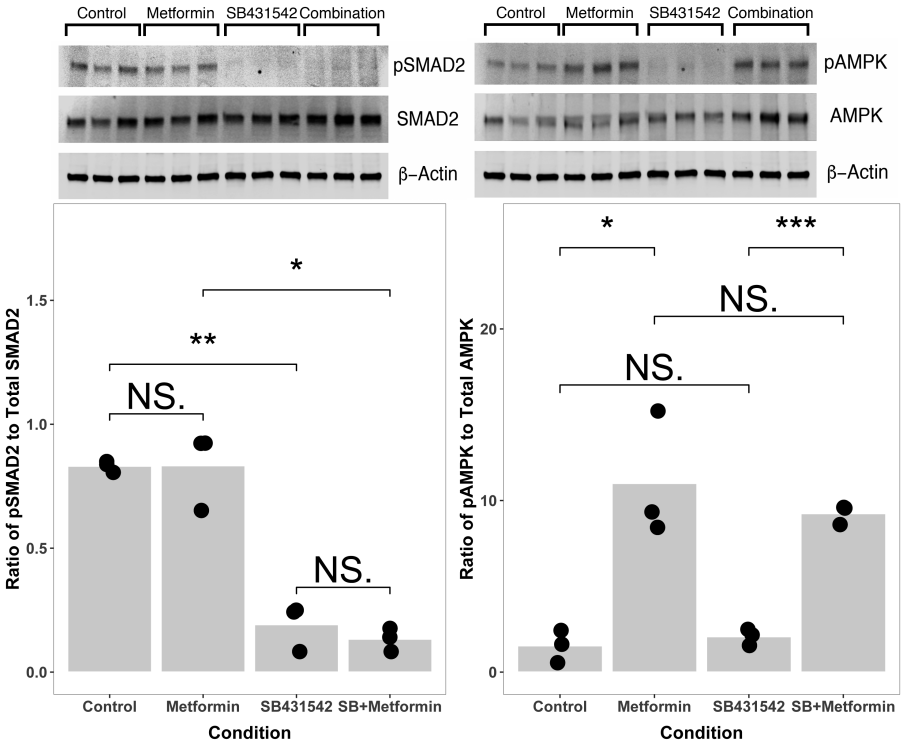

Figure 4.5: **Metformin does not increase Smad2 phosphorylation in primary renal tubule cells, and SB431542 does not alter APMK phosphorylation.** An inhibitor of TGF-β signaling SB43152 alone or in combination with metformin decreased Smad2 phosphorylation (left panel, *: $p < 0.05$;**: $p < 0.01$), but metformin alone does not significantly decrease Smad2 phosphorylation (left panel). Metformin alone or in combination with SB431542 increases AMPK phosphorylation (right panel, *: $p < 0.05$; ***: $p< 0.001$) but SB431542 alone has no effect on AMPK phosphorylation. The apparent additive effect of metformin and TGF-β inhibition may be attributable to independent signaling events rather than crosstalk between the two pathways. Data points indicate the number of biological replicates for each condition.

commercially available TERT-immortalized proximal tubule cells yielded a cuboidal epithelium with a brush border, that reabsorbed glucose and albumin fromapical perfusate (Homan et al., 2016; Lin et al., 2019), yet cadaver-derived tubule cells seeded on porcine small intestine submucosa also formed a cuboidal epithelium with a mature brush border, strongly suggesting that three-dimensional culture was not essential to tubule cell differentiation (Hoppensack et al., 2014).

4.4.2 TGF-β and tubule cell function

The influence of TGF-β signaling on tubule cell differentiated function has been extensively studied. TGF-β signaling seems to be implicated in decisions between recovery as function versus recovery as fibrosis, and inhibition improved recovery in animal models of renal failure (Geng et al., 2009; Lan et al., 2012). Deletion of TGF-β receptor attenuated acute kidney injury in a mouse model, but was separately seen to worsen CKD (Geng et al., 2009; Lan et al., 2012; Gewin and Zent, 2012; Khodo et al., 2016; Nlandu-Khodo et al., 2017). In previous studies, we found that primary renal tubule cells on conventional porous substrates exhibited diuretic-inhibitable apicobasal transport when cultured with SB431542, a small molecule inhibitor of TGFR1 (Love et al., 2020). We wanted to identify the pathways through which TGF-β was acting and learn whether TGF-β inhibition in vitro allowed renal tubule cells on conventional culture materials to display differentiated features in addition to fluid transport. TGF-β appeared to increased transporter function through transcriptional upregulation of transporter abundance for SGLT2 and possibly OAT1, but SB431542 alone did not appear to affect NHE3 mRNA or protein concentrations, suggesting that the effects of the TGF-β pathway might occur through post-translational effects. One possibility might be that TGF-β activates protein kinase A (PKA) through an interaction of Smad3-Smad4 complex and the regulatory subunit of PKA. PKA activation phosphorylates/inhibits NHE3 and acts as a signal for NHE3 endocytosis (Honegger et al., 2006).

We reinforced our conclusion that TGF-β signaling was causally related to the differentiation we observed, as multiple inhibitors of canonical TGF-β signaling reproduced the phenotype of increased transport. The role of metformin remains intriguing, as it affects transcription levels, but there was no evidence of increased Smad2 phosphorylation when metformin was added to media. AMPK is a pleiotropic enzyme that appears to regulate a variety of energy-consuming and energy-generating processes in mammalian cells (Banko et al., 2011). AMPK activation in renal tubule cells is thought to be in the causal pathway of ischemic preconditioning through mTORC1 and the PI3/Akt pathway, reducing apoptosis of tubule cells with subsequent ischemia (Lieberthal et al., 2019). Conversely, AMPK activation by metformin in tubule cells with mutations in tuberous sclerosis complex gene TSC1 was associated with mitigation of the pathologic phenotype via increased apoptosis (Fang et al., 2020). Together, these examples of metformin's interactions with renal tubule cells highlight that AMPK's role in these cells is highly tissue-and context-dependent.

4.4.3 Comparison of in vitro transport versus in vivo transport

TGF-β inhibition in vitro led to the appearance of functions characteristic of the in vivo renal tubule cell, including diuretic-inhibitable fluid transport, phlorizin-inhibitable glucose uptake, probenecid-inhibitable organic anion excretion, and apical acid extrusion. It is worth asking whether the magnitude of these desired phenotypes agrees to any extent with in vivo function. This is a vexing question as most in vivo or immediately ex vivo studies were performed decades ago and sometimes report results in different units and contexts than our work here. Our transport measurements in cells treated with TGF-β inhibitors correspond to about 12 μmol/cm^2/day sodium transport. How does that compare to in vivo sodium transport? Giebish conducted numerous micropuncture studies of the rat proximal tubule, and measured transport ranging from 400-700 pmol/min/mm tubule (Chang et al., 2013). Using electron microscope images to estimate tubule diameter and luminal area, Giebish's measurements in the rat proximal tubule extrapolate to 35-60 μmol/cm^2/day. That we observe sodium transport within the same order of magnitude as in vivo transport is striking, especially as in vitro, our cells were not stimulated with large apicobasal oncotic gradients, catecholamines, or angiotensin, and cells were not perfused with free fatty acids, the preferred energy source for proximal tubule cells in vivo.

We measured total extraction of glucose from apical media to be 3.2 μg/mm2/day, less than the approximately 10 μg/mm^2/day Lewis measured in renal tubule cells continuously perfused with media in 3D culture, but much more than the 0.5 μg/mm^2/day Lewis reported for tubule cells grown on Transwells similar to ours (Homan et al., 2016). Some of this apparent difference may be attributable to the decrease in apical glucose concentration over the 24-hour observation window. In our experiments, media was exchanged every 48-72 hours, over which time the apical media glucose concentration decreased, whereas Lewis continuously perfused cells at a constant glucose concentration. The starting concentration of glucose in our media was 5 mmol/L or 900 μg/mL, and the end concentration averaged 171 μg/ml or 943 μmol/L, closer to the reported Michaelis constant (Km) of 500 μmol/L for SGLT2 (Chang et al., 2013). This suggests that the glucose transport we observed might have submaximal due to substrate concentration.

Our goal is to develop differentiated renal tubule cells for use in an artificial kidney. A major barrier to progress has been the generally accepted observation that primary renal tubule cells undergo significant dedifferentiation and may not survive in conventional artificial culture. Modulation of the TGF-β signaling pathway is sufficient to enhance differentiation in renal proximal tubule cells subject to the stresses of artificial culture. It is indeed possible for cells to perform multiple specific differentiated functions characteristic of a healthy proximal tubule cell even at over 40 weeks in culture. Collectively, our work suggests that renal proximal tubule cells cultured under similar circumstances will be able to perform key functions for an implantable artificial kidney. There remain significant challenges between this work and a practical

clinical device. Primary among these challenges is the mass of cells required for clinical effect. Humes developed protocols that, depending on donor age, led to greatly expanded number of cells from donor tissue(Westover et al., 2012). Conditional reprogramming of epithelial cells using feeder fibroblasts and rho-kinase inhibitors may provide a pathway for cell mass production without the need for potentially oncogenic immortalization(Palechor-Ceron et al., 2019). Finally, in the future, biohybrid devices may provide an early clinical opportunity for organoid-derived cells(Freedman, 2022; Dorison et al., 2022).

4.4.4 Bridging the in vitro-in vivo gap

We find that the dedifferentiation typically observed with cell culture is not intrinsic to the in vitro environment. Indeed, the uses to which cell culture has been put over the past seven decades have not previously asked that cells in culture bear quantitative fidelity to their in vivo counterparts. We seek to bridge the gap between the natural niche and the petri plate without resorting to the intricacies of 3-D culture systems, precisely because our biologic research and manufacturing infrastructures are geared to flat-sheet conditions. In this chapter we have shown that control of specific signal transduction pathways is sufficient to reverse the erosion of at least some of the functional phenotypes associated with cell culture in conventional flat inelastic scaffolds for extended periods of time. This is an important enabling discovery for regenerative medicine and tissue engineering.

4.5 Materials and Methods

Hereafter, we provide further details regarding materials and methods used in this chapter. Section 4.5.1 focuses on cell culture, Section 4.5.2 focuses on transport measurement while Section 4.5.3 focuses on RNA isolation and real-time PCR and 4.5.4 deals with western blotting. Section 4.5.5 details liquid chromatography and Section 4.5.6 deals with glocuse measurement. Finally, Section 4.5.7 provides further information regarding statistical analysis performed.

4.5.1 Cell Culture

Primary human renal tubule cells were purchased from Lonza (Cat CC-2553, Basel, Switzerland) or Innovative Biotherapies (Ann Arbor, MI). Cells were used up to 4th passage. Cells were seeded onto 1.12 cm^2 permeable supports (Transwell, Corning, Oneonta, NewYork). Expression of claudin-2, claudin-7, aquaporin-1, and megalin was measured by PCR to confirm proximal tubule origin of the primary cells.All other materials were purchased from Sigma (St.Louis, MO) unless otherwise indicated. Cells were cultured in 50:50 DMEM:F12 with hydrocortisone, triiodothyronine, ascorbic acid, insulin,transferrin, and selenium, with 5% fetal bovine serum in the basolateral media only. Small molecule inhibitors of TGF-β inhibitor type 1 (SB431542, 10μM,

A8301, 1μM, both from Cayman Chemical, Ann Arbor), SMAD3 (SIS3, 5μM, Cayman Chemical, Ann Arbor), as well as LY294002 (1μM, inhibitor of phosphoinositide 3-kinase, Cayman), rapamycin (40nM, inhibitor of the mammalian target of rapamycin, or mTOR, Cayman), SB203580 (1μM, inhibitor of p38 mitogen-activated protein kinase or p38 MAPK, Cayman), and takinib (2nM, inhibitor of TGF-β activated kinase 1 or TAK1, Cayman), and metformin(200μM, Sigma) were added to cell culture media for the indicated experiments.Texas red isothiocyanate-conjugated dextran (TRITC dextran, 10,000 kD Thermo Fisher #D1868) was added in some experiments to evaluate monolayer confluence. TRITC-Dextran was added to the apical compartment of the cell culture insert to a final concentration of 100 μg/ml. 24 hours later, aliquots of apical and basolateral media were sampled. Fluorescence at 550nm excitation and 571 nm emission was measured to quantify dextran concentrations in apical and basolateral compartments. Cells were grown on a shaker table (73rpm; equivalent average fluid shear stress 2dyne/cm^2) in 95% air 5% CO_2 at 37 degrees Celsius. Media was changed every 72 hours.

4.5.2 Transport Measurement

Primary proximal tubule cells (Lonza) at 19-42 weeks of stable culture with and without SB431542 had media changed to identical media with or without addition of tenapanor (1μM - AdooQ Bioscience LLC). 24 hours later, apical and basolateral media were aspirated and weighed. A blank well with the porous membrane occluded with epoxy was used as an evaporative control. The difference between initial volumes and final volume as estimated by weight, was taken as the transported volume.

4.5.3 RNA Isolation and Real-Time PCR

Total RNA was isolated using the Micro or Mini RNeasy kits (Qiagen, Hilden, Germany). RNA quality was determined by measuring absorbance at 260 nm and 280 nm on a Nanodrop Spectrometer. First-strand cDNA was synthesized from total RNA using the iScript cDNA Synthesis Kit (Bio-Rad, Hercules, CA) according to the manufacturer's instructions. Real-time PCR was performed on triplicate samples using SsoAdvanced Universal SYBR Green Supermix (Bio-Rad) and a Bio-Rad CFX96 Real-Time PCR System. Data were normalized to human GAPDH mRNA levels as an endogenous control. Relative expression (RE) levels are expressed relative to static control using the $\Delta\Delta$Ct formula:

$$\begin{aligned} \text{RE} = 2 - \big[&(\text{Ct(gene, test sample) - Ct(GAPDH, test sample)}) \\ &-(\text{Ct(gene, static sample) - Ct(GAPDH, static sample)})\big], \end{aligned}$$

in which Ct is the threshold cycle number. Bio-Rad CFX Manager Software version 3.1 was used to determine Ct numbers and relative expression levels. PCR primer sequences were from PrimerBank database[1] and oligonucleotides were synthesized by the Vanderbilt University Molecular Biology Core.

4.5.4 Western Blotting

Protein concentration was quantified using Pierce BCA assay (ThermoFisher, Waltham, MA). Samples were prepared at a concentration of 10µg protein per well with 4X protein loading buffer (LICOR, Lincoln, NE) supplemented with 1% DTT (Abcam, Cambridge, UK). Prior to running gels, samples were denatured at 95°C for 5 minutes. Samples were loaded into 4-20% gradient polyacrylamide gels and ran for 35min at 200 volts at room temperature. Gels were then transferred to nitrocellulose membranes via wet transfer for 1 hour at 100 volts at 4°C. Membranes were incubated with primary antibodies (1:500-1:1000) overnight at 4°C, then washed three times for 5 minutes with 1X TBST. Membranes were incubated with secondary antibodies (1:25,000-1:50,000) for 1 hour at room temperature then washed three times for 15 minutes with 1X TBS. Membranes were imaged with an Odyssey XF Imaging System (LICOR). Protein expression was quantified using ImageStudioLite or Empiria Studio (LICOR) and normalized to β-actin using the built-in normalization function in Empiria Studio. Antibodies to phospho-AMPK, phospho-Smad2, total Smad2, and SLGT2 were purchased from Cell Signaling (Danvers, Massachusetts). Antibodies to NHE3 and β-actin were purchased from Santa Cruz Biotechnologies (Dallas, TX). Antibodies to total AMPK were purchased from Invitrogen (Waltham, MA). Antibodies to OAT1 were purchased from ProteinTech (Rosemont, IL).

4.5.5 Liquid Chromatography

Chromatography was performed on an Agilent 1200 series HPLC system. Concentrations were determined using a diode array detector (Agilent G1315C, Santa Clara, CA) at 245nm. An Aeris 3.6μm, 150x4.6 Widepore XB-C18 (Phenomenex) column was used for separation. A phosphate buffer was prepared from (Sodium Phosphate Dibasic Heptahydrate, Fisher Chemical, Ottawa, ON) and (Sodium Phosphate Monohydrate, Fisher Chemical, Ottawa, ON) and adjusted to a pH of 4.1. HPLC grade methanol (Sigma-Aldrich 34860) was added to equal 10% (vol%/vol%) for the mobile phase in an isocratic method. The method had a flow rate of 1 ml/min, injection volume of (15 μL), and a total run time of 8 minutes. Retention time for PAH and acetaminophen were (1.5) and (2.1) respectively. Powdered PAH (Sigma-Aldrich A1422) was used to prepare standards and QC. Acetaminophen (MP Biomedicals, LLC, Solon, OH) was used as the internal standard. Samples were filtered with 30K centrifuge filters (Sartorius, United Kingdom). Standards were prepared at (5, 10, 30, 50, 70, 100 μg/ml (QCS at 20, 60, 80)) levels in 30% methanol and distilled water. The working range

[1] https://pga.mgh.harvard.edu/primerbank/index.html

for the method was 1μg/mL-100μg/mL PAH. Three QC levels per run were prepared directly into cell media.

4.5.6 Glucose Measurement

Fresh cell culture media was added to both apical and basolateral compartments for twenty-four hours. After twenty-four hours, 100 µl of cell culture media from each sample was added to 1mL Glucose Assay Reagent (Glucose (HK) Assay Kit, Sigma) and incubated at room temperature for fifteen minutes. Approximately 2 μl from each sample was then placed on the spectrophotometer (Nanodrop, Thermo Scientific) and absorbance measured at 340nm.

4.5.7 Statistical Analysis

All statistical inference testing was performed on results from prespecified experiments. Differences in means were assessed by Welch's t-test with two tails and assumption of unequal variance using R (The R Foundation for Statistical Computing). Statistical significance was assigned at an alpha threshold of 0.05.

CHAPTER 5

Metformin and TGF-β inhibition direct renal tubule cell metabolism toward increased glycolysis and oxidative phosphorylation

5.1 Introduction

The function of the kidneys is to maintain fluid and electrolyte balance while also eliminating waste from the bloodstream. Blood is filtered in the glomerulus forming an ultrafiltrate consisting of waste, glucose, ions, amino acids, and small proteins, which then enters the renal tubule. Renal proximal tubule epithelial cells (RPTEC) use active transport to reabsorb approximately 65% of the salt and water that is filtered by the glomerulus to concentrate wastes into a small fluid volume (Zhuo and Li, 2013). This is continuous and energy-intensive, making the kidneys the body's second most energy-demanding organ in terms of both mitochondrial content and O_2 consumption. About 95% of ATP in a healthy RPTEC is produced by oxidative phosphorylation (OXPHOS), the oxygen-consuming process that couples ATP synthesis to the movement of electrons through the mitochondrial electron transport chain (ETC)(Soltoff, 1986). Although RPTEC do not preferentially use glucose for energy production, glycolysis aids in RPTEC survival and preservation of transport activity under conditions of oxidative stress and hypoxia (Schaub et al., 2021). In chronic kidney disease (CKD), RPTEC undergo metabolic reprogramming that directs cells towards glycolysis to compensate for impaired OXPHOS due to significant downregulation of oxidative enzymes and upregulation of glycolytic enzymes (Kang et al., 2015; Mutsaers et al., 2015). This effect is mimicked when human renal tubule epithelial cells are cultured in vitro, where cells tend to metabolize glucose using anaerobic glycolysis, rather than OXPHOS despite the presence of oxygen.

Our group has identified Transforming Growth Factor-β (TGF-β) as a key modulator of RPTEC functional phenotype in vitro. Inhibition of TGF-β in cultured RPTEC is sufficient to increase apicobasal fluid transport, glucose uptake, organic anion excretion, and apical acid extrusion. These effects are enhanced with the addition of AMP-activated protein kinase (AMPK) activator metformin (Love et al., 2020; Hunter et al., 2022). TGF-β is a pleiotropic cytokine that plays a critical role in tissue development and homeostasis, fibrosis, and oncogenesis across many tissue types (Li et al., 1999; Matsuki et al., 2015; Meng et al., 2015). Canonical TGF-β signaling is transduced by the Smad proteins, which form a multiprotein complex and translocate to the nucleus to cooperatively activate or repress expression of target genes (Zhang et al., 2015; Morikawa et al., 2013). TGF-β reduces the transcription of Tricarboxylic Acid Cycle (TCA) cycle-related enzymes in numerous cell types (Sohn et al., 2012; Hoffmann et al., 2018; Sarah et al., 2019; Smith et al., 2019; Smith

and Hewitson, 2020). TGF-β induces mitochondrial fractionization in renal tubule epithelial cells (Krick et al., 2008). Metformin is a first-line hypoglycemic drug used for the treatment of type II diabetes mellitus. Metformin inhibits respiratory complex I of the mitochondrial ETC, resulting in mild leakage of electrons before the formation of ATP, causing a decrease in cellular ATP generation (Mráček et al., 2013; El-Mir et al., 2000). This reduction in ATP activates AMPK, which increases glucose uptake and metabolism resulting in lowered blood glucose and insulin levels (Polianskyte-Prause et al., 2019).

We hypothesize that metformin and TGF-β modulate renal tubule cell metabolism by governing activation of metabolic transcription factor PGC-1α. PGC-1α enhances oxidative phosphorylation by increasing pyruvate dehydrogenase (PDH) expression, mitochondrial DNA synthesis and altering voltage dependent anion channel (VDAC) activity.

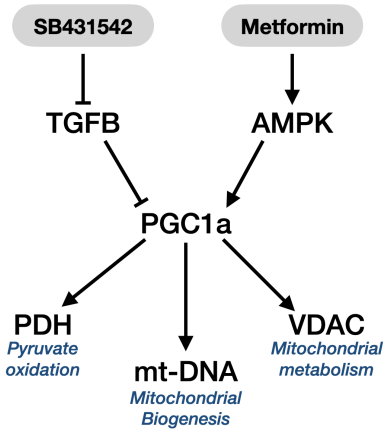

Figure 5.1: **Graphical abstract.** We hypothesize that metformin and TGF-β modulate renal tubule cell metabolism by governing activation of metabolic transcription factor PGC-1α. PGC-1α enhances oxidative phosphorylation by increasing pyruvate dehydrogenase (PDH) expression, mitochondrial DNA synthesis and altering voltage dependent anion channel (VDAC) activity.

5.2 Results

To study the bioenergetics underlying RPTEC differentiation, we exposed primary human RPTEC to AMPK activator metformin and the TGF-β inhibitor SB431542. After four weeks in culture, metformin and SB431542 additively increased transepithelial electrical resistance (TEER) (Fig. 5.2A). Control cells were not significantly different from cells cultured with metformin (245.3 $\pm$ 4.4 Ohms-cm^{-}2 vs 281.7 $\pm$ 14.0 Ohms-$^{c}m-2$; p = 0.0754). When compared to equivalent control cells, cells cultured with SB431542 and combination treatment had increased TEER (control: 245.3 $\pm$ 4.4 Ohms-cm^{-}2 vs SB431542: 496.2 $\pm$ 18.5 Ohms-cm^{-}2, p=0.0005; combination: 636.4 $\pm$ 19.15 Ohms-cm^{-}2, p=0.0001), which suggests an increase in tight junction formation and monolayer integrity (Cereijido et al., 1978; Martinez-Palomo et al., 1980).

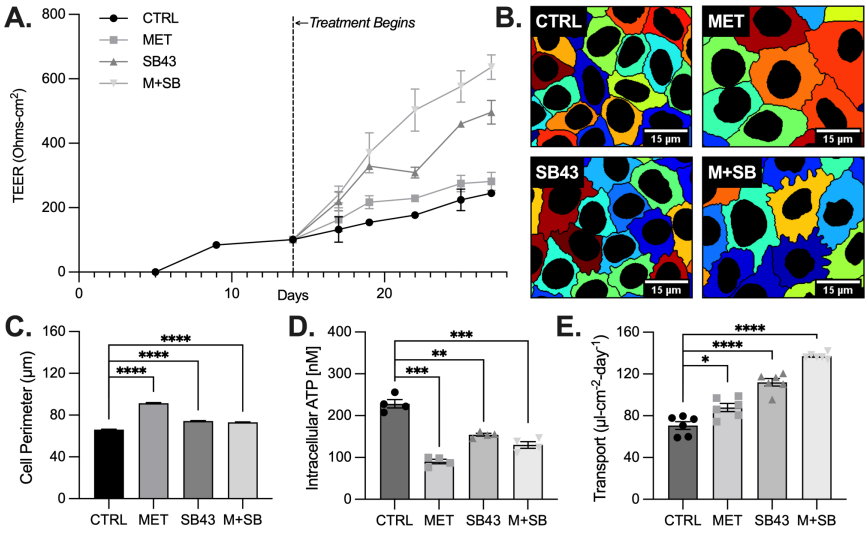

Figure 5.2: **Metformin and SB431542 induce differentiation in renal tubule epithelial cells. A.** Transepithelial electrical resistance. **B.** Cell segmentation using DAPI and ZO-1 immunofluorescent staining; **C.** Cell perimeter analysis (n≥1509); **D.** Intracellular ATP (n=4); **E.** Apicobasal fluid transport (n=6). Data are mean ± SEM. *p<0.05, **p<0.01, ***p<0.001, ****p<0.0001.

Cell metabolism is innately linked to macromolecular biosynthesis. Metabolites govern cell growth by acting as building blocks for biomass accumulation and by regulating the activity of signaling pathways that regulate cell growth and division (Figlia et al., 2020). RPTEC dedifferentiation is associated with depolarization and changes in cytoskeletal reorganization, so we next investigated whether cell morphology altered in response to treatments. As seen in Figure 5.2B, treatments increased cell membrane interdigitation, characteristic of proximal tubule cells. When compared to equivalent control cells, metformin, SB421542, and combination treatment all increased cell perimeter (control: 66.17 ± 0.35 vs metformin: 91.42 ± 0.64; SB431542: 74.25 ± 0.43; combination: 73.10 ± 0.34, respectively; p<0.0001 for all comparisons; Fig 5.2C).

ATP turnover increases with differentiation in human embryonic stem cells, as cells are using ATP more rapidly to support biological processes (Birket et al., 2011). We next examined whether treatment with metformin or SB431542 altered intracellular ATP concentrations. All treatments decreased intracellular ATP concentrations compared to controls (control: 228.4 ± 20.17 vs metformin: 90.35 ± 10.83 (p=0.0024); SB431542: 154.4 ± 6.54 (p=0.029); combination: 129.9 ± 15.93 (p=0.0096), respectively). This is consistent with the fact that metformin reduces the concentration of ATP through the suppression of mitochondrial complex I. We then performed a transport assay to test cell water reabsorption to confirm prior our results and demonstrate that treatments altered cell functional phenotype. Apicobasal fluid transport increased when treated with SB431542, and the effect was increased with combination treatment (Fig 5.2E).

5.2.1 TGF-β inhibition increases glucose uptake while metformin increases glycolysis and glycolytic reserve

TGF-β inhibition increases RPTEC apical glucose transport, so we examined the effect of TGF-β inhibition on glycolysis and expression of glucose-metabolizing enzymes. Sodium-glucose linked transporters (SGLT) are apical membrane transporters responsible for RPTEC glucose absorption from the glomerular filtrate (Fig 5.3A). In comparison to control cells, SB431542 increased SGLT1 transcription approximately 2-fold (p=0.0005; Fig 5.3B). Other than the liver, the kidney is the only organ capable of releasing glucose to the circulation, due to the presence of two of the rate-limiting enzymes for gluconeogenesis glucose-6-phosphatase (G6Pase) and phosphoenolpyruvate carboxylase (PEPCK). SB431532 increased G6Pase transcription in comparison to control cells ($p<0.0001$, Fig 5.3C), as did combination treatment ($p<0.0001$). All treatments reduced PEPCK transcription (Fig 5.3D). Very little glucose is metabolized in healthy tubule cells. Instead, it is reabsorbed into the peritubular capillaries by glucose facilitative transporters (GLUTs, Fig 5.3A). In comparison to control cells, combination treatment increased GLUT2 transcription over 7-fold (p=0.0118, Fig 5.3E).

To better understand if these changes in gene expression resulted in functional changes to cell metabolic activity, a glycolytic stress test was performed to assess whether treatments altered cell glycolytic capacity (Fig 5.3F). Glycolytic rate may be estimated from the extracellular acidification rate (ECAR) (Mookerjee and Brand, 2015). Metformin and combination treatment significantly increased basal glycolysis compared to control cells (control: 34.3 ± 5.83 mpH/min/10^4 cells vs. metformin: 145.4 ± 11.53 mpH/min/10^4 cells ($p<0.0001$), combination: 153.5 ± 6.8 mpH/min/10^4 cells ($p<0.0001$), Fig. 5.3G). Glycolytic capacity was tested by adding an acute injection of glucose to induce maximal glycolysis. Metformin and combination treatment significantly increased glycolytic capacity (control: 47.3 ± 4.5 mpH/min/10^4 cells vs. metformin: 104.0 ± 9.83 mpH/min/10^4 cells (p=0.0003), combination: 111.7 ± 4.67 mpH/min/10^4 cells ($p<0.0001$); Fig 5.32H). The F_0F_1-ATPase inhibitor oligomycin was used to assess glycolytic reserve, the difference between basal glycolysis, and maximum glycolytic capacity. In comparison to control cells, SB431542 increased glycolytic reserve (control: 12.90 ± 2.333 mpH/min/10^4 cells vs SB431542: 24.00 ± 1.933 mpH/min/10^4 cells (p=0.0022), Fig 5.3I). Oligomycin, however, suppressed ECAR significantly in metformin and combination-treated cells (Fig. 5.3E). 2-deoxy-D-glucose (2-DG) inhibits glycolysis by acting as a D-glucose mimic to inhibit the function of hexokinase, allowing an estimate of non-glycolytic ECAR. No treatment significantly affected non-glycolytic acidification (Fig. 5.3J).

5.2.2 Metformin and SB431542 increase transcription of electron transport chain machinery

Healthy RPTEC generate ATP primarily through mitochondrial OXPHOS in vivo, whereas cells become glycolytic in vitro. Mitochondrial biogenesis requires the coordinated expression of nuclear and mitochondrial-

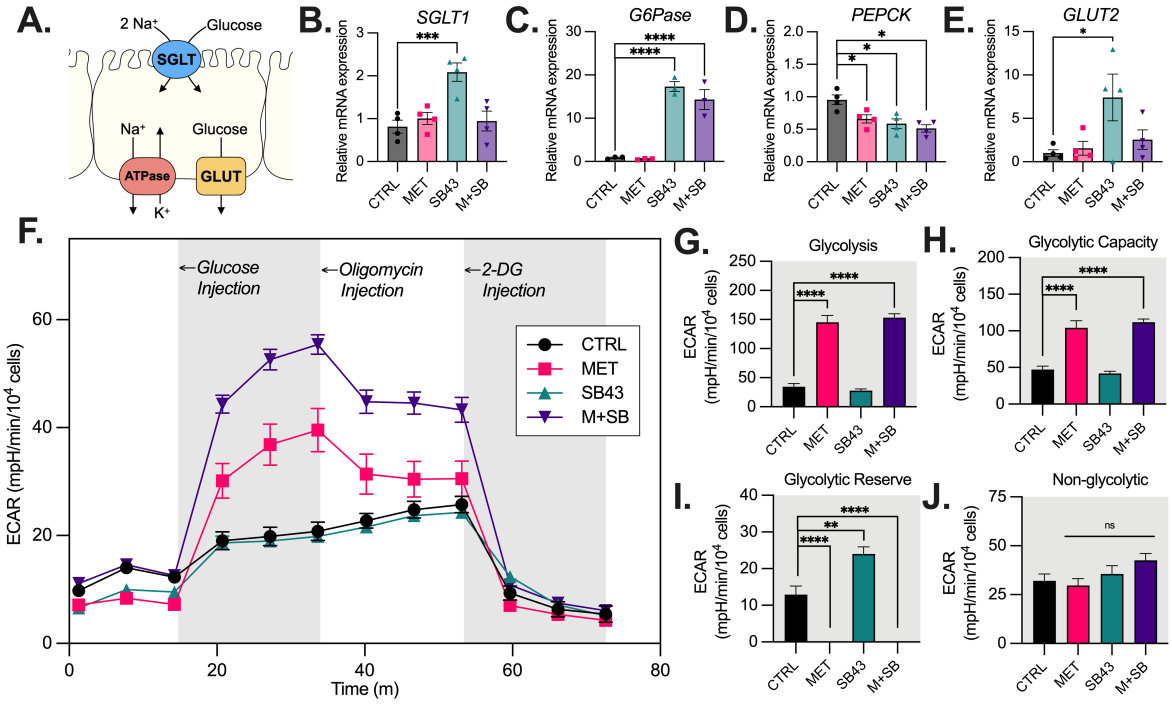

Figure 5.3: **Metformin increases glycolysis and SB431542 increases glycolytic reserve in renal tubule epithelial cells. A.** Sodium glucose transporters (SGLTs) and facilitated glucose transports (GLUTs) govern glucose reabsorption in the renal tubule. **B.** Normalized RNA expression of SGLT1, **C.** G6Pase, **D.** PEPCK, and **E.** GLUT2.($n \geq 3$).) **F.**Glycolytic stress test (n=9). **G.** Glycolysis, **H.** Glycolytic capacity, **I.** Glycolytic reserve, **J.** Non-glycolytic acidification (n=9). Data are mean ± SEM.*p<0.05, **p<0.01, ***p<0.001, ****p<0.0001.

encoded subunits of the mitochondrial respiratory complexes (Tang et al., 2020), so we next examined whether treatments altered the expression of mitochondrial enzymes. Metformin and combination treatments increased transcription of nuclear-encoded uncoupling protein 2 (UCP2), and mitochondrially encoded complex I (mt-ND1), but not SB431532 alone (Fig. 5.4A-B). SB431542 increased expression of nuclear-encoded complex III (UQCRC) (Fig. 5.4C). SB431542 and combination treatment increased nuclear-encoded complex I (NDuFB8) and complex IV (mt-CO2) transcription, but not metformin alone (Fig. 5.4D-E). Mitochondrially-encoded F_0F_1-ATPase (mt-ATP6) and cytochrome B (mt-CYTB), however, increased with combination treatment only (Fig. 5.4F-G). Complex II (SDHB) transcription was not significantly altered by any treatment (Fig. 5.4H). Metformin and SB431542 have different effects on ETC gene transcription; when given jointly, the two treatments result in an additive increase in ETC gene transcription, implying that the treatments control ETC gene transcription through independent pathways.

To determine if changes in RNA expression were translated to changes in protein expression, we employed western blot to assess protein level expression of metabolic genes. Total AMPK expression increased additively with treatments, while metformin and combination treatment increased AMPK phosphorylation (Fig. 5.4I). Activated AMPK phosphorylates PPAR gamma coactivator 1α (PGC1α), which regulates the expression of proteins involved in fatty acid uptake and oxidation (Tran et al., 2011). PGC1α phosphorylation increased significantly with SB431542 and combination treatments (Fig. 5.4I-J). In control cells, glucose metabolism appears to be decoupled from pyruvate oxidation, so carbohydrates are not used for maximal ATP production, despite high oxygen availability. Pyruvate dehydrogenase E1-alpha (PDHE1α) catalyzes the conversion of pyruvate to acetyl-CoA and CO_2 and provides the primary link between glycolysis and the TCA cycle. Voltage-dependent anion channel (VDAC) governs the entry and exit of mitochondrial metabolites (Varughese et al., 2021). PDHE1α and VDAC protein expression increased significantly with all treatments (Fig. 5.4K-L). We examined mitochondrial architecture by staining control and treated cells for VDAC, which outlines mitochondrial shape (Fig. 5.4M). VDAC immunofluorescence labeling is sparse and punctate in control cells. VDAC staining increased with treatments (Fig. 5.4K). The increase in VDAC density and continuity is consistent with a reduction in mitochondrial fragmentation.

5.2.3 Metformin and SB431542 additively increase mitochondrial respiratory capacity

To determine if changes in mitochondrial gene expression were correlated to changes in mitochondrial function, we performed a mitochondrial stress test using the Complex I inhibitor Rotenone, the Complex III inhibitor Antimycin A, the Complex V inhibitor Oligomycin and the mitochondrial uncoupler carbonyl cyanide m-chlorophenylhydrazone (CCCP) (Fig. 5.5A-B). When normalized to cell number, basal respiration rate increased by 54.9% in SB431542-treated cells (control: 24.4$\pm$1.3 pmol O_2/min/10^4 cells vs SB431542:

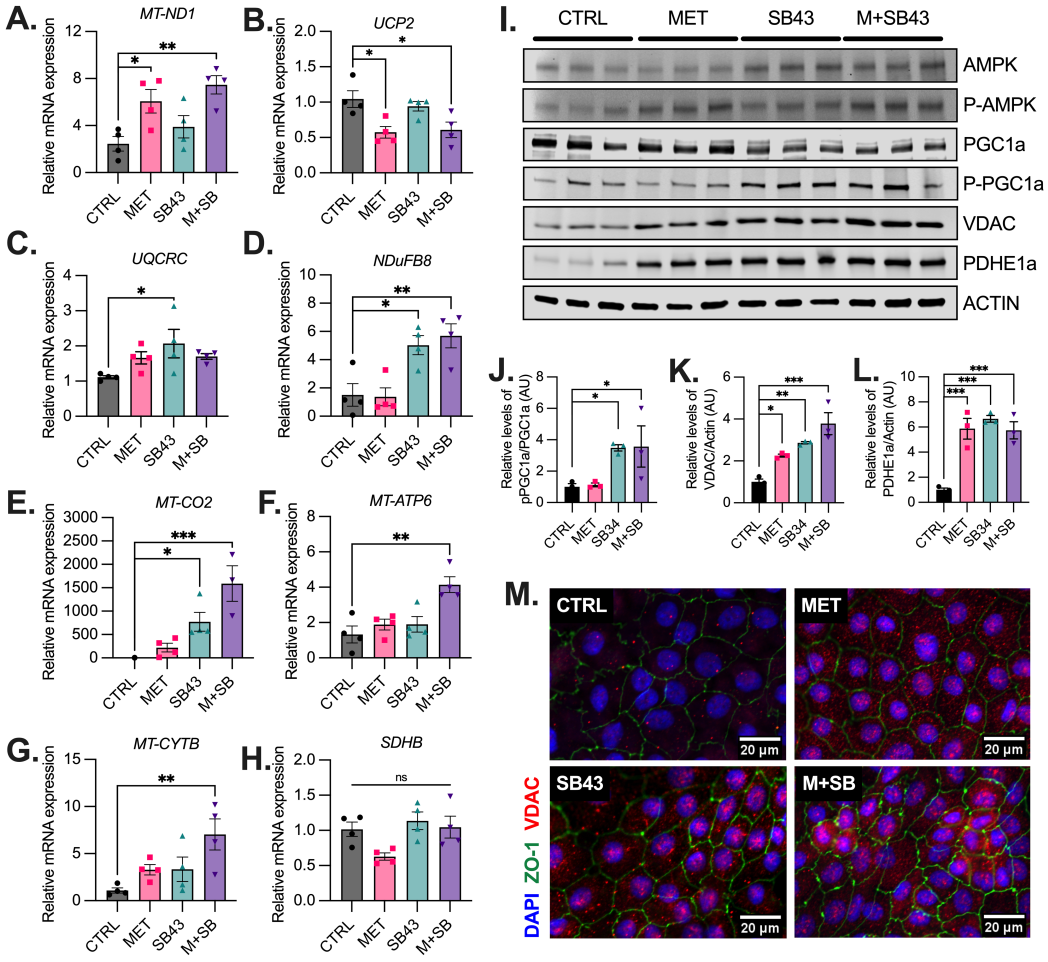

Figure 5.4: **Metformin and SB431542 increase transcription of electron transport chain (ETC) genes.** **A.** RNA expression of MT-ND1, **B.** Uncoupling protein 2 (UCP2); **C.** UQCRC, **D.** NDuFB8, **E.** MT-CO2, **F.** MT-ATP6, **G.** MT-CYTB, **H.** SDHB (n=4). **I.** Western blot metabolic protein analysis; **J.** Protein densitometry analysis of PGC1α phosphorylation, K. Total voltage dependent anion channel (VDAC), **L.** Total PDHE1a. Data are mean $\pm$ SEM. (n$\geq$3).) *p<0.05, **p<0.01, ***p<0.001, ****p<0.0001.

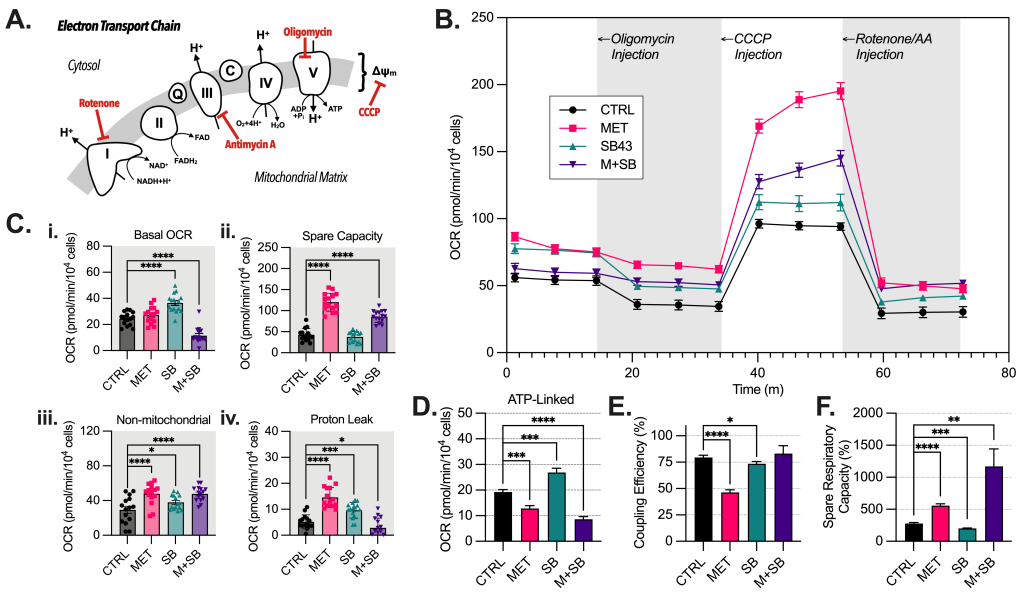

Figure 5.5: **Metformin and SB431542 increase spare respiratory capacity. A.** Diagram of the Electron Transport Chain (ETC) and respiratory inhibitors used to probe cell respiratory capacity. **B.** Mitochondrial stress test. **Ci**. Basal oxygen consumption rate (OCR), **ii.** Non-mitochondrial OCR, **iii.** Spare respiratory capacity, **iv.** Proton leak. **D.** ATP-linked OCR; **E.** Coupling efficiency (%); **F.** Spare respiratory capacity (%). Data are mean ± SEM. (n=15).) *p<0.05, **p<0.01, ***p<0.001, ****p<0.0001.

36.5±1.8 pmol O_2/min/10^4 cells (p<0.0001)). Basal OCR was 53.1% lower in combination-treated cells (control: 24.4±1.3 pmol O_2/min/10^4 cells vs combination: 11.46±1.6 pmol O_2/min/10^4 cells (p<0.0001), Fig. 5.5Ci), while metformin did not significantly affect basal OCR. CCCP may be used to uncouple mitochondrial respiration and determine cell maximal respiration capacity. Metformin and combination treatments significantly increased maximal respiration upon exposure to CCCP (Fig. 5.5B). Spare respiratory capacity, which measures a cell's capacity to respond to rising energy demands or stress, is defined as the difference between maximal OCR and basal OCR. When compared to control cells, metformin and combination treatments improved spare respiratory capacity (control: 42.6±3.9 pmol O_2/min/10^4 cells vs metformin: 120.0±5.5 pmol O_2/min/10^4 cells (p<0.0001), combination: 86.0±3.6 pmol O_2/min/10^4 cells (p<0.0001)).

Non-mitochondrial sources of oxygen consumption include reactive oxygen species (ROS) formation and cell surface electron transport (Starkov, 2008; Herst and Berridge, 2007). The Complex I inhibitor rotenone and Complex III inhibitor antimycin A were used to isolate non-mitochondrial oxygen consumption. Non-mitochondrial OCR increased with metformin and combination treatments (control: 29.3±4.0 pmol O_2/min/10^4 cells vs metformin: 48.0±3.1 pmol O_2/min/10^4 cells (p<0.0001), combination: 47.7±2.20 pmol O_2/min/10^4 cells (p<0.0001)). This is supported by metformin's ability to inhibit complex I, which leads to

an increase in ROS production as NADH cannot transport electrons to the electron acceptor, preventing the formation of water and NAD+ (Warkad et al., 2021). Non-mitochondrial OCR was also significantly increased by SB431542 (37.91±2.1 pmol O_2/min/10^4 cells (p=0.04)).

Oligomycin, which stops ATP synthesis by inhibiting the F_0 unit of F_0F_1-ATPase, was used to evaluate leak and ATP-linked respiration. The term "leak respiration" refers to the difference between respiration that occurs in the presence of oligomycin and non-mitochondrial respiration. When compared to control cells, proton leak increases about 3-fold with metformin and roughly 2-fold with SB431542, but decreases about 44.4% when the two treatments are combined (control: 5.2±0.7 pmol O_2/min/10^4 cells vs metformin:15.0±1.0 pmol O_2/min/10^4 cells (p<0.0001); SB431542: 9.6±1.0 pmol O_2/min/10^4 cells (p=0.0001), combination: 2.88±1.0 pmol O_2/min/10^4 cells (p=0.0114), Fig. 5.5Civ). ATP-linked respiration may be calculated as the difference between the OCR before and after an injection of oligomycin. ATP-linked respiration decreased 33.6% with metformin and 55.5% with combination treatment but increased 39.6% with SB43152 (control: 19.25±0.9 pmol O_2/min/10^4 cells vs metformin: 12.79±1.1 pmol O_2/min/10^4 cells (p=0.0002), SB431542: 26.88±1.7 pmol O_2/min/10^4 cells (p=0.0008), combination: 8.574±1.1 pmol O_2/min/10^4 cells (p<0.0001), Fig. 5.5D). Coupling efficiency is defined as the ratio between oxygen consumed to drive ATP synthesis to that used to cause proton leak, normalized to basal OCR. When compared to control cells, metformin and SB431542 both reduced coupling efficiency (control 79.51±2.05% vs metformin: 46.33±2.58% (p<0.0001), SB431542: 73.47±2.09% (p=0.0486)). Combination treatment, however, did not affect coupling efficiency (Fig. 5.5E). Finally, normalized spare respiratory capacity (SPR%) can be calculated as the difference between basal and maximal OCR expressed as a percentage of baseline OCR. In comparison to raw spare respiratory capacity, SPR% gives an indication of the cell's mitochondrial fitness, or its capacity to meet extra energy requirements in response to acute cellular stress. SB431542 decreased %SPR by approximately 76% (control: 278.3±15.5% vs SB431542: 202.4±6.0% (p=0.0002), Fig. 5.5F). %SPR increased by approximately two-fold with metformin and four-fold with combination treatment (control: 278.3±15.5% vs metformin: 557.0±29.0% (p<0.0001); combination: 1171±270.3% (p=0.0048), Fig. 5.5 F).

5.2.4 Metformin and SB431542 regulate renal tubule epithelial cell substrate dependency

CKD alters tubule cell metabolism by suppressing fatty acid oxidation and increasing glycolysis (Gewin, 2021). We assessed the effect of treatments on cell dependence on glucose, fatty acids, and glutamine using a series of respiratory inhibitors (Fig 5A-D). Mitochondrial pyruvate carrier inhibitor UK5009 was used to inhibit glucose oxidation (Fig. 5.6A-Bi). Glutaminase 1 (GLS1) inhibitor BPTES was used to inhibit glutamine oxidation (Fig. 5.6A, Ci). Carnitine palmitoyl transferase 1 (CPT1) inhibitor etomoxir was used to inhibit fatty acid oxidation (Fig. 5.6A, Di). After inhibition of the target pathway, the two alternate inhibitors were

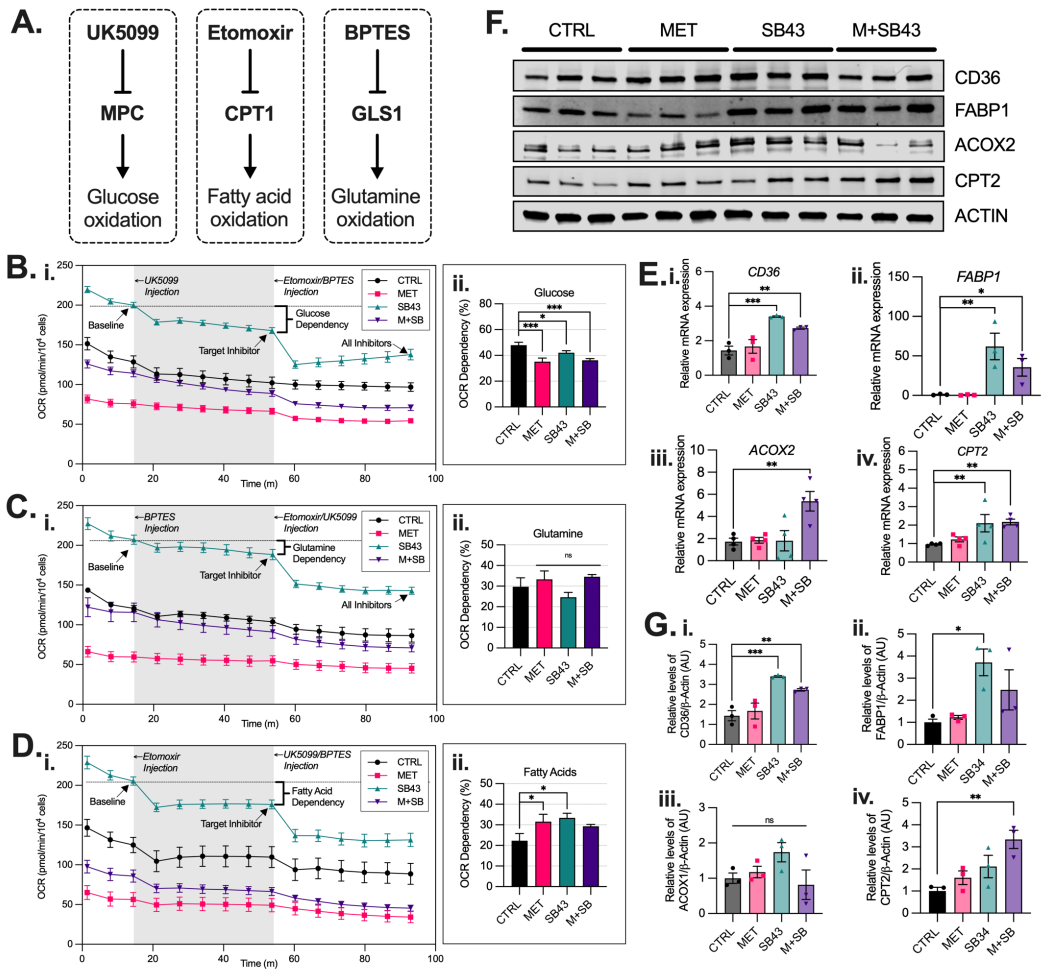

Figure 5.6: **Metformin reduces glucose dependency while SB431542 increases fatty acid oxidation (FAO).A.** Substrate inhibitor pathways. **B.** Glucose dependency test (n=5). **C.** Glutamine dependency test. **D.** Fatty acid dependency test. **E.** RNA expression of FAO genes CD36, FABP1, ACOX2, and CPT2. **F.** Western blot protein analysis of CD36, FABP1, ACOX2, CPT2, and Actin. **G.** Protein densitometry of data in panel F relative to loading control b-Actin: **i.** CD36 expression, **ii:** FABP1 expression, **iii.** ACOX2, **iv.** CPT2. Data are mean ± SEM. (n≥3).) *p<0.05, **p<0.01, ***p<0.001, ****p<0.0001.

added to suppress the remaining oxidation pathways. Target pathway dependency was then calculated as a percentage of the total inhibition achieved by all three inhibitors (Fig. 5.6Bii, Cii, Dii). All treatments reduced OCR glucose dependency (Fig. 5.6Bii). No treatment significantly changed OCR glutamine dependency (Fig. 5.6Cii).

When administered separately metformin and SB431542 both increased OCR fatty acid dependency, although combination treatment had no significant effect on OCR fatty acid dependency (Fig. 5.6Dii). To determine whether this was caused by an increase in the expression of fatty acid oxidation metabolic machinery, we assessed whether the treatments altered the transcription of genes associated with fatty acid metabolism.

SB431542 increased transcription of Cluster of differentiation 36 (CD36), the primary translocase that governs fatty acid cell import (Fig. 5.6Ei). All treatments significantly increased the transcription of fatty acid binding protein 1 (FABP1), a carrier protein involved in fatty acid transport (Fig. 5.6Eii). Combination treatment increased mRNA expression of acyl-CoA oxidase 2 (ACOX2), which catalyzes the first step of fatty acid beta-oxidation in the peroxisome (Fig. 5.6Eiii). SB431542 and combination treatment increased the expression of mitochondrial enzyme carnitine palmitoyl transferase 2 (CPT2), which governs fatty acid import to the mitochondria (Fig. 5.6Eiv). Protein expression of CD36 and FABP1 expression increased with SB431542 and combination treatments (Fig. 5.6Gi-ii). ACOX2 protein expression did not significantly increase with any treatment, although CPT2 protein expression significantly increased with combination treatment.

5.3 Discussion

We conducted this study to identify and investigate the effects of metformin and TGF-β signaling on the metabolism of renal tubule epithelial cells in vitro. We previously found that TGF-β signaling negatively regulates fluid transport, glucose uptake, organic anion excretion, and apical acid extrusion in vitro, yet the mechanisms by which TGF-β governs RPTEC metabolism are incompletely understood. Our data indicate that metformin increases glycolysis while reducing glucose oxidation dependency, while TGF-β inhibition increases oxidative phosphorylation and fatty acid dependency while reducing glucose oxidation dependency. Interestingly, the addition of metformin to TGF-β inhibition provides an increased effect that is greater than the effects of either treatment alone.

RPTEC have high energy requirements which render them exquisitely dependent on mitochondrial health. As such, they are the cell type most frequently injured in renal ischemia. Most of the energy produced in the kidneys is used to sustain renal tubular transport. In vivo, renal tubule cells exhibit intricate intra- and intercellular interdigitation (Welling and Welling, 1988; Takahashi-Iwanaga, 1992). We find that metformin and SB431542 increase cell perimeter and TEER, suggesting an increase in tight junctions and monolayer integrity (Fig. 5.2B-D) (Takahashi-Iwanaga, 1992). Further, metformin and SB431542 observably altered cell energy status as determined by ATP concentration and AMPK phosphorylation (Fig 5.2E, 5.4). We found that metformin, but not SB431542, boosted AMPK phosphorylation (Fig. 5.4). Interestingly, however, both treatments increased the phosphorylation of PGC1a, which is phosphorylated by AMPK and governs the transcription of numerous metabolic genes (Fig. 5.4). Both treatments increased the transcription of PGC-1α-dependent nuclear- and mitochondrially encoded ETC proteins (Fig. 5.4A-H) and the expression of mitochondrial proteins VDAC and PDHE1α (Fig. 5.4I-J). PGC-1α expression is epigenetically downregulated by Smad3-dependent TGF-β signaling through direct binding to the PGC-1α enhancer. PGC-1α increases PDH expression (Kiilerich et al., 2010) and increases mitochondrial DNA (mt-DNA) synthesis through

activation of NRF1/2. Increased PGC-1α activation may be contributing to an increase in VDAC activity, as PGC-1α by regulates VDAC conformation through HK2 protein binding (Li et al., 2021).

Glucose handling is strictly regulated in RPTEC. We found that modulation of the AMPK and TGF-β signaling pathways altered glucose handling in RPTEC. TGF-β inhibition increased the expression of glucose transporters (e.g. SGLT1, GLUT2, G6Pase) and glucose reabsorption, as we have previously observed (Hunter et al., 2022). PEPCK catalyzes the first irreversible step in gluconeogenesis, the conversion of oxaloacetate into phosphoenolpyruvate, while G6Pase hydrolyzes the phosphorylated form of glucose, enabling its cellular export (Gerich, 2010). Both treatments reduced PEPCK transcription, implying a reduction in the diversion of TCA intermediate oxaloacetate toward gluconeogenesis. SB431542 increased G6Pase transcription, which supports our previous data demonstrating that TGF-β inhibition increases glucose reuptake. This is in agreement with prior work which has shown that TGF-β1 increases gluconeogenesis via the c-Jun/G6P axis in zebrafish embryos (Zhang et al., 2018).

When administered independently, metformin and SB431542 demonstrate the reciprocal balance between glycolysis and OXPHOS. Metformin increases the utilization of glycolysis, while reducing the spare capacity of OXPHOS, while SB431542 increases OXPHOS while reducing glycolytic spare capacity. Metformin increased basal glycolysis and glycolytic capacity while reducing glycolytic reserve, as cells were unable to further increase glycolytic flux as measured by ECAR upon the addition of ATP-synthase inhibitor oligomycin. Conversely, SB431542 increased glycolytic reserve while also reducing glycolytic capacity, as indicated by a lesser response to the acute glucose injection.

Metformin did not change basal OCR but increased spare respiratory capacity (Fig. 5.5C). Metformin increased proton leak because complex I inhibition increases ROS generation as electrons from NADH cannot be transferred to the electron acceptor to form water. This increase in proton leak led to a significant reduction in ATP-linked OCR and coupling efficiency (Fig. 5.5D-E). Overall, however, due to the increase in the uncoupler-induced maximal respiratory capacity, metformin significantly increased spare respiratory capacity when expressed as a percent of basal OCR (%SPR). The renoprotective effects of metformin have been demonstrated in a mouse model of streptozotocin-induced diabetes, where metformin attenuated renal oxidative stress and tubulointerstitial fibrosis (chun Han et al., 2021). On the other hand, SB431542 increased basal O_2 consumption and ATP-linked oxygen consumption (Fig. 5.5C-D). Unexpectedly, SB431542 also increased proton leak which led to a reduction in coupling efficiency (Fig. 5.5C, E). Overall, SB431542 decreased %SPR due to the increase in basal OCR (Fig. 5.5C, F).

When administered together, the two treatments had a synergistic effect that increases both glycolytic and oxidative phosphorylation capacities, imparting greater metabolic flexibility. Combination-treated cells have decreased basal and ATP-linked OCR (Fig. 5.5C, D) due to the significant increase in glycolytic metabolism

(Fig. 5.3G). Conversely, combination treatment reduced proton leak in comparison to control cells, and did not affect coupling efficiency, leading to a considerable improvement in spare respiratory capacity over metformin or SB431542 alone (Fig. 5.5C, E, F).

Treatment-induced metabolic uncoupling may be beneficial to cells in our model by minimizing ROS formation. Reactive oxygen species (ROS), like superoxides and hydrogen peroxide, are produced by the ETC as a byproduct of metabolism. Due to H^+ leak pathways, mitochondrial ATP generation and O_2 consumption are not perfectly coupled. Mitochondrial uncoupling may allow a cell to remain glycolytic in an aerobic environment and is hypothesized to aid in maintaining homeostasis by decreasing oxidative damage (Bouillaud, 2009). This is beneficial when directing metabolic intermediates toward cell growth. All treatments increased non-mitochondrial OCR, suggesting an increase in non-mitochondrial peroxisomal respiration (Fig 5.5C). UCP2 expression was reduced with metformin and combination treatments (Fig 5.4B). UCP2 contributes to the maintenance of mitochondrial integrity by minimizing the loss of membrane potential and thus lowering mitophagy. Mitochondrial uncoupling may have adverse effects in the kidneys as it elevates oxygen consumption and promotes hypoxia (Schiffer and Friederich-Persson, 2017). UCP2 is linked to mitochondrial damage, but it also protects renal tubule cells from oxidative stress brought on by high salt levels (Qin et al., 2019; Forte et al., 2021). According to Brand's "uncoupling to survive" theory, H^+ leaks help to reduce ROS generation by reducing the proton motive force (Brand and Esteves, 2005). By delaying systemic lactic acidosis, elevated UCP2 is hypothesized to have a positive impact on mitochondrial activity in the heart (Kukat et al., 2014).

Metformin and SB431542 treatments were sufficient to alter RPTEC substrate dependency. Metformin and SB431542 demonstrate the reciprocal regulation between fatty acid oxidation and glycolysis, the Randle cycle, in RPTEC. Metformin reduced the dependence of oxygen consumption on glucose, whereas SB43142 increased fatty acid uptake and utilization as determined by the expression of FAO enzymes and the heightened response to etomoxir. Defective FAO plays a key role in the development of kidney fibrosis. Mice are protected from developing tubulointerstitial fibrosis by restoring fatty acid metabolism (Kang et al., 2015). SB431542 has been shown to alleviate TGF-β-attenuated expression of CD36 (Han et al., 2000). CPT1a expression is lower in kidneys of diabetic patients and mice with tubulointerstitial fibrosis (Kang et al., 2015). Renal tubule CPT1a overexpression protects from kidney fibrosis by restoring mitochondrial homeostasis (Miguel et al., 2021). No treatment affected glutamine oxygen consumption dependency, although inhibition of glutamine oxidation caused significant increases in extracellular acidification, which is consistent with the fact that glutamine metabolism plays an important role in acid-base balance in RPTEC.

5.4 Conclusion

In summary, through gene expression analysis and functional studies, we demonstrate that metformin and SB431542 synergistically increase mitochondrial biogenesis and oxidative phosphorylation capacity. These cellular mechanisms could explain the direct roles of metformin in mediating RPTEC glucose utilization and its connection to functional apicobasal fluid transport. Together our results suggest that correcting metabolic defects via TGF-β signaling and metformin may be useful for both the development of in vitro cell culture systems and for the prevention and treatment of CKD.

5.5 Materials and methods

5.5.1 Cell culture

Primary human renal tubule epithelial cells (HREC) were obtained from Innovative Biotherapies (Ann Arbor, MI). Cells were maintained in a 1:1 ratio of glucose-free DMEM/F12 media supplemented with 5.5mM glucose, 10mg/L insulin, 5.5mg/L transferrin, 6.7μg/L selenium, 25μg/L hydrocortisone, 25μg/L prostaglandin E1, 10μg/L epidermal growth factor, and 10μg/L triiodothyronine. Cells were seeded onto polycarbonate Transwell cell culture inserts (Corning Inc., Corning, NY) or polystyrene Seahorse 96-well tissue culture plates (Agilent Technologies, Santa Clara, CA) at a density of 100,000 cells cm^{-2} and left overnight to facilitate cell attachment. After 24 hours, cells were moved to an orbital shaker to simulate physiological shear stress (2 dyne cm^{-2}). After one week in culture for 96-well plates and two weeks in culture for tissue culture supports, cells were supplemented apically with AMPK activator Metformin (200μM; Cayman Chemical, Ann Arbor, MI), TGF-β receptor I inhibitor SB431542 (10μM; Cayman Chemical), or a combination of both. Control cells were treated with DMSO vehicle control (1μl/ml). Cells were cultured with treatments for four weeks prior to staining, mRNA, protein harvest, and respirometry assays.

5.5.2 Transepithelial electrical resistance

HREC were cultured on Transwell inserts as described above. Trans-epithelial electrical resistance measurements (TEER) were taken using an EVOM2 voltohmeter (World Precision Instruments, Sarasota, FL) at three different locations per well. TEER measurements were corrected using a blank membrane. Average TEER measurements were corrected to membrane surface area.

5.5.3 Apicobasal transport

HREC were cultured on Transwell inserts as described above. After four weeks of treatment, cultures were aspirated and changed to fresh media. 24 hours later, apical media was aspirated and weighed. Three blank wells with the porous membrane occluded with epoxy were used as an evaporative control. Volume transport

was assessed by determining the differences between initial volumes and final volumes, as estimated by weight, and correcting for evaporation.

5.5.4 ATP concentration

HREC at six weeks of culture were changed to fresh media. 24 hours later, apical media was aspirated, and ATP concentration was determined using a luminescence-based ATP Detection Assay Kit (Cayman Chemical, Ann Arbor, MI) according to the manufacturer's instructions.

5.5.5 RNA preparation and cDNA synthesis

RNA was extracted using an RNeasy kit with on-column DNase I digestion (Qiagen, Valencia, CA). First-strand cDNA was synthesized using a high-capacity cDNA reverse transcription kit (Applied Biosystems, Carlsbad, CA) according to the manufacturer's instructions.

5.5.6 Quantitative RT-PCR

Primers were selected from the Harvard-Massachusetts General Hospital Primerbank or generated using PrimerBLAST (NCBI, Bethesda, MD) and purchased from Sigma-Aldrich (St. Louis, MO). Reactions were performed using a CFX96 Real-Time PCR System (Bio-Rad, Hercules, CA) under standard running conditions with SSO Advanced Supermix (Bio-Rad). mRNA transcripts were quantified relative to the housekeeping gene GAPDH.

5.5.7 Immunoblotting

Cells were rinsed once with PBS and lysed in ice-cold lysis buffer (PBS containing 0.05% SDS, protease inhibitor, and phosphatase inhibitor). Cells were then scraped, collected, and sheared. Total protein concentration was determined using a bicinchoninic acid assay (Pierce Biotechnology, Waltham, MA). Cell lysates were resolved on Mini-PROTEAN TGX 4-20% polyacrylamide gels (Bio-Rad), at a concentration of 10µg protein per lane, under reducing conditions with SDS-glycine running buffer according to the manufacturer's instructions. Proteins were transferred to a nitrocellulose membrane using a wet blotter. Blots were fully dried and blocked with 5% (wt/vol) bovine serum albumin (BSA) in Tris-buffered saline with 0.1% Tween-20 (TBST). Membranes were incubated overnight at 4°C with primary antibody diluted in 5% BSA in TBST and detected using the appropriate near infrared secondary antibody. Products were visualized by NIR fluorescence on an Odyssey CLx (LI-COR, Lincoln, NE). Band intensities were measured and normalized to loading using beta-actin using ImageStudio (LI-COR). For each protein target, the mean density of the control sample bands was assigned the value of 1 with all individual densitometries being expressed relative to this mean.

5.5.8 Seahorse respirometry experiments

After four weeks of treatments, cell oxygen consumption (OCR) and extracellular acidification rates (ECAR) were assessed using a Seahorse XFe96 (Agilent, Santa Clara, CA). Basal OCR and ECAR levels were obtained from an average of three independent measurements per well. Cells were glucose-starved for one hour prior to the glycolytic stress test. In the glycolytic stress test, glucose (100mM), oligomycin (12μM), and 2-deoxyglucose (2-DG, 500mM) were injected to determine cellular glycolytic capacity. For mitochondrial stress tests, oligomycin (2μM), CCCP (12μM), rotenone (0.5μM), and antimycin A (0.5 μM) were injected to determine cellular mitochondrial capacity. For these experiments, three serial OCR/ECAR measurements were taken to determine OCR/ECAR in the presence of each respiratory inhibitor. In separate experiments, glutamine oxidation inhibitor BPTES (10µM), fatty acid oxidation inhibitor etomoxir (100µM), and glucose oxidation inhibitor UK5099 (10µM) were injected to determine the cellular response to substrate inhibition. For these experiments, five serial OCR/ECAR measurements were taken to determine OCR/ECAR in the presence of each respiratory inhibitor. Once respiration experiments were complete, cells were washed with PBS and fixed with 4% paraformaldehyde on ice for 20 minutes. Substrate dependency was calculated by determining the change in OCR caused by the target substrate inhibitor and dividing it by the total change in OCR after administration of all substrate inhibitors. Cells were then mounted with VectaShield containing DAPI (ThermoFisher, Waltham, MA). Nuclear count was obtained using an ImageXpress automated cell imaging system (Molecular Devices, San Jose, CA). OCR and ECAR values were then normalized to cell count.

5.5.9 Immunofluorescence imaging

Cells were washed with ice-cold PBS and fixed with 4% paraformaldehyde for 20 minutes on ice. Cells were then permeabilized with 0.1% Triton-X in PBS for 10 minutes and then washed three times with PBS. Cells were blocked for one hour at room temperature, then incubated with primary antibody (1:200) at room temperature for one hour. Cells were then washed three times with PBS, then incubated for one hour in the dark with fluor-conjugated secondary antibody (1:10,000) for one hour at room temperature. Cells were then washed overnight in PBS and then fixed with mounting medium. Images were taken with a Zeiss LSM 710 confocal microscope using Zen Black (Zeiss, Oberkochen, Germany).

5.5.10 Cell perimeter analysis

Cell images for DAPI and ZO-1 were obtained at a 20X objective using the above methods. At least three different fields of view were analyzed for each sample with at least 1500 cells in total being examined. CellProfiler (Broad Institute, Cambridge, MA) was used to threshold and segment nuclei and cell perimeters.

5.5.11 Quantification and statistical analysis

All results are expressed at mean ± SEM of a minimum of three independent experiments. Differences in means were assessed with one-way ANOVA tests following the Two-stage step-up method of Benjamini, Krieger, and Kekutieli with individual variances for each comparison between means using Prism 9 (GraphPad, San Diego, CA). Statistical significance was accepted at a level of $p< 00.05$. At least three samples per group were used for statistically meaningful interpretation of results.

5.6 Supplemental Tables

Hereafter we gather three tables providing further details on the experiments conducted in this chapter. Table 5.1 provides a summary of the glycolytic stress test results. Table 5.2 provides a summary of the mitochondrial respiratory stress test results. Table 5.3 details the list of primers used to perform quantitative RT-PCR for each gene. Finally, Table 5.4 describes the primary antibodies used to perform immunoblotting.

Table 5.1: **Glycolytic stress test summary data**

	Control		Metformin		SB431542		Met+SB43	
Parameter	Average	SEM	Average	SEM	Average	SEM	Average	SEM
Non-Glycolytic Acidification	32.0	3.5	29.7	3.4	35.6	4.2	42.5	3.5
Glycolysis	34.4	5.8	145.4	11.5	27.8	3.1	153.3	6.8
Glycolytic Capacity	47.3	4.5	104.0	9.8	41.8	3.2	111.7	4.5
Glycolytic Reserve	12.9	2.3	0.0	0.0	14.0	1.9	0.0	0.0
Glycolytic Reserve (%)	155.1	15.0	71.0	2.3	169.4	24.1	73.3	2.5

Table 5.2: **Mitochondrial respiratory stress test summary data**

	Control		Metformin		SB431542		Met+SB43	
Parameter	Average	SEM	Average	SEM	Average	SEM	Average	SEM
Basal	24.4	1.3	27.3	1.6	36.5	1.8	11.5	1.6
Proton Leak	5.2	0.7	14.5	1.0	9.6	0.8	2.9	1.0
Maximal Respiration	67.0	4.4	147.5	6.2	74.4	4.8	97.4	4.4
Spare Respiratory Capacity	42.6	3.9	120.2	5.5	37.9	3.2	86.0	3.6
Non Mitochondrial O_2 Consumption	29.3	4.0	47.7	3.1	37.9	2.1	47.7	2.2
ATP Production	19.3	0.9	12.8	1.1	26.9	1.7	8.6	1.1
Coupling Efficiency (%)	79.5	2.0	46.3	2.6	73.5	2.1	83.2	7.3
Spare Respiratory Capacity (%)	278.3	15.5	557.3	29.0	202.4	6.0	1171.3	270.3

Table 5.3: **RNA primers used to perform quantitative RT-PCR.**

Gene	Forward (5'-3')	Reverse (3'-5')
ACOX2	GCACCCCGACATAGAGAGC	CTGCGGAGTGCAGTGTTCT
CD36	GGCTGTGACCGGAACTGTG	AGGTCTCCAACTGGCATTAGAA
CPT2	CATACAAGCTACATTTCGGGACC	AGCCCGGAGTGTCTTCAGAA
FABP1	GTGTCGGAAATCGTGCAGAAT	GACTTTCTCCCCTGTCATTGTC
G6Pase	GTGTCCGTGATCGCAGACC	GACGAGGTTGAGCCAGTCTC
GAPDH	AATCCCATCACCATCTTCCA	TGGACTCCACGACGTACTCA
GLS1	AGGGTCTGTTACCTAGCTTGG	ACGTTCGCAATCCTGTAGATTT
GLUT2	GCTGCTCAACTAATCACCATGC	TGGTCCCAATTTTGAAAACCCC
MT-ATP6	TAGCCATACACAACACTAAAGGACGA	GGGCATTTTTAATCTTAGAGCGAAA
MT-CO2	CTGAACCTACGAGTACACCG	TTAATTCTAGGACGATGGGC
MT-CYTB	ATCACTCGAGACGTAAATTATGGCT	TGAACTAGGTCTGTCCCAATGTATG
MT-ND1	CCACCTCTAGCCTAGCCGTTTA	GGGTCATGATGGCAGGAGTAAT
NDuFB8	ACAGGAACCGTGTGGATACAT	CCCCACCCAGCACATGAAT
PEPCK	GCCATCATGCCGTAGCATC	AGCCTCAGTTCCATCACAGAT
SDHB	ACAGCTCCCCGTATCAAGAAA	GCATGATCTTCGGAAGGTCAA
SGLT1	TACCTGAGGAAGCGGTTTGGA	CGAGAAGATGTCTGCCGAGA
SGLT2	TCCTGCTGACATCCTAGTCATT	GAAGAGCGCATTCCACTCC
SLC38A3	GGAGCTGTATGGAGGGCAAG	GAACACTGACATCCCGAATGAT
UCP2	GGAGGTGGTCGGAGATACCAA	ACAATGGCATTACGAGCAACAT
UQCRC2	TTCAGCAATTTAGGAACCACCC	GGTCACACTTAATTTGCCACCAA

Table 5.4: **Primary antibodies used to perform immunoblotting.**

Gene	Manufacturer	Catalog number
AMPK	Invitrogen	MA5-15815
Beta-actin	Santa Cruz Biotechnologies	SC-47778
P-AMPK	Cell Signaling	2535S
P-PGC1a	Bio-Techne	AF6650
PDHE1a	Abcam	AB110330
VDAC	Cell Signaling	4661S

CHAPTER 6

Canonical Smad-dependent TGF-β signaling governs NKCC2 transcription and fluid transport via HNF-1α in renal tubule epithelial cells

6.1 Introduction

As detailed in Chapter 1, Chronic kidney disease is the ninth leading cause of death in the US and is characterized by the progressive, irreversible stiffening of renal parenchyma and phenotypic erosion of surviving renal tubule epithelial cells. At present, there are no treatments to reverse or even halt established kidney disease. Cell-based models of the renal tubule offer a potentially inexhaustible source for immunosuppression-free transplants to treat CKD. However, the development of these bioartificial devices, is limited by an inability to maintain cell differentiation in vitro.

Transforming Growth Factor-β (TGF-β) is a pleiotropic cell signaling pathway, involved in the regulation of epithelial cell fate and plasticity, but also the development of renal fibrosis and CKD (Gu et al., 2020; Sureshbabu et al., 2016). TGF-β initiates canonical and non-canonical pathways to exert multiple signaling cascades. Canonical TGF-β is mediated by the receptor-activated Smad (r-Smads) proteins, Smad2 and Smad3, which form a complex with the common Smad (co-Smad), Smad4, and translocate to the nucleus to regulate target gene expression (Frick et al., 2017; Hata and Chen, 2016; Massague, 2000). We have previously found that TGF-β inhibition using small molecule SB431542 increases differentiation in renal tubule epithelial cells, as indicated by increased transepithelial electrical resistance, glucose reabsorption, and apicobasal fluid transport (Love et al., 2020; Hunter et al., 2022). This effect is amplified with the addition of AMP-protein kinase (AMPK) activator metformin.

Hepatic Nuclear Factor-1α (HNF-1α) is a master regulator of renal tubule epithelial cell differentiation,

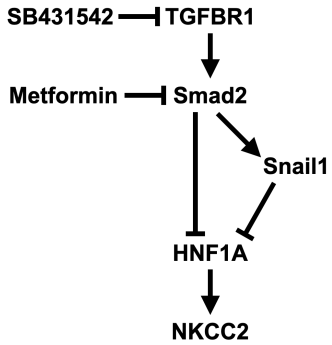

Figure 6.1: **Graphical Abstract** Proposed signal transduction pathway

where it regulates the expression of drug-metabolizing enzymes and membrane transporters, including Multi-drug resistance protein 2 (MDRP2), Organic ion transporters 1/3 (OAT1/3), Sodium-glucose transporter 2 (SGLT2), and Na-K-Cl cotransporter 2 (NKCC2)(Martovetsky et al., 2013; Markadieu and Delpire, 2014; Hiratsuka et al., 2019). HNF-1α regulates target gene transcription by binding to the palindromic consensus sequence GTTAATNATTANC and recruiting histone acetyltransferases CBP/p300 to target gene promoters (Ban et al., 2002; Dohda et al., 2004). HNF-1α dependent nucleosome hyperacetylation is required for the activation of tissue-specific target genes (Marcelina et al., 2001). HNF-1α is expressed in the proximal and distal tubules (Lazzaro et al., 1992; Massa et al., 2013). The HNF-1α binding site is conserved in the mammalian NKCC2 gene promoter, suggesting that it is essential to renal NKCC2 expression and functional integrity (Markadieu and Delpire, 2014). TGF-β signaling is known to functionally inactivate HNF-1α by impairing its ability to recruit CBP/p300 acetyltransferases to target gene promoters (Bisceglia et al., 2019). We hypothesize that canonical Smad2-dependent TGF-β signaling attenuates HNF-1α activated NKCC2 expression. The goal of this study is to determine the mechanisms by which TGF-β governs NKCC2 expression in renal tubule epithelial cells.

6.2 Results

The results hereafter describe experiments validating the effects of TGF-β inhibition and AMPK activation on governing NKCC2 expression and activity. Sections 6.2.1 and 6.2.2, demonstrate the utility of ALK5 small molecule inhibitors in increasing NKCC2 expression. The roles of non-canonical and canonical TGF-β signaling pathways in governing NKCC2 expression are explored in Sections 6.2.3 and 6.2.4, respectively. Section 6.2.5 presents genetic Smad2, Smad3, Smad4, and Snail1 knockout and rescue models. Sections 6.2.6 and 6.2.7 explore the role in HNF-1α in mediating TGF-β dependent NKCC2 expression.

6.2.1 SB431542 and metformin induce NKCC2 expression and function

The small molecule TGF-β inhibitor SB431542 is found to increase transport. Although, metformin does not increase transport when administered alone, it enhances the effect of SB431542 when the two are administered together (Fig. 6.2A). To further investigate the mechanism by which TGF-β governs fluid transport, we administered loop diuretic furosemide, which inhibits the electroneutral sodium transporter NKCC2. Control, SB431542, and combination treated cells are responsive to furosemide-induced NKCC inhibition (Fig 6.2A). RNA expression of NKCC2 expression significantly increases with combination treatment, but not SB431542 alone (Fig. 6.21B). Protein expression of NKCC2 significantly increases with SB431542 and combination treatment (Fig. 6.2C-D). Immunofluorescent staining of NKCC2 reveals significant increases in NKCC2 expression with SB431542 and combination treatment (Fig. 6.2E).

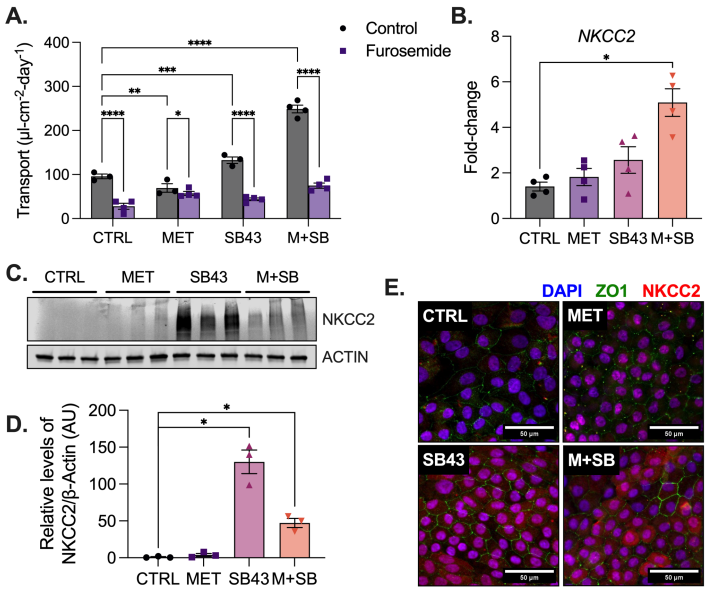

Figure 6.2: **SB431542-induced TGF-β inhibition enhances renal tubule cell transporter expression and activity. A.** Volume transport with and without loop diuretic furosemide. **B.** RNA expression of NKCC2 normalized to GAPDH. **C.** Protein expression of NKCC2 and loading control β-actin. **D.** Protein densitometry of western blots in 6.2C. **E.** Immunofluorescent staining HREC treated with metformin, SB431542, and combination treatment. Blue=DAPI, green=ZO-1, red=NKCC2.Data are mean $\pm$ SEM.*p<0.05, **p<0.01, ***p<0.001, ****p<0.0001.

6.2.2 ALK5 inhibition governs NKCC2 expression and fluid transport

Small molecule TGF-β inhibitor SB431542 inhibits the ALK4, ALK5 (also known as TGF-β receptor I/TβRI), and ALK7 receptors, so we next verify the specificity of SB431542. Transcription of ALK5 is suppressed with SB431542, but not ALK4 or ALK7 (Fig. 6.3A-C). Next, we assess whether metformin and SB431542 alter the transcription of fibrotic genes Collagen 4 alpha chain 1 (Col4α1) and Snail1 (Snai1). Transcription of Col4α1 decreases with all treatments, while Snai11 transcription decreases with SB431542 and combination treatment, but not metformin alone (Fig. 6.3D-E). To confirm that ALK5 inhibition is governing this change in HREC differentiation, we test whether the administration of ALK5-specific inhibitors, A7701, LY3200882, RepSox, and SB525334, can recapitulate the effects of SB431542. All ALK5 inhibitors significantly increase fluid transport as well as RNA and protein-level expression of NKCC2 (Fig. 6.3F-H). NKCC2 staining also increases with ALK5 inhibitors (Fig. 6.9). All ALK5 inhibitors suppress transcription of Col4α1, supporting the hypothesis that ALK5-dependent signaling is mediating this change in phenotype (Fig. 6.3I).

6.2.3 Non-canonical TGF-β signaling pathways do not govern NKCC2 expression

ALK5 activation governs several canonical and non-canonical signaling pathways (Fig. 6.4A). SB431542 and metformin lead to additive suppression of Akt and Extracellular signal-regulated kinases (ERK) 1/2, as

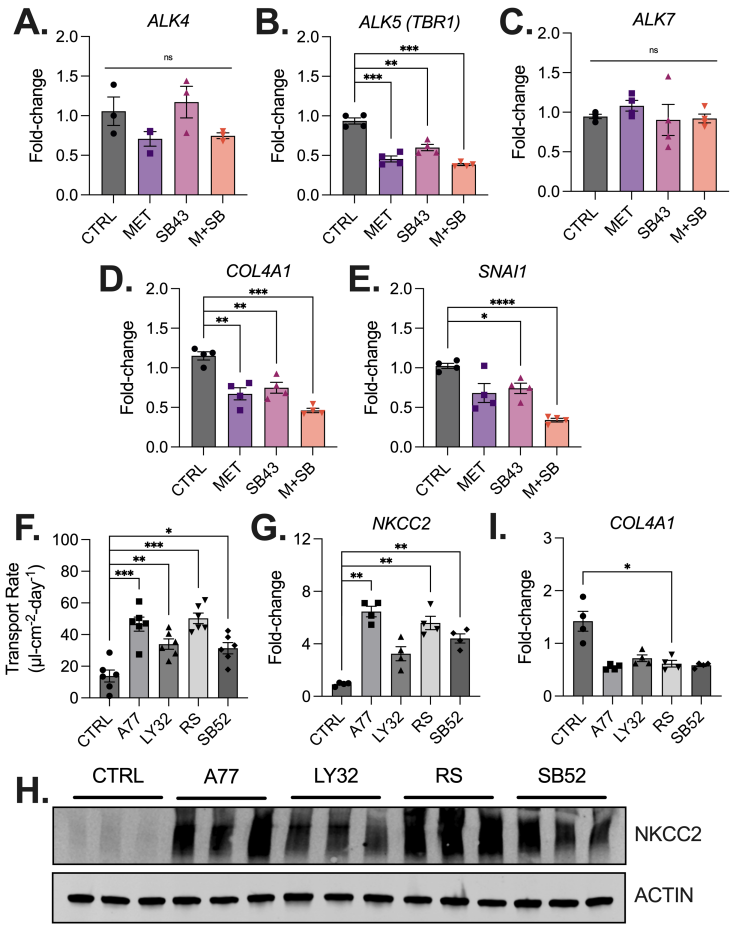

Figure 6.3: **ALK5 governs NKCC2 expression. A.** RNA expression of ALK4, **B.** ALK5 (TGF-β receptor I), **C.** ALK7, **D.** Collagen 4 alpha chain 1 (Col4α1), and **E.** Snail1 (Snai1). **F.** Apicobasal volume transport. **G.** RNA expression of NKCC2. **H.** Protein expression of NKCC2 and β-actin. **I.** RNA expression of Col4α1. Data are mean $\pm$ SEM.*p<0.05, **p<0.01, ***p<0.001, ****p<0.0001.

shown by the decrease in phosphorylation of each protein with treatment (Fig. 6.4B). Total P70S6K expression increases with treatments, though P70S6K phosphorylation does not significantly change for any treatment. There is a reduction in total TGF-activated kinase 1 (TAK1) expression with SB431542 and combination treatment. To determine if inhibition of non-canonical TGF-β signaling pathways can recapitulate the effects of SB431542 on NKCC2 expression, we test several non-canonical TGF-β inhibitors, including the PI3K inhibitor LY294002, the Mechanistic target of Rapamycin (mTOR) inhibitor Rapamycin, the p38 Mitogen-activated protein kinase (MAPK) inhibitor SB203580, TAK1 inhibitor Takinib, and the Mitogen-activated protein kinase kinase (MEK)1/2 inhibitor Trametinib. As shown in Chapter 5, we have previously demonstrated that inhibition of non-canonical TGF-β signaling pathways do not increase apicobasal fluid transport. Here, we find that none of the non-canonical inhibitors significantly increased NKCC2 mRNA or protein expression (Fig. 6.4C-D), nor do they alter the expression of fibrotic marker Col4α1 (Fig. 6.4E).

6.2.4 Canonical Smad-dependent TGF-β signaling governs NKCC2 transcription

Modulation of non-canonical TGF-β pathways does not alter NKCC2 expression, so we next investigate whether modulation of canonical Smad-transduced TGF-β signaling will alter NKCC2 expression. First, we determine whether SB431542 has any effect on Smad activity. SB431542 suppresses Smad2 and Smad3 activity, as shown by reductions in Smad2 and Smad3 protein phosphorylation (Fig. 6.5A). There is no significant change in Smad4 protein expression. We next test Smad3 inhibitor SIS3 to determine if Smad3 inhibition is sufficient to recapitulate the effects of SB431542 on NKCC2 expression. Smad2 and Smad4 are not tested in this manner, because to the best of our knowledge there are currently no known direct inhibitors of Smad2 or Smad4. SIS3 increases NKCC2 transcription (Fig. 6.5B) and decreases both Col4α1 and Snai1 transcription (Fig. 6.5C-D), suggesting that SB431542 is alleviating Smad3-dependent repression of NKCC2 transcription.

6.2.5 Smad/Snail1 signaling axis governs NKCC2 expression

Smads have weak DNA binding affinity, so Smad complexes interact with a wide variety of DNA-binding proteins to cooperatively regulate the expression of target genes. Snail1 is a target of canonical Smad-dependent TGF-β signaling that is directly upregulated by the Smads (Medici et al., 2011; Yu et al., 2015a). Snail1 is itself a transcription factor involved in epithelial-mesenchymal transition that drives renal fibrosis and can be targeted to reverse established disease (Kaufhold and Bonavida, 2014; Grande et al., 2015). To investigate whether Snail1 may be an intermediary in the TGF-β induced repression of NKCC2, we perform an in silico analysis to determine the number of Smad2, Smad3, and Snail1 binding sites present in the NKCC2 promoter (Table 6.1). Smad2 has 12 binding sites on the NKCC2 promoter, while Smad3 has 3, and Snail1 has 15. This

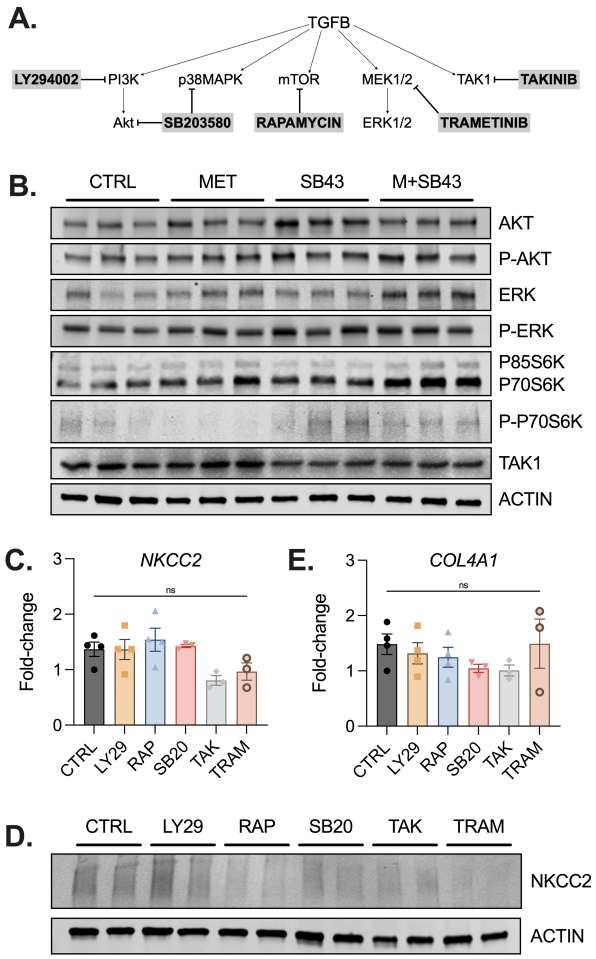

Figure 6.4: **Non-canonical TGF-β signaling does not govern NKCC2 expression**. **A.** . Diagram of non-canonical TGF-β pathways and small molecule inhibitors. **B.** Protein analysis of non-canonical TGF-β pathway activation. **C.** mRNA expression of NKCC2 in the presence of non-canonical TGF-β inhibitors. **D.** Protein analysis of NKCC2 expression in the presence of non-canonical TGF-β inhibitors. **E.** mRNA expression of Col4α1 in the presence of non-canonical TGF-β inhibitors. Data are mean $\pm$ SEM.*p<0.05, **p<0.01, ***p<0.001, ****p<0.0001.

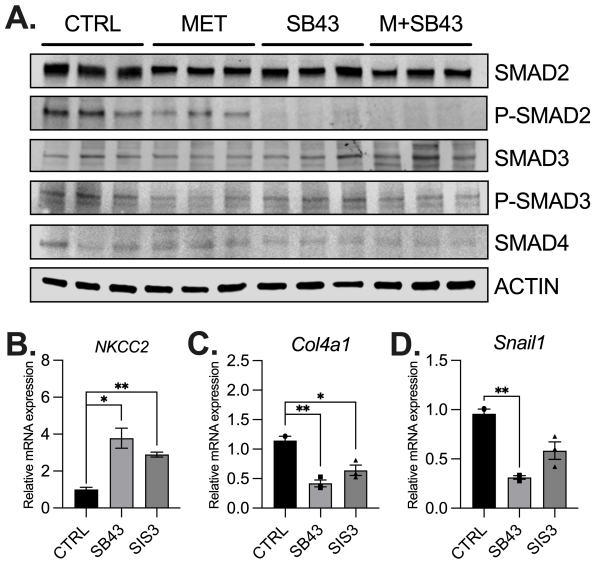

Figure 6.5: **Canonical Smad-dependent TGF-β signaling governs NKCC2 transcription. A.** Protein analysis of canonical TGF-β signaling intermediates. **B.** Effect of Smad inhibition on mRNA expression of NKCC2, **C.** Col4α1, and **D.** Snail1. Data are mean $\pm$ SEM.*p<0.05, **p<0.01, ***p<0.001, ****p<0.0001.

suggests that the Smads may be acting on NKCC2 directly or through their downstream target Snail1.

Next, we construct knockout (KO) models of Smad2, Smad3, Smad4, and Snail1, respectively, to determine if the inactivation of these genes can modulate NKCC2 expression. CRISPR-Cas9 targeting causes significant decreases in mRNA and protein expression in each of the targeted genes (Fig. 6.6A-D,F). NKCC2 mRNA expression, however, significantly increases with only Smad2 and Smad4 KO (Fig. 6.6E). Protein expression of NKCC2, however, is increased with only Smad2 KO (Fig. 6.6G). PiggyBac transposons are then used to induce overexpression of Smad2, Smad3, Smad4, and Snail1 in each of their knockout models, respectively. Rescue of Smad2, Smad3, Smad4, and Snail1 significantly increase the mRNA expression of each gene (Fig. 6.6H-K). Smad2 and Smad4 rescue causes increases in Smad2 and Smad4 protein expression, while Smad3 rescues causes increases in Smad2, Smad3, and Smad4 protein expression, and Snail1 rescues causes increases in Snail1 protein expression (Fig. 6.6M). Although NKCC2 mRNA expression does not significantly change in any overexpression group (Fig. 6.6L), NKCC2 protein expression significantly decreases in Smad2, Smad3, Smad4, and Snail1 rescue groups (Fig. 6.6M), supporting the hypothesis that the Smad/Snail1 signaling axis suppresses NKCC2 expression in renal tubule epithelial cells.

6.2.6 Smad/Snail1 signaling axis suppresses HNF-1α

Negative regulation of transcription cannot fully explain what induces positive expression of a certain gene. Therefore, we next investigate whether the Smads are repressing HNF-1α, a known transcriptional activator of

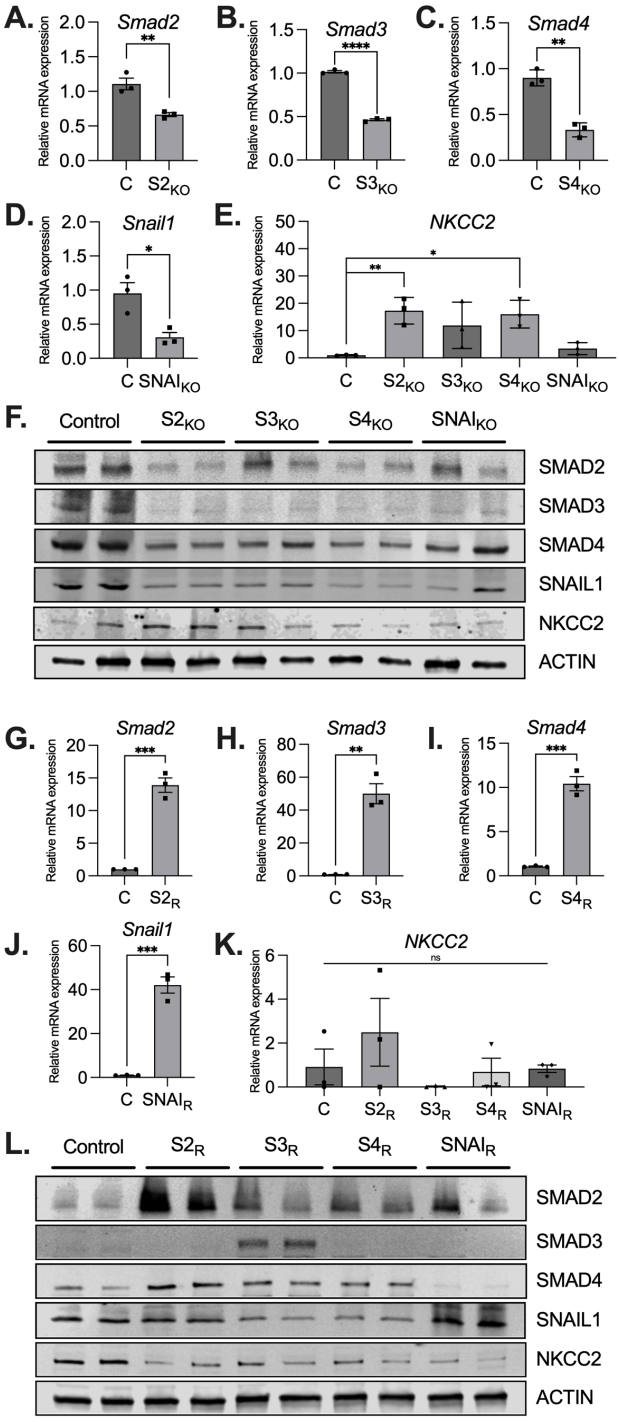

Figure 6.6: **The Smad/Snail1 axis governs NKCC2 expression. A.** mRNA expression of Smad2 CRISPR knockout (KO), **B.** Smad3 CRISPR KO, **C.** Smad4 CRISPR KO, **D.** Snail1 CRISPR KO, and **E.** NKCC2 in Smad2/3/4 and Snail1 KO cells. **F.** Protein expression analysis of Smad2/3/4 and Snail1 KO cells. **G.** mRNA expression of Smad2 PiggyBac (Pb) overexpression, **H.** Smad3 Pb overexpression, **I.** Smad4 Pb overexpression, **J.** Snail1 Pb overexpression, and **K.** NKCC2 in Smad2/3/4 and Snail1 Pb overexpression cells. **L.** Protein expression analysis of Smad2/3/4 and Snail1 KO cells. Data are mean ± SEM.*p<0.05, **p<0.01, ***p<0.001, ****p<0.0001.

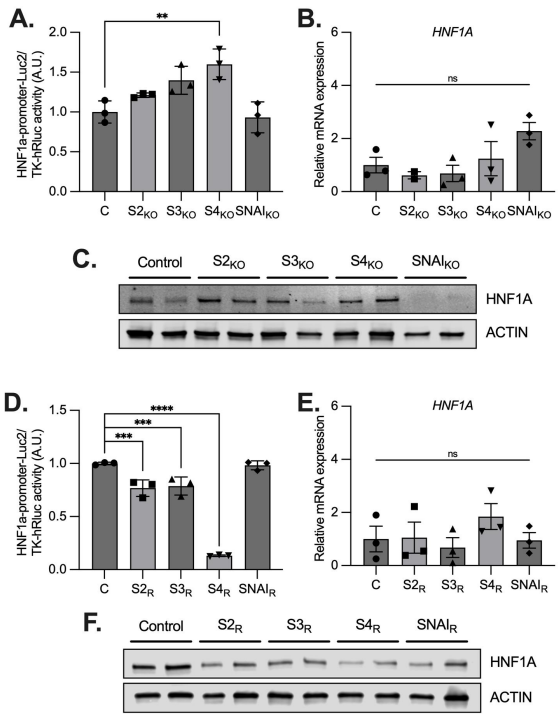

Figure 6.7: **The Smad/Snail1 signaling axis suppresses HNF-1α A.** Luciferase HNF-1α promoter activation assay in Smad2/3/4 and Snail1 KO cells. **B.** mRNA expression of HNF-1α in Smad2/3/4 and Snail1 KO cells. **C.** Protein expression of HNF-1α and loading control β-actin in Smad2/3/4 and Snail1 KO cells. **D.** Luciferase HNF1α promoter activation assay of Smad2/3/4 and Snail1 overexpression cells. **E.** mRNA expression of HNF-1α in Smad2/3/4 and Snail1 overexpression cells. **F.** Protein expression of HNF-1α and loading control β-actin in Smad2/3/4 and Snail1 overexpression cells. Data are mean $\pm$ SEM.*p<0.05, **p<0.01, ***p<0.001, ****p<0.0001.

NKCC2. First, we perform an in silico analysis to assess the number of Smad2, Smad3, and Snail1 binding sites present in the HNF-1α promoter (Table 6.1). We also verify the number of HNF-1α binding sites present in the NKCC2 promoter (Table 6.1). To determine if Smad2, Smad3, Smad4, and Snail1 KO and overexpression alters the activation of the HNF-1α promoter, we perform a luciferase reporter assay on the HNF-1α promoter. Smad4 KO increases HNF-1α promoter activity (Fig. 6.7A), while Smad2, Smad3, and Smad4 rescue decreases HNF-1α promoter activity (Fig. 6.7B). Next, we assess whether Smad2, Smad3, Smad4, and Snail1 KO and overexpression changes mRNA expression of HNF-1α. (Fig. 6.7C-D). Protein expression significantly increases with Smad2, Smad3, Smad4, and Snail1 KO, confirming luciferase assay results (Fig. 6.7E-F). While HNF-1α mRNA expression does not significantly change with Smad2, Smad3, Smad4, and Snail1 KO, HNF-1α protein expression decreases for all groups.

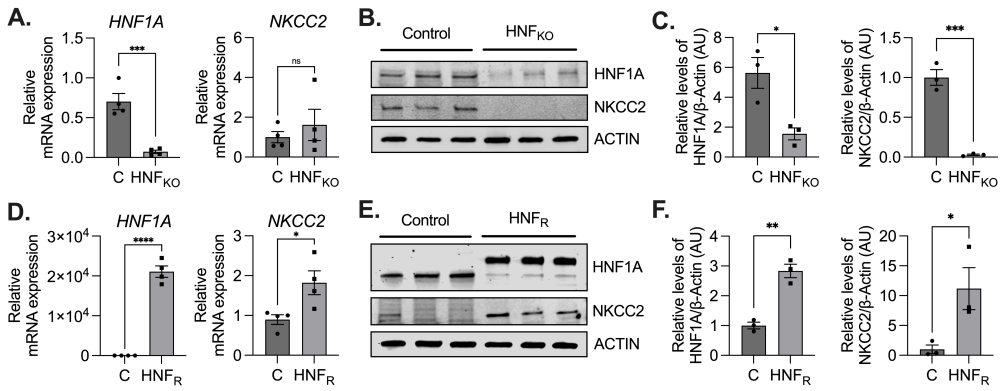

Figure 6.8: **HNF-1α governs NKCC2 expression. A.** HNF-1α and NKCC2 mRNA expression in HNF-1α CRISPR knockout (KO) cells **B.** Western blot protein expression analysis of HNF-1α, NKCC2, and loading control β-actin in HNF-1α CRISPR KO cells. **C.** Protein densitometry analysis of data in panel B. **D.** HNF-1α and NKCC2 mRNA expression in HNF-1α PiggyBac (Pb) overexpression cells. **E.** Western blot protein expression analysis of HNF-1α, NKCC2, and loading control β-actin in HNF-1α Pb overexpression cells. **D.** Protein densitometry analysis of data in panel E. Data are mean $\pm$ SEM.*p$<$0.05, **p$<$0.01, ***p$<$0.001, ****p$<$0.0001.

6.2.7 HNF-1α governs NKCC2 expression

To determine if modulation of HNF-1α is sufficient to change NKCC2 expression, we construct a HNF-1α KO and overexpression models. First, we perform a luciferase reporter assay to verify that HNF-1α KO and overexpression alter NKCC2 promoter activation (Fig. 6.10. NKCC2 activity is significantly reduced with HNF-1α, increased with HNF-1α overexpression. HNF-1α KO causes a significant reduction in HNF-1α mRNA and protein expression (Fig. 6.8A-B), while HNF-1α overexpression causes a significant increase in HNF-1α mRNA and protein expression (Fig. 6.8D-E). Although HNF-1α KO does not significant alter NKCC2 mRNA expression, HNF-1α overexpression significantly increases NKCC2 mRNA (Fig.6.8A,D). NKCC2 protein expression follows the same trend (Fig. 6.8E-F). Lastly, we perform a luciferase assay to determine if modulation of HNF-1α is sufficient to change activation of the NKCC2 promoter. HNF-1α KO significantly reduces the activity of the NKCC2 promoter while HNF-1α overexpression increases the activity of the NKCC2 promoter (Fig. 6.8E).

6.3 Discussion

Native renal epithelia are characterized by an elaborate array of sodium transporters which enable the orchestrated reabsorption and secretion of a diverse array of ions whilst maintaining normal cellular homeostasis. Understanding the intricacies of how these transporters are regulated will enable the development of in vitro culture conditions that enable cells to phenocopy their in vivo counterparts for use in the bioartificial kidney. We found that small molecule TGF-β inhibitor SB431542 increased NKCC2 expression and habitable

apicobasal fluid transport (Fig. 6.2). Further, this effect was increased with the addition of metformin. NKCC2 is primarily found in the thick ascending limb (TAL) of the loop of Henle. TAL cells perform approximately 30% of tubular water reabsorption making them an appealing cell type in the implementation of a bioartificial kidney (Ares et al., 2011).

The biological effects of TGF-β family members are highly context-dependent, responses may differ across tissue types, local environments, and stages of disease progression. TGF-β suppresses epithelial cell tumorigenesis at early stages and activates cytostatic and cell death processes that maintain homeostasis in mature tissues. The TGF-β signaling cascade is initiated when the TGF-β1 ligand is released from the TGF-β latency complex in the extracellular matrix and binds with one of its type II receptors, ALK4, ALK5 or ALK7. mRNA expression of ALK5 significantly decreased with metformin, SB431542, and combination treatment, while mRNA expression of ALK4 and ALK7 remained unchanged (Fig. 6.3A-C). Metformin, SB431542, and combination treatment all significantly suppressed the transcription of Col4α1 and Snai1 (Fig. 6.3D-E). Administration of specific ALK5 inhibitors was sufficient to increase NKCC2 mRNA and protein level expression, in addition to apicobasal fluid transport (Fig. 6.3F-H). All ALK5 inhibitors suppressed transcription of Col4α1 (Fig. 6.3I). ALK4 and ALK7 do not appear to be significantly involved in governing NKCC2 expression. ALK5 initiates the canonical TGF-β signaling cascade when bound to the TGFβI ligand. ALK4 primarily initiates the activin signaling pathway while ALK7 primarily initiates the nodal signaling pathway. Both activin and nodal, when activated, however, recruit and phosphorylate the r-Smads, Smad2 and Smad3. While we did not genetically suppress the expression of ALK4 and ALK7 to isolate these responses, the corresponding data suggests that ALK5-dependent signaling is governing the effect of TGF-β inhibition on NKCC2 expression.

TGF-β initiates numerous signaling pathways involved in cell growth and tissue homeostasis (Fig. 6.4A). Metformin and SB431542 suppress phosphorylation of non-canonical TGF-β signaling pathways, including Akt, ERK, and P70S6K, and reduce expression of TAK1 (Fig. 6.4B), yet inhibition of these pathways using small molecule inhibitors, does not alter NKCC2 mRNA or protein expression (Fig. 6.4C-D). Interestingly, none of the inhibitors significantly altered Col4α1 transcription. These data suggest that non-canonical TGF-β signaling pathways are not involved in the mechanism by which SB431542 increases NKCC2 expression.

Smad2 and Smad3 are the primary regulators of canonical Smad-dependent TGF-β signaling. SB431542 reduces phosphorylation of Smad2 (Fig. 6.5A). SIS3-induced Smad3 inhibition is sufficient to increase NKCC2 transcription (Fig. 6.5B) and decrease Col4α1 transcription (Fig. 6.5C). SIS3, however, does not significantly alter Snail1 mRNA expression (Fig. 6.5D). We generated Smad2, Smad3, Smad4, and Snail1 KO and rescue models to elucidate the role of each protein in governing the effect of TGF-β inhibition on NKCC2 expression.

It is still unclear what exactly controls the DNA-binding specificity of different types of Smad complexes in

vivo. Smads have weak DNA binding affinity, so Smad complexes interact with a wide variety of DNA-binding proteins to cooperatively regulate the expression of target genes. A single Smad-binding element is not sufficient to bind an activated Smad complex, rather, Smad recruitment to DNA usually requires additional TF. Smad4 KO increased HNF-1α promoter activity (Fig. 6.7A), while Smad2 and Smad3 KO had no significant effect on HNF-1α promoter activity. This may be because Smad4, as the common Smad, has a role in transducing both Smad2 and Smad3 activity. Knockout of a singular r-Smad (e.g. Smad2 or Smad3) may not be sufficient to alleviate endogenous HNF-1α repression of its counterpart. Smad2, Smad3, and Smad4 overexpression reduced HNF-1α promoter activity (Fig. 6.7B), demonstrating that all three Smads repress HNF-1α activation. Smads function predominantly via chromatin remodeling. Activated Smad complexes show no transcriptional activity on naked DNA templates, but the same Smad complexes efficiently activated transcription from chromatin templates (Ross et al., 2006). Smad2 and Smad3 demonstrate differential transcriptional activity due to their nonoverlapped target gene binding specificity (Liu et al., 2016), which may explain why SIS3-induced Smad3 inhibition did not suppress Snail1 transcription (Fig. 6.3D), but Smad2 overexpression increased Snail1 protein expression (Fig. 6.7) The short DNA-binding site may be the key to the Smads' versatility since it allows the Smads to derive specificity primarily from the interacting factors (e.g. transcription factors, coactivators, and corepressors), rather than from the nucleotide sequence per se. TF can actively recruit Smads to DNA and can also bind adjacent to repeated Smad binding elements and synergize with the Smads to activate transcription.

Interventions on Snail1 expression did not affect HNF-1α promoter activity, although Snail1 KO and rescue both changed NKCC2 protein expression (Fig. 6.7, Fig. 6.6). Comparison between the two aforementioned figures suggests that Snail1 is governing NKCC2 expression independently of HNF-1α. Snail1 can directly bind the NKCC2 promoter sequence or may be interacting with other TF to modulate NKCC2 expression. Smad2, Smad3, and Smad4 overexpression were not sufficient to drive increased Snail1 protein expression in our model (Fig. 6.6L).

Hereafter, we discuss at length the clinical relevance of interactions between TGF-β, HNF-1α, and NKCC2. NKCC2 is encoded by 27 exons in the SLC12A1 gene. The human NKCC2 gene promoter contains consensus binding sites for various transcription factors (TF) (Igarashi et al., 1996). Nuclear run-off assays have demonstrated that kidney-specific expression of NKCC2 is due to interactions between kidney-enriched TF and regulatory elements in the 5'-flanked region of the SLC12A1 gene (Markadieu and Delpire, 2014). In a mouse model of renal organogenesis, expression of HNF-1α immediately precedes the expression of NKCC2 (Lazzaro et al., 1992). Deletion of a 280-bp segment of the NKCC2 promoter containing the putative HNF-1α binding site led to a 76% reduction in promoter activity (Igarashi et al., 1996). HNF-1α dysregulation in renal tubule epithelial cells is associated with various pathologies. HNF-1α mutations cause an autosomal

dominant form of diabetes mellitus (MODY3), renal dysplasia, and tubular dysfunction (Yamagata et al., 1996). Dysregulation of HNF-regulated genes is an integral part of the clear cell renal carcinoma and papillary renal cell carcinoma transcriptomes (Lindgren et al., 2017).

Evidence is emerging of cross-regulation between the TGF-β and HNF-1α signaling pathways. TGF-β causes transcriptional downregulation of HNF-1α within three hours of treatment, and of HNF-1α target genes within three to six hours of treatment (Bisceglia et al., 2019). Downregulation of HNF-1α target genes occurs before there is a significant change in HNF-1α protein expression, suggesting that TGF-β causes functional inactivation of HNF-1α before its transcriptional downregulation. HNF-1α knockdown is known to activate Akt and its downstream target mTOR in pancreatic cancer cells (Luo et al., 2015). In the liver, Akt2 phosphorylates and inhibits HNF-1α, thus relieving the suppression of hepatic PPARy expression and promoting tumorigenesis (Patitucci et al., 2017).

6.4 Conclusion

In this chapter, we demonstrate that TGF-β signaling suppresses NKCC2 transcription through the Smad/Snail signaling axis and by repressing transcription factor Hepatic Nuclear Factor 1α (HNF-1α). Genetic knockout of Smad2 increases protein expression of NKCC2, while genetic rescue of Smad2, Smad3, and Smad4 and Snail1 suppress NKCC2 protein expression. Independently, constituent HNF1α overexpression is sufficient to increase NKCC2 expression. Increased understanding of the interactions of these pathways provides relevant information for the development of cultured renal tubule epithelial cells with greater functional fidelity. This study also reveals new pharmacological and genetic targets that may be targeted for the treatment of CKD.

6.5 Materials and methods

6.5.1 Cell culture

Primary human renal tubule epithelial cells (HREC) were obtained from Innovative Biotherapies (Ann Arbor, MI). Cells were maintained in a 1:1 ratio of glucose-free DMEM/F12 media supplemented with 5.5mM glucose. Cells were seeded on polycarbonate Transwell inserts (Corning, Corning, NY) at a density of 100,000 cells cm-2 and left overnight to facilitate cell attachment. After 24 hours, cells were moved to an orbital shaker to simulate physiological shear stress (2 dyne cm^{-2}). After two weeks in culture, cells were supplemented apically with AMPK activator metformin (200μM), TGF-β receptor I inhibitor SB431542 (10μM), or a combination of both. Control cells were treated with DMSO vehicle control (1μl/ml). For ALK5 inhibition experiments, cells were treated apically with A7701 (0.5μm), LY3200882 (5μm), RepSox (1μm), or SB525334 (1μm). For non-canonical inhibition experiments, cells were treated apically with LY294002 (1μM), Rapamycin (40nM), SB203580 (1μM), Takinib (2nM), or Trametinib (2nM). Cells were cultured with

treatments for four weeks prior to staining and RNA and protein harvest.

6.5.2 Apicobasal transport

HREC were cultured on Transwell inserts as described above. After four weeks of treatment, cultures were aspirated and changed to fresh media. 24 hours later, apical media was aspirated and weighed. Three blank wells with the porous membrane occluded with epoxy were used as an evaporative control. Volume transport was assessed by determining the differences between initial volumes and final volumes, as estimated by weight, and correcting for evaporation.

6.5.3 RNA preparation and cDNA synthesis

Total RNAs were extracted with RNeasy kit (Qiagen, Valencia, CA) according to manufacturer's protocol and single-strand cDNA was synthesized using a high-capacity cDNA reverse transcription kit (Applied Biosystems, Carlsbad, CA).

6.5.4 Quantitative RT-PCR

Quantitative real-time polymerase chain reaction (RT-PCR) was used to assess RNA transcription. Primers were selected from the Harvard-Massachusetts General Hospital Primerbank and purchased from Sigma-Aldrich (St. Louis, MO) or designed using PrimerBLAST (NCBI, Bethesda, MD). RT-PCR was performed using Sso7d fusion protein polymerase (Bio-Rad Laboratories, Hercules, CA) using a Bio-Rad CFX96. RNA expression levels were normalized to the expression of the housekeeping gene GAPDH.

6.5.5 Immunoblotting

Cells were rinsed once with PBS and lysed in ice-cold lysis buffer (PBS containing 0.05% SDS, protease inhibitor, and phosphatase inhibitor). Cells were then scraped, collected, and sheared with a syringe. Total protein concentration was determined using bicinchoninic acid assay (Pierce Biotechnology, Waltham, MA). Protein lysates were separated on 4-20% precast linear gradient gels (Invitrogen). Blots were then transferred onto nitrocellulose membranes (Bio-Rad). Membranes were incubated overnight at 4°C with primary antibody diluted in 5% BSA (wt/vol) in TBST and detected using the appropriate near infrared (NIR) secondary antibody. Products were visualized by NIR fluorescence on an Odyssey CLx (LI-COR, Lincoln, NE). Band intensities were measured and normalized to loading using beta-actin using ImageStudio (LI-COR). For each protein target, the mean density of the control sample bands was assigned the arbitrary value of 1 with all individual densitometries being expressed relative to this mean.

6.5.6 Immunofluorescence imaging

Cells were washed three times with ice-cold PBS then fixed with 4% paraformaldehyde on ice for 20 minutes. Cells were washed three times with PBS then permeabilized with 0.1% Triton X-100 and rinsed with PBS. Cells were then blocked with 5% goat serum in PBS/BSA for 1 hour. Cells were then incubated for 1 hour with primary antibody at 1:200 dilution. Cells were washed three times with PBS, then incubated for 1 hour at room temperature with the fluor-conjugated secondary antibody at 1:10,000 dilution. Cells were then washed overnight with PBS. Polycarbonate membranes were then cut from the Transwell supports and mounted face up on glass slides with mounting media with DAPI (SouthernBiotech, Birmingham, AL). Cells were imaged using a Zeiss LSM710 confocal microscope with ZEN Black software (Carl Zeiss AG, Oberkochen, Germany).

6.5.7 In silico promoter analysis

Promoters for each gene were located using UCSC Genome Browser. Promoter sequences were scanned for putative binding sites using Jaspar (Castro-Mondragon et al., 2022).

6.5.8 Plasmid preparation

Competent *E. coli* were obtained from VectorBuilder (Chicago, IL). Single colonies were isolated by streaking *E. coli* on LB-agar plates supplemented with 100μg/ml ampicillin. Individual colonies were used to inoculate LB broth supplemented with 100μg/ml ampicillin and shaken at 200rpm overnight at 37C. The following day, plasmids were isolated using a GenElute Maxi Prep kit (Sigma) according to the manufacturer's instructions. Plasmid concentrations were quantified using a NanoDrop.One (Thermo-Fisher).

6.5.9 Gene knockdown and rescue

HEK293 (ATCC, Manassas, VA) were plated at a density of 5x105 in 6-well (35mm) plates to achieve 60-70% confluence the following day. For CRISPR experiments, cells were co-transfected with CRISPR sgRNA with PiggyBac (Pb) hygromycin resistance and eGFP vectors and the m7pB hyperactive Pb transposase. Cells were co-transfected with 2.5μg total of donor vector and helper vector plasmids at a 3:1 ratio. For control transfection, cells were transfected with a scramble sequence. 48 hours post-transfection, cells were supplemented with 200μg/mL hygromycin. Hygromycin selection pressure was maintained for one week. Cells were passaged once then harvested for RNA and protein analysis. CRISPR knockout cells were then transfected with Pb rescue plasmids encoding an overexpression cassette for the gene of interest, a puromycin resistance cassette and an mCherry expression cassette. 48 hours post-transfection, cells were supplemented with 1μg/mL puromycin. Puromycin selection pressure was maintained for one week. Cells were passaged once then harvested for RNA and protein analysis.

6.5.10 Luciferase promoter activation

DNA promoter primers were designed using NEBuilder Assembly Tool (NEB) and synthesized by Sigma. Genomic DNA was harvested using a DNeasy Blood and Tissue Kit (Qiagen) according to the manufacturer's instructions. Promoter sequences were replicated by PCR using Q5 High-Fidelity 2X Master Mix (NEB) according to the manufacturer's instructions. Promoter sequences were then ligated to an empty firefly Luciferase pGL4.10 (*Luc2*) vector (Promega) using Blunt/TA Ligase Master Mix (NEB) according to the manufacturer's instructions. Previously transfected HEK293 gene knockout and rescue cells were then co-transfected with the ligated pGL4.10 vectors and a pGL4.74(*hRluc-TK*) renilla Luciferase vector with Lipofectamine LTX Plus according to the manufacturer's instructions. Cells were harvested 96 hours post-transfection and luminescence was measured using a Dual-Luciferase Reporter Assay (Promega). Experimental *Luc2* luminescence was normalized to *hRluc* luminescence to account for transfection efficiency.

6.5.11 Quantification and statistical analysis

All results are expressed at mean $\pm$ SEM of a minimum of three independent experiments. For comparison between two groups, statistical analysis was performed with a Student's t-test using Prism 9 (GraphPad, San Diego, CA). For comparison between three or more groups, statistical analysis was performed with one-way ANOVA using Prism 9. Significance was accepted at a level of $p<0.05$. At least three samples per group were used for statistically meaningful interpretation of results.

6.6 Appendix

Supplementary material is deferred to the following section. Section 6.6.1 provides further informative tables and Section 6.6.2 provide further supplemental figures.

6.6.1 Supplemental tables

Table 6.1 presents the results of the in silico transcription factor binding analysis. Table 6.2 presents the primers used to RT-PCR. Table 6.3 presents the primary antibodies used for immunoblotting and immunofluorescent staining. Table 6.4 presents the guide RNA sequences used for CRISPR-Cas9 knockout studies. Table 6.5 presents the primer sequences used to replicate the DNA promoter sequences for the luciferase reporter assays.

Table 6.1: **Putative transcription factor binding site analysis.**

		Number of binding sites			
Promoter		Smad2	Smad3	Snail1	HNF-1α
	Snail1	11	2	11	6
	HNF-1α	15	3	13	3
	NKCC2	12	2	15	6

Table 6.2: **RT-PCR primers.**

Target	**Forward (5' to 3')**	**Reverse (5' to 3')**
ALK4	CCGGGAAGCCCTTCTACTG	CTCAAGTCGATCCTGTTGCAG
ALK5 (TBR1)	ACGGCGTTACAGTGTTTCTG	GCACATACAAACGGCCTATCTC
ALK7	TGAACAGGGCTCCTTATATGACT	GTGTGCCAGACCACTAGCAA
Col4α1	GGGATGCTGTTGAAAGGTGAA	GGTGGTCCGGTAAATCCTGG
GAPDH	AATCCCATCACCATCTTCCA	TGGACTCCACGACGTACTCA
HNF-1α	AACACCTCAACAAGGGCACTC	CCCCACTTGAAACGGTTCCT
NKCC2	GCCAGTTTTCACGCTTATGATTC	CTATCTTGGGAACGGCATCCA
Smad2	CCGACACACCGAGATCCTAAC	GAGGTGGCGTTTCTGGAATATAA
Smad3	TGGACGCAGGTTCTCCAAAC	CCGGCTCGCAGTAGGTAAC
Smad4	CTCATGTGATCTATGCCCGTC	AGGTGATACAACTCGTTCGTAGT
Snail1	TCGGAAGCCTAACTACAGCGA	AGATGAGCATTGGCAGCGAG

Table 6.3: **Primary antibodies used for immunoblotting and immunofluorescence imaging.**

Target	Manufacturer	Catalog number
Akt (total)	Cell Signaling	4685S
Beta-Actin	Santa Cruz Biotechnologies	sc-47778
ERK1/2	Cell Signaling	9102S
HNF-1α	Cell Signaling	89670S
NKCC2	ProteinTech Group	18970-1-AP
P70S6K	Cell Signaling	2708S
Phospho-Akt	Cell Signaling	4060s
Phospho-AMPK	Cell Signaling	2535S
Phospho-ERK1/2	Cell Signaling	9101S
Phospho-P70S6K	Cell Signaling	9204S
Phospho-Smad2	Cell Signaling	18338S
Phospho-Smad3	Cell Signaling	9520S
Smad2 (total)	Cell Signaling	5339S
Smad3 (total)	Cell Signaling	9523S
Smad4	ProteinTech Group	10231-1-AP
Snail1	ProteinTech Group	13099-1-AP
TAK1	Cell Signaling	4505S
ZO-1	Invitrogen	33-9100

Table 6.4: **CRISPR guide RNA (gRNA) design.**

Name	Guide sequence (5' to 3')	Strand	Target location
Scramble	GTGTAGTTCGACCATTCGTG	-	-
Smad2	TATATTGCCGATTATGGCGC	Coding	61811-61830
Smad3	GGAATGTCTCCCCGACGCGC	Template	115679-115698
Smad4	TCTGTCGATGCACGATTACT	Template	24670-24689
Snail1	AGTTGAAGGCCTTTCGAGCC	Template	1210-1229
HNF-1α	TCGCTGCTTGCGGACGTACC	Template	11211-11230

Table 6.5: **DNA PCR primer design for promoter sequences.**

Name	Sequence (5' to 3')	Length
Snai1-promoter-fwd	TCAACAAGCTAAAGAAAAT AAAATCACATGACCGTATC AATAGATGCAGAAAACGAA TTTGGCAAAATCCAACATTC	77
Snai1-promoter-rev	CCCCCGCCTCCTCCCGCG	18
HNF-1α-promoter-fwd	CTGGCTTGCCTTCAGTCATTTG	22
HNF-1α-promoter-rev	AAGCTGAGGCAGAGAGTG	18
NKCC2-promoter-fwd	TAATCAACAATGAATTAT TTTTATTATTAAAAGTATATGGTAAT CAACTCAAGGTTTATGTATTGG	66
NKCC2-promoter-rev	GAAGCAGCAGCCGCAGCA	18

6.6.2 Supplemental figures

Figure 6.9 presents NKCC2 immunofluorescent staining in HREC treated with ALK5 (TβRI) inhibitors A7701, LY3200882, RepSox, and SB525334. Figure 6.10 presents luciferase reporter assays conducted on HNF-1α knockout and over expression models that probe activation of the NKCC2 promoter.

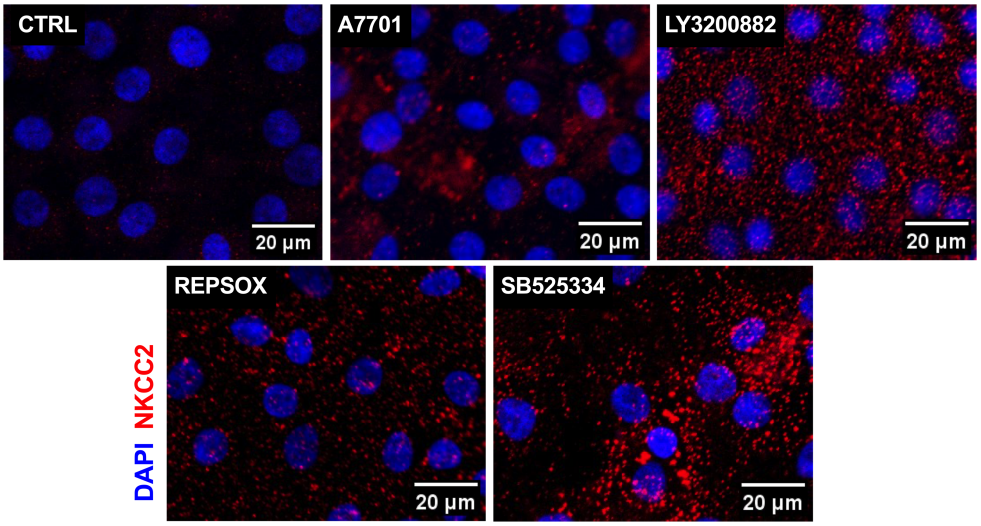

Figure 6.9: **NKCC2 staining increases with ALK5 inhibition.**

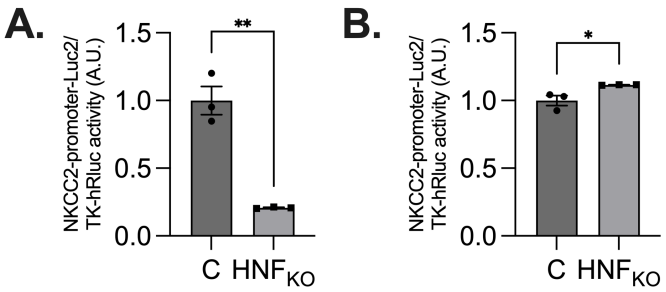

Figure 6.10: **HNF-1α governs activation of the NKCC2 promoter.**

CHAPTER 7

Conclusions & future directions

7.1 Conclusions

Chronic kidney disease is a major cause of death worldwide, yet the mechanisms underlying its development are still not fully understood. Metabolic dysregulation and fibrosis of the renal parenchyma are increasingly appreciated to be both causes and consequences of CKD that contribute to renal tubule epithelial cell dedifferentiation and loss of function. This dissertation is devoted to the study of the mechanisms underlying these phenomena. The contributions presented in this dissertation are the following:

First, we studied whether modulation of the TGF-β signaling pathway is sufficient to enhance differentiation in renal proximal tubule epithelial cells. We found that inhibition of the canonical TGF-β signaling pathway is sufficient to induce multiple specific differentiation functions characteristic of a healthy proximal tubule cell, even with prolonged (more than approximately 40 weeks) culture. Differentiated cells performed sodium reabsorption, para-amino hippurate excretion, and glucose uptake. The specificity of each response was demonstrated using inhibitors of each transport protein.

In the second part of this dissertation, we studied the mechanisms by which AMPK and TGF-β cooperatively govern renal tubule epithelial cell glycolytic and oxidative metabolism. Metabolic dysregulation is a critical feature of renal tubule cell dedifferentiation in vitro, that limits the functional fidelity of these cells. We observed that AMPK activation and TGF-β inhibition synergistically increase the expression and activity of human renal tubule cell glycolytic and mitochondrial metabolic machinery. AMPK activator metformin increased glycolysis and reduced electron transport chain glucose dependency, thus decreasing coupling efficiency while increasing spare respiratory capacity. TGF-β inhibitor SB431542 reduced glycolysis while increasing cell oxidative phosphorylation and electron transport chain fatty acid dependency. We found that metformin and SB431542 ameliorate the metabolic dysregulation brought on by cell culture stress by increasing the flux of glucose towards oxidative phosphorylation, suggesting that these two pathways may be the key to reversing in vitro metabolic dysfunction of renal tubule cells.

In the third part of this dissertation, we explore the Smad/Snail/HNF1α signaling axis and its role in governing NKCC2 expression. We find that genetic knockdown of Smad2 is sufficient to increase NKCC2 protein expression in vitro, and rescue of Smad2, Smad3, Smad4, and Snail1 are sufficient to suppress this effect. The role of the Smad/Snail signaling axis in suppressing NKCC2 transcription factor HNF-1α is explored. Smad4 knockout was found to be sufficient to increase activity of the HNF-1α promoter,

while Smad2, Smad3, and Smad4 overexpression suppressed HNF-1α promoter activation. Finally, genetic overexpression of HNF-1α was demonstrated to be sufficient to increase NKCC2 expression.

These contributions further advance the development of fully differentiated cultured renal tubule epithelial cells suitable for use in the bioartificial kidney. They also provide insights that may be useful for developing new therapeutic and genetic targets for the treatment of renal metabolic disorders, loop disorders, and chronic kidney disease.

7.2 Concerns & limitations

In this section, concerns and limitations of the work depicted in this dissertation are addressed.

Posttranslational modifications of NKCC2. Posttranslational mechanisms of transporter regulation include protein trafficking, phosphorylation and protein-protein interactions. In this manuscript it was not explored in depth although, posttranslational mechanisms of NKCC2 activation should be further explored. In order to lay some background first, NKCC2 is a direct substrate of AMPK at Ser126. AMPK remains an important regulator of NKCC2-mediated salt retention in the medullary thick ascending limb of the loop of Henle. AMPK phosphorylation of NKCC2 may be further examined as a mechanism of NKCC2 activation. AMPK also indirectly modulates NKCC2 activity via the Renal outward medullary potassium channel (ROMK). ROMK is a membrane protein that is required for NKCC2 function as it allows recirculation of absorbed K^+ ions. AMPK inhibits ROMK by down-regulating channel activity and membrane abundance.

With no lysine kinase 4 (WNK4) is another protein that modulates NKCC2 activity that can be further explored. Non-canonical TGF-β intermediaries PI3K and Akt modulate the stability of WNK4 via Ketch-Like family member 3 (KLHL3), regulates WNK protein degradation. Yoshizaki et al. (2015) have demonstrated that Akt-mediated phosphorylation of KLHL3 reduces its interaction with WNK4, leading to sustained WNK4 expression. WNK4 may also contribute to a feedback loop between NKCC2 activation and TGF-β signaling because WNK4 binds and phosphorylates TGF-β signaling intermediates Smad2 and Smad3. Expanding on the work shown in Chapter 6, TGF-β strongly effects posttranslational modification patterns on the HNF-1α protein, which may account for altered interactions of HNF-1α and its coactivator CBP/p300 in the presence of TGF-β.

Transcription factor DNA binding activity. To expand on Chapter 6, the DNA binding activity of HNF-1α and the receptor-actived Smads (r-Smads), Smad2 and Smad3, can be further explored. Chromatin immunoprecipitation or electrophoretic mobility shift assays may be used to assess the occupancy of HNF-1α binding sites in the NKCC2 promoter in the presence and absence of TGF-β inhibitors or genetic manipulations. TGF-β has been found to override HNF-1α constitutive expression, so co-immunoprecipitation assays may also be conducted to assess the protein-protein interactions of the r-Smads, HNF-1α, and CBP/p300.

Transcription factors other than HNF-1α, such as cAMP response element-binding protein (CREB), may also be playing a role in the mechanisms by which AMPK and TGF-β modulate NKCC2 expression and activation. Mammalian NKCC2 promoters share a conserved 21bp CREB binding sequence. Two overlapping CREB sites are also located very close to the TATA box in the human NKCC2 promoter. AMPK phosphorylates the CREB activator CREB Regulated Transcription Coactivator 2 (CRTC2). TGF-β is known to modulate CREB activity through Smad3, ERK1/2, and MAPK signaling. Similarly to HNF-1α, CREB requires additional regulatory partners, such as CBP/p300, for recruitment to target gene promoters. For this reason, CREB may be suppressed by TGF-β sequestration of the CBP/p300 complex.

7.3 Future work

The work depicted in this manuscript invites further exploration of the interactions between cell signaling pathways and metabolic reprogramming. These contributions should not considered as a dead end and can be leveraged toward new directions. Hence, several points discussed in this dissertation can be further developed. This section depicts some perspectives related to the problems tackled in this thesis.

Smad dependent fatty acid oxidation. As mentioned in Chapters 3 and 5, fatty acid β-oxidation is key contributor to renal tubule ATP generation. In Chapter 5, TGF-β inhibition is demonstrated to increase fatty acid oxidation dependency. While we demonstrate an increase in fatty acid oxidation machinery (e.g. CPT2, ACOX2, FABP1, CD36), the specific mechanisms driving these changes in mRNA and protein expression remain obscure. To further characterize the metabolic switch that occurs in renal tubule epithelial cells in vitro, the role of the Smad proteins in mediating fatty acid oxidation must be elucidated. For example, one may rely on models developed in Chapter 6 to perform RNA sequencing, proteomic, or respirometry experiments. Differential suppression of the Smad proteins may uncover new insights that are overshadowed by the use of off-target effects caused by small molecule inhibitors.

HNF-1α dependent metabolism. HNF-1α is a key regulator of numerous essential metabolic processes in the adult kidney. The methodology used in Chapter 5 can be extended to further examine the role of HNF-1α in governing renal tubule epithelial cell metabolism. HNF-1α regulates G6P and GLUT2 transcription, in addition to transporters that impact amino acid metabolism, and sodium-dependent phosphate transporters NPT1 and NPT4 (Hiraiwa et al., 2001; Pontoglio et al., 2000; Cheret et al., 2002). It is feasible that TGF-β may be negatively regulating renal tubule cell metabolism through suppression of HNF-1α.

HNF-1α is also known to interact with several non-canonical TGF-β signaling pathways, which could alter tubule cell metabolic processes. HNF-1α knockdown activates Akt and its downstream target mTOR in pancreatic cancer cells (Luo et al., 2015). In the liver, Akt2 phosphorylates and inhibits HNF-1α, thus relieving the suppression of hepatic PPAR-γ expression and promoting tumorigenesis (Patitucci et al., 2017). Further,

HNF-1α-null mice express a loss of renal membrane transporters of the SLC6A family which manifests as increased proline and urine, and overexpression of aldosterone (Bonzo et al., 2010).

Role of inhibitory Smads. Chapter 6 explores the role of the receptor-activated Smads, Smad2 and Smad3, and the common Smad, Smad4, in mediating the effect of TGF-β in governing the expression of NKCC2, but the roles of the inhibitory Smads (i-Smads), Smad4 and Smad7, has yet to be explored. Building on Chapter 6, Smad4 and Smad7 overexpression experiments may be conducted to determine if the i-Smads are involved in the regulation of HNF-1α or NKCC2. Similarly, one may examine whether overexpression of the i-Smads is sufficient to reverse cell glycolytic phenotype.

Role of micro-RNAs. Micro RNAs (miRs) are small noncoding RNAs that regulate gene expression and renal tubule maturation through mRNA decay and translational repression. miR-192 and miR-194 are highly expressed in the human kidney and are involved in renal fluid handling. Knockdown of miR-192 leads to upregulation of Atp1b1 in mice (Mladinov et al., 2013). Microarray analysis of microdissected tubule segments has determined that various tubule segments (e.g. glomerulus, proximal tubule, thick ascending limb) are uniquely enriched for different miRNAs (Mladinov et al., 2013). Hence, miRNA may feasibly contribute to the segment-specific enrichment of renal transporters. The role of miRs in mediating the effect of TGF-β on NKCC2 expression and protein activation is another avenue that can be further explored.

Several miRNA are known to potentiate the development of CKD and alter renal cell metabolic programming. To illustrate, miR-21 promotes fibrosis of the kidney by silencing metabolic pathways (Chau et al., 2012). One may investigate whether miR-21 is mediating the changes in renal metabolism observed in Chapter 5. A second illustration is provided by miR-132 as it directly targets cyclooxygenase-2 (COX-2), an enzyme involved hypertension and the metabolism of essential fatty acids van Zonneveld et al. (2020). The direct link between cell respiration and transport phenotype may be explained by miR-132.

CHAPTER 8

Appendix

8.1 Experimental protocols

Hereafter are detailed the experimental protocols utilized to reproduce experiments depicted in this dissertation.

8.1.1 Mitochondrial respiratory stress test

1. One day prior to running the assay, hydrate a sensor cartridge with hydration buffer and incubate at 37C in a non-CO_2 incubator
2. Warm assay medium to 37C
3. Adjust pH to 7.3 with 0.1N NaOH and sterile filter; Keep medium at 37C until ready to use
4. Prepare injection compounds by diluting stocks in pre-warmed media
   - Oligomycin: Prepare 3mL of 16μm working solution
   - CCCP: Prepare 3mL of 108μm working solution
   - Rotenone+Antimycin A: Prepare 3mL of 5mM working solution
5. Load prepared compounds into the hydrated sensor cartridge using an electronic pipette
   - 25μl oligomycin in Port A (final concentration 2μM)
   - 25μl CCCP in Port B (final concentration 12μM)
   - 25μl Rotenone+Antimycin A in Port C (final concentration 0.5μM)
6. Return the loaded sensor cartridge to a 37C non-CO_2 incubator for one hour to degas
7. Change media in the cell plate to the pH-adjusted, pre-warmed media using a plate washer. Ensure that wells have a final volume of 175μl of media
8. Return the cell plate to a 37C non-CO_2 incubator for one hour to degas
9. After one hour, run the assay using the saved assay template on the Seahorse XFe96
10. When the assay is completed, gently wash cells three times with 1X PBS using a multichannel pipette
11. Fix cells with 4% paraformaldehyde on ice for 20 minutes
12. Wash cells three times with 1X PBS
13. (*Optional*) Stain cells as desired for immunofluorescent analysis
14. Mount cells with VectaShield containing DAPI and let dry overnight
15. Image cells for DAPI (and other fluors as desired) using the ImageXpress Micro Confocal High-Content Imaging System
16. Quantify staining (e.g. nuclear count) using MetaXpress
17. Normalize respiratory data by adding well-by-well nuclear count

8.1.2 Glycolytic respiratory stress test

1. One day prior to running the assay, hydrate a sensor cartridge with hydration buffer and incubate at 37C in a non-CO_2 incubator
2. Prepare glucose-free assay medium and warm to 37C
3. Adjust pH to 7.3 with 0.1N NaOH and sterile filter; Keep medium at 37C until ready to use
4. Prepare injection compounds by diluting stocks in pre-warmed media
    - Glucose: Prepare 3mL of 100mM working solution
    - Oligomycin: Prepare 3mL 20μm working solution
    - 2-deoxy-D-glucose (2-DG): Prepare 3mL of 500mM working solution
5. Load prepared compounds into the hydrated sensor cartridge using an electronic pipette
    - 25μl glucose in Port A (final concentration 10mM)
    - 25μl oligomycin in Port B (final concentration 2μM)
    - 25μl 2-DG in Port C (final concentration 50mM)
6. Return the loaded sensor cartridge to a 37C non-CO_2 incubator for one hour to degas
7. Change media in the cell plate to the pH-adjusted, pre-warmed media using a plate washer. Ensure that wells have a final volume of 175μl of media
8. Return the cell plate to a 37C non-CO_2 incubator for one hour to degas; cells will be glucose starved for one hour prior to assay, so be sure to time the assay properly
9. After one hour, run the assay using the saved assay template on the Seahorse XFe96
10. When the assay is completed, gently wash cells three times with 1X PBS using a multichannel pipette
11. Fix cells with 4% paraformaldehyde on ice for 20 minutes
12. Wash cells three times with 1X PBS
13. (*Optional*) Stain cells as desired for immunofluorescent analysis
14. Mount cells with VectaShield containing DAPI and let dry overnight
15. Image cells for DAPI (and other fluorophores as desired) using the ImageXpress Micro Confocal High-Content Imaging System
16. Quantify staining (e.g. nuclear count) using MetaXpress
17. Normalize respiratory data by adding well-by-well nuclear count

8.1.3 Metabolic substrate dependency assay

1. One day prior to running the assay, hydrate a sensor cartridge with hydration buffer and incubate at 37C in a non-CO_2 incubator.
2. Prepare glucose-free assay medium and warm to 37C.
3. Adjust pH to 7.3 with 0.1N NaOH and sterile filter; Keep medium at 37C until ready to use.
4. Prepare injection compounds by diluting stocks in pre-warmed media.
   - BPTES: Prepare 3mL of 100μM working solution.
   - Etomoxir: Prepare 3mL 10mM working solution.
   - UK5099: Prepare 3mL of 100μM working solution.
5. Load prepared compounds into the hydrated sensor cartridge using an electronic pipette:
   - Put 25μL inhibitor of the substrate of interest in Port A (e.g. BPTES to assess glutamine oxidation dependency, etomoxir to assess fatty acid oxidation dependency, and UK5099 to assess glucose oxidation dependency.
   - Put 27μl of the remaining inhibitors in Ports B and C, respectively.
6. Return the loaded sensor cartridge to a 37C non-CO_2 incubator for one hour to degas.
7. Change media in the cell plate to the pH-adjusted, pre-warmed media using a plate washer. Ensure that wells have a final volume of 175μl of media.
8. Return the cell plate to a 37C non-CO_2 incubator for one hour to degas; cells will be glucose starved for one hour prior to assay, so be sure to time the assay properly.
9. After one hour, run the assay using the saved assay template on the Seahorse XFe96. Program the software to:
   (a) Acquire $\geq$ five basal respiration measurements
   (b) Inject the contents of Port A (target inhibitor).
   (c) Acquire $\geq$ five respiration measurements in the presence of inhibitor A.
   (d) Inject the contents of Ports B and S (alternate substrates).
   (e) Acquire $\geq$ five respiration measurements in the presence of all three inhibitors.
10. When the assay is completed, gently wash cells three times with 1X PBS using a multichannel pipette.
11. Fix cells with 4% paraformaldehyde on ice for 20 minutes.
12. Wash cells three times with 1X PBS.
13. (*Optional*) Stain cells as desired for immunofluorescent analysis.
14. Mount cells with VectaShield containing DAPI and let dry overnight.
15. Image cells for DAPI (and other fluorophores as desired) using the ImageXpress Micro Confocal High-Content Imaging System.
16. Quantify staining (e.g. nuclear count) using MetaXpress.
17. Normalize respiratory data by adding well-by-well nuclear count.

8.1.4 Volume transport assay

Day prior to assay: determination of cell confluence

1. Prepare a 25X stock of sterile FITC-inulin by diluting 2.5mg in 1mL of sterile growth media
2. Dilute sterile FITC-inulin in sterile growth media (Add 20μL 25X stock for every 480μ media for a final concentration of 100μg/mL)
3. Change media on cells of interest:
    - Add 500μl of FITC-inulin supplemented media to the apical compartment
    - Add 1.5ml of FITC-inulin-free media in the basolateral compartment
4. Incubate at 37C in a 5% CO_2 for 24 hours
5. After 24 hours, collect 100μL samples from the apical and basolateral compartments of each transwell in a 96-well plate
6. Measure the fluorescence of the samples using a microplate reader
7. Plot the fluorescence data to determine if cells are confluent; confluent cells will have very little basolateral fluorescence; leaky cells will have fluorescence in the basolateral compartment and may have reduced apical fluorescence due to the dilution of FITC

Prior to the assay

- Mass and number sterile microtubes (equal to the number of transwells to be examined)
- Prepare ”blanks” by occluding the membrane of a transwell with medical grade epoxy; let cure for at least 96 hours prior to use in assay
- Sterilize ”blanks” by soaking in 70% ethanol for 24 hours prior to assay

Day of the assay

1. Change media on cells of interest
    - Distribute sterile ”blanks” so there are at least three in each cell plate
    - Aspirate media from cells
    - Add 500μL of media to the apical compartments of all transwell inserts, including ”blanks”
    - Add 1.5mL of media to the basolateral compartments of all transwell inserts, including ”blanks”
2. Incubate cells for 24 hours at 37C in 5% CO_2
3. After 24 hours, collect apical and basolateral media of each transwell (separately) into sterile microtubes
4. Add fresh growth media to cells
5. Mass tubes containing apical and basolateral samples
6. Calculate mass transfer by finding the difference in apical mass after 24 hours accounting for evaporation, surface area, and time

8.1.5 Immunoblotting of primary cell cultures

Sample preparation

1. Prepare 1X cell lysis buffer:
   - 1ml 10X cell lysis buffer (CellSignaling) + 9mL of dH_2O
   - 50μL 200mM phenylmethylsulfonyl fluoride (PMSF)
   - 1 tablet phosphatase inhibitor (Roch)
   - 100ul protease inhibitor 3 cocktail (Sigma)
2. Aspirate media from cells of interest
3. Gently wash cells with 1X PBS three times for two minutes
4. Harvest protein with 1X cell lysis buffer (200μL per well for a 6-well plate or 1mL for a 60-mm dish)
5. Immediately transfer lysed samples to a labeled microtube on ice.
6. Shear samples with a 21-27 gauge syringe 5-6 times to complete cell lysis, shear DNA, and reduce sample viscosity
7. Centrifuge samples at 10,000rpm for 1 minute to collect debris
8. Transfer supernatant to new labeled tubes and discard the pellet
9. Store samples at -20C

Protein sample quantification

1. Measure sample protein concentration using Pierce BCA Kit
2. Calculate volumes needed for 10μg/lane for each sample with equal loading volume

Loading gels

1. Prepare sample dilutions to achieve 10ug/lane (with 15-20% excess)
2. Add 30% volume of (4X loading buffer + 10% DTT)

Note: Use orange LICOR loading buffer for IR detection and blue Laemmeli buffer for ECL detection. Blue Laemmeli buffer will auto-fluoresce under infrared light causing high background signal.

3. Heat sample to 95-100C for five minutes
4. Microcentrifuge samples for one-two minutes at 4,000rpm to
5. Load lysate onto SDS-PAGE gel (4-20% Mini-PROTEAN TGX Precast Gels (Bio-Rad)); Be sure to load 1.5µl standard ladder in the first lane

Note: Samples should be at ROOM TEMPERATURE when loading. If kept on ice, samples will precipitate, which will cause uneven loading

6. Run gel at 200 volts for 35 minutes at room temperature (or until dye front reaches the bottom of the gel; if the tank starts to overheat, reduce the voltage and run for a longer period of time)

Protein transfer

1. Rinse tank and cassettes with deionized water.
2. Fill the tank half-way with transfer buffer.
3. Put a cold pack in the transfer tank.
4. Cut membrane to appropriate size. Take care not to touch the membrane. Cut one corner of the membrane to indicate the where the top of the standard will be.

Note: Use nitrocellulose if performing infrared detection (IR); use PVDF if using enhanced chemilumines-

cence (ECL) detection.

5. Wet membrane with transfer buffer.

Note: If using PVDF: Wet cut membrane with methanol (about 1ml), then add transfer buffer to membrane to thoroughly wet.

Note: If using nitrocellulose, transfer buffer alone may be used.

6. Carefully open plastic gel casing and place gel in distilled water.
7. Assemble transfer cassette in the following order: black side-sponge-filter paper-gel-membrane-filter paper-sponge-clear side.
8. Close the cassette and place into the transfer tank.
9. Transfer protein to the membrane at 100 volts for 60 minutes in the cold room on the stir plate.
10. After transfer, carefully remove paper-gel-membrane sandwich from the plastic cassette and place into container of deionized water.
11. Carefully remove the membrane from the sandwich.
12. Rinse the membrane with deionized water for a few seconds, then allow to completely dry

Note: Make sure membrane is completely dried before proceeding to the next step. Failure to fully dry membrane may result in loss of proteins on the membrane.

Membrane blotting and antibody incubations

1. If using nitrocellulose: wet PVDF membrane with methanol.
2. Incubate membrane with blocking buffer for 1 hour at room temperature on shaker.
3. Incubate membrane with primary antibody (at the appropriate dilution and diluent as recommended in the product datasheet) in blocking buffer with gentle agitation overnight at 4C.
4. Wash three times for 5min each with 15mL of TBST.
5. Incubate membrane with the species appropriate secondary antibody in 3-4mL of blocking buffer with gentle agitation (tilting shaker) for 1 hour at room temperature.
    - For ECL detection: use HRP-conjugated secondary antibody at concentration of (1:2000)
    - For IR detection: use LICOR IRDye secondary antibody at concentration of (1:25,000-40,000)
6. Wash three times for 15min each with 15ml of TBS.

Note: be sure to use TBS for the final wash before IR detection. Tween present in TBST will fluoresce and cause increased background signal.

Note: TBS or TBST may be used for the final ECL washes.

7. Proceed with detection.

Detection of proteins

<u>For ECL Detection</u>

1. Incubate membrane with 2-4mL Immobilon solution (HRP substrate peroxide solution + equal volume of luminol solution 1mL of each can do several blots) with gentle agitation for 1min at room temperature
2. Drain membrane of excess developing solution and visualize with ChemDoc system

Note: Due to the kinetics of the detection reaction, signal is most intense immediately following incubation and declines over the following 2hr.

<u>For IR Detection</u>

1. Image blots on Odyssey CLx.

Densitometry and quantitative analysis

1. Process using ImageStudioLite.
2. Normalize protein expression to loading control (e.g. GAPDH, β-actin, α-tubulin).
3. For phospho-proteins, normalize to total protein expression.

Drying and storage

1. Rinse blots with deionized water.
2. Dry fully protected by light.
3. Store in aluminum foil (or other photo-resistant material) for future reference.

8.1.6 Immunofluorescent staining of cells cultured on transwells

1. Aspirate media and gently wash three time with 1X PBS. Let PBS sit for at least two minutes for each wash.
2. Gently aspirate PBS.
3. Under a fume hood, fix cells on ice for 20 minutes with 4% paraformaldehyde.
4. Gently wash cells three times with 1X PBS. Let PBS sit for at least two minutes for each wash.
5. (*Optional*) Cells may be stored with storage buffer (2% goat serum in PBS) at this time for later analysis. Wrap plate with parafilm and store at 4C.
6. Gently wash cells three times with 1X PBS. Let PBS sit for at least two minutes for each wash.
7. Permeabilize cells for 10 minutes at room temperature using permeabilization buffer (100μL 10% Triton X-100 in 9.9mL 1X PBS).
8. Gently wash cells three times with 1X PBS. Let PBS sit for at least two minutes for each wash.
9. Block cells for one hour at room temperature with blocking buffer (2mL goat serum + 5g bovine serum albumin in 500mL 1X PBS).
10. Dilute desired primary antibody in blocking buffer (1:200) and incubate with cells for one hour at room temperature.
11. Aspirate antibody solution and perform three two-minute washes with PBS.
12. Dilute desired fluor-conjugated secondary antibodies in blocking buffer (1:200) and incubate with cells in the dark for one hour at room temperature on a rocking shaker.
13. Aspirate antibody solution and wash three times with 1X PBS at room temperature.
14. Wash cells overnight with 1X PBS on a rocking shaker at 4C.
15. When cells are ready to be mounted, gather glass microscope slides, coverslips, and mounting media.
16. Place a drop of mounting media on the microscope slide in the position where the sample will go.
17. Using a scalpel, carefully cut the membrane out of the transwell support.
18. Carefully place the membrane on the pre-positioned mounting media, apical side up.
19. Gently add another drop of mounting media onto the top of the membrane.
20. Gently place the coverslip on top of the membrane to seal it in place. Take care not to create bubbles.
21. Repeat until all membranes are mounted.
22. Dry slides in a light protected box at 4C.

8.1.7 Bacterial transformation and plasmid preparation

Bacterial transformation

1. Thaw a vial of competent E. coli on ice.
2. Remove agar plates (containing the appropriate antibiotic) from storage at 4C and let warm to room temperature.
3. Mix 1-5μg of DNA with 20-50μl of competent cells.
4. Gently flick the bottom of the tube to mix.
5. Incubate the competent cell/DNA mixture on ice for 20-30 minutes.
6. Heat shock each transformation tube by placing it in a 42C water bath for 30-60 seconds.
7. Incubate the microtube on ice for two minutes.
8. (Optional) Add 500μl antibiotic-free LB Broth or SOC media and incubate at 37C for 45 minutes.
9. Streak transformed cells on the pre-warmed agar plate.
10. Incubate the plates upside-down at 37C overnight.

Inoculating a liquid culture

1. Prepare sterile LB broth.
2. Add appropriate antibiotic.
3. Using a sterile pipette tip or toothpick, select a single colony from your LB agar plate.
4. Drop the tip or toothpick into the liquid LB + antibiotic and swirl.
5. Loosely cover the top of the flask with sterile aluminum foil.
6. Incubate the bacterial culture at 37C for 12-18hr in a shaking incubator.
7. When the bacteria has sufficiently grown, isolate the plasmid DNA using a Plasmid Prep Kit.

Preparing a glycerol stock

1. Once you have a liquid culture, add 500μ of the culture medium+cell mixture to 50% glycerol in a sterile 2ml cryovial.
2. Pipette gently to mix, ensuring that the solution is uniform (i.e. there are no visible layers).
3. Label the cryovial appropriately.
4. Freeze the stock at -80C.
5. To recover bacteria from the stock, open the tube and use a sterile inoculating loop to scrape off some bacteria off the top.
6. Streak the bacteria onto an LB agar plate (with the appropriate selection antibiotic). Incubate the plate overnight at 37C.

8.1.8 CRISPR gene knockout and Piggybac antibiotic selection co-transfection for renal cell lines

This is a protocol for transfecting mammalian cells with Lipofectamine LTX PLUS reagent (Invitrogen). Seed cells at 100,000 cells per well. When cells reach about 60% confluency, begin transfection.
Instructions for transfecting two 6-well plates at 3:1 transposon:transposase ratio:

1. Wash cells with 1X PBS.
2. Gently add fresh pre-warmed Opti-MEM to each well (200μL/well).

Note: Opti-MEM must be antibiotic-free and serum-free.

3. Thaw components to RT:
   - 3μL PLUS reagent per well
   - 6μL LTX reagent per well
   - 2.5μg total DNA per well
     - 1μg CRISPR sgRNA
     - 0.5μg HA-m7pB PiggyBac plasmid DNA
     - 0.5μg Neomycin resistance plasmid DNA
     - 0.5μg eGFP plasmid DNA
4. Vortex PLUS and LTX reagents gently to mix
5. Dilute the LTX reagent:
   (a) Pipette 1.5mL of Opti-MEM into a sterile tube
   (b) Add 72μL LTX reagent (6μL/well)
   (c) Pipette gently to mix
6. Dilute the DNA:
   (a) Add 1.5μL of Opti-MEM into an eppendorff tube
   (b) Add 6μg HA-m7pB PiggyBac plasmid DNA
   (c) Add 6μg Neomycin resistance plasmid DNA
   (d) Add 6μg eGFP plasmid DNA
7. Mix and aliquot 250μL into six sterile eppendorff tubes
8. Add CRISPR sgRNA to each tube (1μg/well; 2μg per tube)
9. Add 6μL of PLUS reagent to each tube
10. Pipette gently to mix
11. Add 250μL of the LTX mix to each tube of DNA mix
12. Pipette gently to mix and incubate five minutes at room temperature
13. Distribute the complexes to the cells by adding 250μL of each mix from step 12 drop-wise to different areas of the well in a 6-well plate. Gently rock the culture vessel back-and-forth and from side-to-side to evenly distribute the DNA complexes.
14. Incubate for two hours at 37C with 5% CO2.
15. Change the wells to fresh growth media. Incubate at 37C with 5% CO2. Begin antibiotic selection after 48 hours.

8.1.9 PiggyBac gene overexpression transfection for renal cell lines

This is a protocol for transfecting mammalian cells with Lipofectamine LTX PLUS reagent (Invitrogen). Seed cells at 100,000 cells per well. When cells reach about 60% confluency, begin transfection.
Instructions for transfecting two 6-well plates at 3:1 transposon:transposase ratio:

1. Wash cells with 1X PBS.
2. Gently add fresh pre-warmed Opti-MEM to each well (200μL/well).

Note: Opti-MEM must be antibiotic-free and serum-free.

3. Thaw components to room temperature:
   - 3μL PLUS reagent per well
   - 6μL LTX reagent per well
   - 2.5μg total DNA per well
     - 0.6μg HA-m7pB PiggyBac sgRNA
     - 1.9μg Overexpression plasmid DNA (containing puromycin resistance and mCherry cassettes)
4. Vortex PLUS and LTX reagents gently to mix.
5. Dilute the LTX reagent:
   (a) Pipette 1.5mL of Opti-MEM into a sterile tube
   (b) Add 72μL LTX reagent (6μL/well)
   (c) Pipette gently to mix
6. Dilute the DNA:
   (a) Add 1.5μL of Opti-MEM into an eppendorff tube
   (b) Add 7.2μg HA-m7pB PiggyBac plasmid DNA
7. Mix and aliquot 250μL into six sterile eppendorff tubes.
8. Add 3.8μg Pb overexpression plasmid to each tube.
9. Add 6μL of PLUS reagent to each tube.
10. Pipette gently to mix.
11. Add 250μL of the LTX mix to each tube of DNA mix.
12. Pipette gently to mix and incubate five minutes at room temperature.
13. Distribute the complexes to the cells by adding 250μL of each mix from step 12 drop-wise to different areas of the well in a 6-well plate. Gently rock the culture vessel back-and-forth and from side-to-side to evenly distribute the DNA complexes.
14. Incubate for two hours at 37C with 5% CO2.
15. Change the wells to fresh growth media. Incubate at 37C with 5% CO2. Begin antibiotic selection after 48 hours.

References

Abecassis, M., Bartlett, S. T., Collins, A. J., Davis, C. L., Delmonico, F. L., Friedewald, J. J., Hays, R., Howard, A., Jones, E., Leichtman, A. B., Merion, R. M., Metzger, R. A., Pradel, F., Schweitzer, E. J., Velez, R. L., and Gaston, R. S. (2008). Kidney transplantation as primary therapy for end-stage renal disease: A national kidney foundation/kidney disease outcomes quality initiative (nkf/kdoqi™) conference. *Clinical Journal of the American Society of Nephrology*, 3:471–480.

Alsabeeh, N., Chausse, B., Kakimoto, P. A., Kowaltowski, A. J., and Shirihai, O. (2018). Cell culture models of fatty acid overload: Problems and solutions. *Biochimica et Biophysica Acta - Molecular and Cell Biology of Lipids*, 1863.

Ares, G. R., Caceres, P. S., and Ortiz, P. A. (2011). Molecular regulation of nkcc2 in the thick ascending limb. *American journal of physiology. Renal physiology*, 301:F1143–59.

Ban, N., Yamada, Y., Someya, Y., Miyawaki, K., Ihara, Y., Hosokawa, M., Toyokuni, S., Tsuda, K., and Seino, Y. (2002). Hepatocyte nuclear factor-1α recruits the transcriptional co-activator p300 on the glut2 gene promoter. *Diabetes*, 51:1409–1418.

Banko, M., Allen, J., Schaffer, B., Wilker, E., Tsou, P., White, J., Villén, J., Wang, B., Kim, S., Sakamoto, K., Gygi, S., Cantley, L., Yaffe, M., Shokat, K., and Brunet, A. (2011). Chemical genetic screen for ampkα2 substrates uncovers a network of proteins involved in mitosis. *Molecular Cell*, 44:878–892.

Batlle, E. and Massagué, J. (2019). Transforming growth factor-β signaling in immunity and cancer. *Immunity*, 50:924–940.

Bays, J. L., Campbell, H. K., Heidema, C., Sebbagh, M., and DeMali, K. A. (2017). Linking e-cadherin mechanotransduction to cell metabolism through force-mediated activation of ampk. *Nature cell biology*, 19:724–731.

Benziane, B., Bjornholm, M., Pirkmajer, S., Austin, R. L., Kotova, O., Viollet, B., Zierath, J. R., and Chibalin, A. V. (2012). Activation of amp-activated protein kinase stimulates na+,k+-atpase activity in skeletal muscle cells. *Journal of Biological Chemistry*, 287:23451–23463.

Birket, M. J., Orr, A. L., Gerencser, A. A., Madden, D. T., Vitelli, C., Swistowski, A., Brand, M. D., and Zeng, X. (2011). A reduction in atp demand and mitochondrial activity with neural differentiation of human embryonic stem cells. *Journal of Cell Science*, 124:348–358.

Bisceglia, F., Battistelli, C., Noce, V., Montaldo, C., Zammataro, A., Strippoli, R., Tripodi, M., Amicone, L., and Marchetti, A. (2019). Tgfβ impairs hnf1α functional activity in epithelial-to-mesenchymal transition interfering with the recruitment of cbp/p300 acetyltransferases. *Frontiers in pharmacology*, 10:942.

Bonzo, J. A., Patterson, A. D., Krausz, K. W., and Gonzalez, F. J. (2010). Metabolomics identifies novel hnf1α-dependent physiological pathways in vivo. *Molecular Endocrinology*, 24:2343–2355.

Border, W. A., Okuda, S., Languino, L. R., Sporn, M. B., and Ruoslahti, E. (1990). Suppression of experimental glomerulonephritis by antiserum against transforming growth factor β1. *Nature*, 346:371–374.

Bottinger, E. P., Factor, V. M., Tsang, M. L., Weatherbee, J. A., Kopp, J. B., Qian, S. W., Wakefield, L. M., Roberts, A. B., Thorgeirsson, S. S., and Sporn, M. B. (1996). The recombinant proregion of transforming growth factor beta1 (latency-associated peptide) inhibits active transforming growth factor beta1 in transgenic mice. *Proceedings of the National Academy of Sciences*, 93:5877–5882.

Bouillaud, F. (2009). Ucp2, not a physiologically relevant uncoupler but a glucose sparing switch impacting ros production and glucose sensing. *Biochimica et Biophysica Acta - Bioenergetics*, 1787.

Brand, M. D. and Esteves, T. C. (2005). Physiological functions of the mitochondrial uncoupling proteins ucp2 and ucp3. *Cell Metabolism*, 2.

Bridges, H. R., Jones, A. J. Y., Pollak, M. N., and Hirst, J. (2014). Effects of metformin and other biguanides on oxidative phosphorylation in mitochondria. *The Biochemical journal*, 462:475–487.

Brown, K. A., Pietenpol, J. A., and Moses, H. L. (2007). A tale of two proteins: Differential roles and regulation of smad2 and smad3 in tgf-β signaling. *Journal of Cellular Biochemistry*, 101:9–33.

Brown, M. A., Collett, G. K., Josland, E. A., Foote, C., Li, Q., and Brennan, F. P. (2015). Ckd in elderly patients managed without dialysis: Survival, symptoms, and quality of life. *Clinical Journal of the American Society of Nephrology*, 10.

Calandrini, C., Schutgens, F., Oka, R., Margaritis, T., Candelli, T., Mathijsen, L., Ammerlaan, C., van Ineveld, R. L., Derakhshan, S., de Haan, S., Dolman, E., Lijnzaad, P., Custers, L., Begthel, H., Kerstens, H. H. D., Visser, L. L., Rookmaaker, M., Verhaar, M., Tytgat, G. A. M., Kemmeren, P., de Krijger, R. R., Al-Saadi, R., Pritchard-Jones, K., Kool, M., Rios, A. C., van den Heuvel-Eibrink, M. M., Molenaar, J. J., van Boxtel, R., Holstege, F. C. P., Clevers, H., and Drost, J. (2020). An organoid biobank for childhood kidney cancers that captures disease and tissue heterogeneity. *Nature Communications*, 11:1310.

Caliskan, Y., Lee, B., Whelan, A. M., Abualrub, F., Lentine, K. L., and Jittirat, A. (2022). Evaluation of genetic kidney diseases in living donor kidney transplantation: Towards precision genomic medicine in donor risk assessment. *Current Transplantation Reports*, 9:127–142.

Cannon, R. M., Jones, C. M., Hughes, M. G., Eng, M., and Marvin, M. R. (2013). The impact of recipient obesity on outcomes after renal transplantation. *Annals of Surgery*, 257:978–984.

Caralt, M., Uzarski, J. S., Iacob, S., Obergfell, K. P., Berg, N., Bijonowski, B. M., Kiefer, K. M., Ward, H. H., Wandinger-Ness, A., Miller, W. M., Zhang, Z. J., Abecassis, M. M., and Wertheim, J. A. (2015). Optimization and critical evaluation of decellularization strategies to develop renal extracellular matrix scaffolds as biological templates for organ engineering and transplantation. *American Journal of Transplantation*, 15:64–75.

Castro-Mondragon, J. A., Riudavets-Puig, R., Rauluseviciute, I., Berhanu Lemma, R., Turchi, L., Blanc-Mathieu, R., Lucas, J., Boddie, P., Khan, A., Manosalva Pérez, N., Fornes, O., Leung, T., Aguirre, A., Hammal, F., Schmelter, D., Baranasic, D., Ballester, B., Sandelin, A., Lenhard, B., Vandepoele, K., Wasserman, W. W., Parcy, F., and Mathelier, A. (2022). Jaspar 2022: the 9th release of the open-access database of transcription factor binding profiles. *Nucleic Acids Research*, 50:D165–D173.

CDC (2021). Chronic kidney disease in the united states,.

Cereijido, M., Robbins, E. S., Dolan, W. J., Rotunno, C. A., and Sabatini, D. D. (1978). Polarized monolayers formed by epithelial cells on a permeable and translucent support. *Journal of Cell Biology*, 77.

Chang, H.-C., Yang, S.-F., Huang, C.-C., Lin, T.-S., Liang, P.-H., Lin, C.-J., and Hsu, L.-C. (2013). Development of a novel non-radioactive cell-based method for the screening of sglt1 and sglt2 inhibitors using 1-nbdg. *Molecular BioSystems*, 9:2010.

Chau, B. N., Xin, C., Hartner, J., Ren, S., Castano, A. P., Linn, G., Li, J., Tran, P. T., Kaimal, V., Huang, X., Chang, A. N., Li, S., Kalra, A., Grafals, M., Portilla, D., MacKenna, D. A., Orkin, S. H., and Duffield, J. S. (2012). Microrna-21 promotes fibrosis of the kidney by silencing metabolic pathways. *Science Translational Medicine*, 4.

Chavez, J. A., Roach, W. G., Keller, S. R., Lane, W. S., and Lienhard, G. E. (2008). Inhibition of glut4 translocation by tbc1d1, a rab gtpase-activating protein abundant in skeletal muscle, is partially relieved by amp-activated protein kinase activation. *The Journal of biological chemistry*, 283:9187–9195.

Cheret, C., Doyen, A., Yaniv, M., and Pontoglio, M. (2002). Hepatocyte nuclear factor 1 α controls renal expression of the npt1-npt4 anionic transporter locus. *Journal of Molecular Biology*, 322:929–941.

Chisolm, D. A. and Weinmann, A. S. (2018). Connections between metabolism and epigenetics in programming cellular differentiation. *Annual review of immunology*, 36:221–246.

Chuasuwan, A., Pooripussarakul, S., Thakkinstian, A., Ingsathit, A., and Pattanaprateep, O. (2020). Comparisons of quality of life between patients underwent peritoneal dialysis and hemodialysis: a systematic review and meta-analysis. *Health and Quality of Life Outcomes*, 18:191.

chun Han, Y., qi Tang, S., ting Liu, Y., mei Li, A., Zhan, M., Yang, M., Song, N., Zhang, W., qin Wu, X., hui Peng, C., Zhang, H., and Yang, S. (2021). Ampk agonist alleviate renal tubulointerstitial fibrosis via activating mitophagy in high fat and streptozotocin induced diabetic mice. *Cell Death and Disease*, 12.

Chung, A. C., Zhang, H., Kong, Y.-Z., Tan, J.-J., Huang, X. R., Kopp, J. B., and Lan, H. Y. (2010). Advanced glycation end-products induce tubular ctgf via tgf-β–independent smad3 signaling. *Journal of the American Society of Nephrology*, 21:249–260.

Ciampi, O., Bonandrini, B., Derosas, M., Conti, S., Rizzo, P., Benedetti, V., Figliuzzi, M., Remuzzi, A., Benigni, A., Remuzzi, G., and Tomasoni, S. (2019). Engineering the vasculature of decellularized rat kidney scaffolds using human induced pluripotent stem cell-derived endothelial cells. *Scientific Reports*, 9:8001.

Cordeiro, M. F., Mead, A., Ali, R. R., Alexander, R. A., Murray, S., Chen, C., York-Defalco, C., Dean, N. M., Schultz, G. S., and Khaw, P. T. (2003). Novel antisense oligonucleotides targeting tgf-β inhibit in vivo scarring and improve surgical outcome. *Gene Therapy*, 10:59–71.

Crabtree, J. H., Shrestha, B. M., Chow, K.-M., Figueiredo, A. E., Povlsen, J. V., Wilkie, M., Abdel-Aal, A., Cullis, B., Goh, B.-L., Briggs, V. R., Brown, E. A., and Dor, F. J. (2019). Creating and maintaining optimal peritoneal dialysis access in the adult patient: 2019 update. *Peritoneal Dialysis International: Journal of the International Society for Peritoneal Dialysis*, 39:414–436.

Cruz, N. M., Song, X., Czerniecki, S. M., Gulieva, R. E., Churchill, A., Kim, Y. K., Winston, K., Tran, L. M., Diaz, M., Fu, H., Finn, L. S., Pei, Y., Himmelfarb, J., and Freedman, B. S. (2017). Organoid cystogenesis reveals a critical role of microenvironment in human polycystic kidney disease. *Nature Materials*, 16:1112–1119.

Datto, M. B., Frederick, J. P., Pan, L., Borton, A. J., Zhuang, Y., and Wang, X.-F. (1999). Targeted disruption of smad3 reveals an essential role in transforming growth factor β-mediated signal transduction. *Molecular and Cellular Biology*, 19:2495–2504.

Declèves, A.-E. and Sharma, K. (2015). Obesity and kidney disease. *Current Opinion in Nephrology and Hypertension*, 24:28–36.

Detaille, D., Guigas, B., Leverve, X., Wiernsperger, N., and Devos, P. (2002). Obligatory role of membrane events in the regulatory effect of metformin on the respiratory chain function. *Biochemical pharmacology*, 63:1259–1272.

Ding, B., Sun, G., Liu, S., Peng, E., Wan, M., Chen, L., Jackson, J., and Atala, A. (2020). Three-dimensional renal organoids from whole kidney cells: Generation, optimization, and potential application in nephrotoxicology in vitro. *Cell Transplantation*, 29:096368971989706.

Dohda, T., Kaneoka, H., Inayoshi, Y., Kamihira, M., Miyake, K., and Iijima, S. (2004). Transcriptional coactivators cbp and p300 cooperatively enhance hnf-1α–mediated expression of the albumin gene in hepatocytes. *The Journal of Biochemistry*, 136:313–319.

Domenech, E., Maestre, C., Esteban-Martinez, L., Partida, D., Pascual, R., Fernandez-Miranda, G., Seco, E., Campos-Olivas, R., Perez, M., Megias, D., Allen, K., Lopez, M., Saha, A. K., Velasco, G., Rial, E., Mendez, R., Boya, P., Salazar-Roa, M., and Malumbres, M. (2015). Ampk and pfkfb3 mediate glycolysis and survival in response to mitophagy during mitotic arrest. *Nature cell biology*, 17:1304–1316.

Dorison, A., Forbes, T. A., and Little, M. H. (2022). What can we learn from kidney organoids? *Kidney International*, 102:1013–1029.

Dupont, S., Mamidi, A., Cordenonsi, M., Montagner, M., Zacchigna, L., Adorno, M., Martello, G., Stinchfield, M. J., Soligo, S., Morsut, L., Inui, M., Moro, S., Modena, N., Argenton, F., Newfeld, S. J., and Piccolo, S. (2009). Fam/usp9x, a deubiquitinating enzyme essential for tgfβ signaling, controls smad4 monoubiquitination. *Cell*, 136:123–135.

El-Mir, M. Y., Nogueira, V., Fontaine, E., Averet, N., Rigoulet, M., and Leverve, X. (2000). Dimethylbiguanide inhibits cell respiration via an indirect effect targeted on the respiratory chain complex i. *The Journal of biological chemistry*, 275:223–228.

Evangelidis, N., Tong, A., Manns, B., Hemmelgarn, B., Wheeler, D. C., Tugwell, P., Crowe, S., Harris, T., Biesen, W. V., Winkelmayer, W. C., Sautenet, B., O'Donoghue, D., Tam-Tham, H., Youssouf, S., Mandayam, S., Ju, A., Hawley, C., Pollock, C., Harris, D. C., Johnson, D. W., Rifkin, D. E., Tentori, F., Agar, J., Polkinghorne, K. R., Gallagher, M., Kerr, P. G., McDonald, S. P., Howard, K., Howell, M., and Craig, J. C. (2017). Developing a set of core outcomes for trials in hemodialysis: An international delphi survey. *American Journal of Kidney Diseases*, 70:464–475.

Evans, M., Lewis, R. D., Morgan, A. R., Whyte, M. B., Hanif, W., Bain, S. C., Davies, S., Dashora, U., Yousef, Z., Patel, D. C., and Strain, W. D. (2022). A narrative review of chronic kidney disease in clinical practice: Current challenges and future perspectives. *Advances in Therapy*, 39:33–43.

Fan, J.-M., Ng, Y.-Y., Hill, P. A., Nikolic-Paterson, D. J., Mu, W., Atkins, R. C., and Lan, H. Y. (1999). Transforming growth factor-β regulates tubular epithelial-myofibroblast transdifferentiation in vitro. *Kidney International*, 56:1455–1467.

Fang, Y., Li, F., Qi, C., Mao, X., Wang, F., Zhao, Z., Chen, J.-K., Zhang, Z., and Wu, H. (2020). Metformin effectively treats tsc1 deletion-caused kidney pathology by upregulating ampk phosphorylation. *Cell Death Discovery*, 6:52.

Fedecostante, M., Westphal, K. G. C., Buono, M. F., Romero, N. S., Wilmer, M. J., Kerkering, J., Baptista, P. M., Hoenderop, J. G., and Masereeuw, R. (2018). Recellularized native kidney scaffolds as a novel tool in nephrotoxicity screening. *Drug Metabolism and Disposition*, 46:1338–1350.

Feng, X.-H. and Derynck, R. (2005). Specificity and versatility in tgf-β signaling through smads. *Annual Review of Cell and Developmental Biology*, 21:659–693.

Ferrell, N., Cheng, J., Miao, S., Roy, S., and Fissell, W. H. (2018). Orbital shear stress regulates differentiation and barrier function of primary renal tubular epithelial cells. *ASAIO Journal*, 64:766–772.

Ferrell, N., Desai, R. R., Fleischman, A. J., Roy, S., Humes, H. D., and Fissell, W. H. (2010). A microfluidic bioreactor with integrated transepithelial electrical resistance (teer) measurement electrodes for evaluation of renal epithelial cells. *Biotechnology and Bioengineering*, 107:707–716.

Ferrell, N., Ricci, K. B., Groszek, J., Marmerstein, J. T., and Fissell, W. H. (2012). Albumin handling by renal tubular epithelial cells in a microfluidic bioreactor. *Biotechnology and Bioengineering*, 109:797–803.

Figlia, G., Willnow, P., and Teleman, A. A. (2020). Metabolites regulate cell signaling and growth via covalent modification of proteins. *Developmental Cell*, 54.

Fissell, W. H. (2006). Developments towards an artificial kidney. *Expert Review of Medical Devices*, 3:155–165. doi: 10.1586/17434440.3.2.155.

Fissell, W. H., Dubnisheva, A., Eldridge, A. N., Fleischman, A. J., Zydney, A. L., and Roy, S. (2009). High-performance silicon nanopore hemofiltration membranes. *Journal of Membrane Science*, 326:58–63.

Fontaine, E. (2014). Metformin and respiratory chain complex i: the last piece of the puzzle? *The Biochemical journal*, 463:e3–5.

Foreman, K. J., Marquez, N., Dolgert, A., Fukutaki, K., Fullman, N., McGaughey, M., Pletcher, M. A., Smith, A. E., Tang, K., Yuan, C.-W., Brown, J. C., Friedman, J., He, J., Heuton, K. R., Holmberg, M., Patel, D. J., Reidy, P., Carter, A., Cercy, K., Chapin, A., Douwes-Schultz, D., Frank, T., Goettsch, F., Liu, P. Y., Nandakumar, V., Reitsma, M. B., Reuter, V., Sadat, N., Sorensen, R. J. D., Srinivasan, V., Updike, R. L., York, H., Lopez, A. D., Lozano, R., Lim, S. S., Mokdad, A. H., Vollset, S. E., and Murray, C. J. L. (2018). Forecasting life expectancy, years of life lost, and all-cause and cause-specific mortality for 250 causes of death: reference and alternative scenarios for 2016–40 for 195 countries and territories. *The Lancet*, 392:2052–2090.

Foretz, M., Guigas, B., Bertrand, L., Pollak, M., and Viollet, B. (2014). Metformin: from mechanisms of action to therapies. *Cell metabolism*, 20:953–966.

Forte, M., Bianchi, F., Cotugno, M., Marchitti, S., Stanzione, R., Maglione, V., Sciarretta, S., Valenti, V., Carnevale, R., Versaci, F., Frati, G., Volpe, M., and Rubattu, S. (2021). An interplay between ucp2 and ros protects cells from high-salt-induced injury through autophagy stimulation. *Cell Death and Disease*, 12.

Freedman, B. S. (2022). Physiology assays in human kidney organoids. *American Journal of Physiology-Renal Physiology*, 322:F625–F638.

Freedman, B. S., Brooks, C. R., Lam, A. Q., Fu, H., Morizane, R., Agrawal, V., Saad, A. F., Li, M. K., Hughes, M. R., Werff, R. V., Peters, D. T., Lu, J., Baccei, A., Siedlecki, A. M., Valerius, M. T., Musunuru, K., McNagny, K. M., Steinman, T. I., Zhou, J., Lerou, P. H., and Bonventre, J. V. (2015). Modelling kidney disease with crispr-mutant kidney organoids derived from human pluripotent epiblast spheroids. *Nature Communications*, 6:8715.

Frick, C. L., Yarka, C., Nunns, H., and Goentoro, L. (2017). Sensing relative signal in the tgf-β/smad pathway. *Proceedings of the National Academy of Sciences*, 114.

Geng, H., Lan, R., Wang, G., Siddiqi, A. R., Naski, M. C., Brooks, A. I., Barnes, J. L., Saikumar, P., Weinberg, J. M., and Venkatachalam, M. A. (2009). Inhibition of autoregulated tgfβ signaling simultaneously enhances proliferation and differentiation of kidney epithelium and promotes repair following renal ischemia. *The American Journal of Pathology*, 174:1291–1308.

Georgas, K., Rumballe, B., Wilkinson, L., Chiu, H. S., Lesieur, E., Gilbert, T., and Little, M. H. (2008). Use of dual section mrna in situ hybridisation/immunohistochemistry to clarify gene expression patterns during the early stages of nephron development in the embryo and in the mature nephron of the adult mouse kidney. *Histochemistry and cell biology*, 130:927–942.

Gerich, J. E. (2010). Role of the kidney in normal glucose homeostasis and in the hyperglycaemia of diabetes mellitus: Therapeutic implications. *Diabetic Medicine*, 27.

Gewin, L. and Zent, R. (2012). How does tgf-β mediate tubulointerstitial fibrosis? *Seminars in Nephrology*, 32:228–235.

Gewin, L. S. (2021). Sugar or fat? renal tubular metabolism reviewed in health and disease. *Nutrients*, 13.

Ghelichi-Ghojogh, M., Ghaem, H., Mohammadizadeh, F., Vali, M., Ahmed, F., Hassanipour, S., Nikbakht, H.-A., Rezaei, F., and Fararouei, M. (2021). Graft and patient survival rates in kidney transplantation, and their associated factors: A systematic review and meta-analysis. *Iranian Journal of Public Health*.

Glassock, R. J., Warnock, D. G., and Delanaye, P. (2017). The global burden of chronic kidney disease: estimates, variability and pitfalls. *Nature Reviews Nephrology*, 13:104–114.

Grande, M. T., Sánchez-Laorden, B., López-Blau, C., Frutos, C. A. D., Boutet, A., Arévalo, M., Rowe, R. G., Weiss, S. J., López-Novoa, J. M., and Nieto, M. A. (2015). Snail1-induced partial epithelial-to-mesenchymal transition drives renal fibrosis in mice and can be targeted to reverse established disease. *Nature Medicine*, 21:989–997.

Groth, T., Stegmayr, B. G., Ash, S. R., Kuchinka, J., Wieringa, F. P., Fissell, W. H., and Roy, S. (2022). Wearable and implantable artificial kidney devices for end-stage kidney disease treatment—current status and review. *Artificial Organs*.

Gu, Y.-Y., Liu, X.-S., Huang, X.-R., Yu, X.-Q., and Lan, H.-Y. (2020). Diverse role of tgf-β in kidney disease. *Frontiers in Cell and Developmental Biology*, 8.

Guigas, B., Detaille, D., Chauvin, C., Batandier, C., Oliveira, F. D., Fontaine, E., and Leverve, X. (2004). Metformin inhibits mitochondrial permeability transition and cell death: a pharmacological in vitro study. *The Biochemical journal*, 382:877–884.

Gélinas, R., Dontaine, J., Horman, S., Beauloye, C., Bultot, L., and Bertrand, L. (2018). Amp-activated protein kinase and o-glcnacylation, two partners tightly connected to regulate key cellular processes. *Frontiers in endocrinology*, 9:519.

Hale, L. J., Howden, S. E., Phipson, B., Lonsdale, A., Er, P. X., Ghobrial, I., Hosawi, S., Wilson, S., Lawlor, K. T., Khan, S., Oshlack, A., Quinlan, C., Lennon, R., and Little, M. H. (2018). 3d organoid-derived human glomeruli for personalised podocyte disease modelling and drug screening. *Nature Communications*, 9:5167.

Hall, M.-C., Young, D. A., Waters, J. G., Rowan, A. D., Chantry, A., Edwards, D. R., and Clark, I. M. (2003). The comparative role of activator protein 1 and smad factors in the regulation of timp-1 and mmp-1 gene expression by transforming growth factor-β1. *Journal of Biological Chemistry*, 278:10304–10313.

Hamidi, A., Song, J., Thakur, N., Itoh, S., Marcusson, A., Bergh, A., Heldin, C.-H., and Landstrom, M. (2017). Tgf-beta promotes pi3k-akt signaling and prostate cancer cell migration through the traf6-mediated ubiquitylation of p85alpha. *Science signaling*, 10.

Han, J., Hajjar, D. P., Tauras, J. M., Feng, J., Gotto, A. M., and Nicholson, A. C. (2000). Transforming growth factor-β1 (tgf-β1) and tgf-β2 decrease expression of cd36, the type b scavenger receptor, through mitogen-activated protein kinase phosphorylation of peroxisome proliferator-activated receptor-γ. *Journal of Biological Chemistry*, 275.

Harder, J. L., Menon, R., Otto, E. A., Zhou, J., Eddy, S., Wys, N. L., O'Connor, C., Luo, J., Nair, V., Cebrian, C., Spence, J. R., Bitzer, M., Troyanskaya, O. G., Hodgin, J. B., Wiggins, R. C., Freedman, B. S., and Kretzler, M. (2019). Organoid single cell profiling identifies a transcriptional signature of glomerular disease. *JCI Insight*, 4.

Harding, H. P., Zhang, Y., Zeng, H., Novoa, I., Lu, P. D., Calfon, M., Sadri, N., Yun, C., Popko, B., Paules, R., Stojdl, D. F., Bell, J. C., Hettmann, T., Leiden, J. M., and Ron, D. (2003). An integrated stress response regulates amino acid metabolism and resistance to oxidative stress otherwise unrelated stresses. stress conditions leading to eif2␣ phosphorylation skirball institute share the potential for accumulation of malfolded or modified proteins, for which the eif2␣ phosphorylation. *Molecular Cell*, 11:619–633.

Hasegawa, T., Bragg-Gresham, J. L., Yamazaki, S., Fukuhara, S., Akizawa, T., Kleophas, W., Greenwood, R., and Pisoni, R. L. (2009). Greater first-year survival on hemodialysis in facilities in which patients are provided earlier and more frequent pre-nephrology visits. *Clinical Journal of the American Society of Nephrology*, 4:595–602.

Hata, A. and Chen, Y.-G. (2016). Tgf-β signaling from receptors to smads. *Cold Spring Harbor Perspectives in Biology*, 8:a022061.

Heiden, M. G. V., Cantley, L. C., and Thompson, C. B. (2009). Understanding the warburg effect: The metabolic requirements of cell proliferation. *Science*, 324:1029–1033.

Herman-Edelstein, M., Scherzer, P., Tobar, A., Levi, M., and Gafter, U. (2014). Altered renal lipid metabolism and renal lipid accumulation in human diabetic nephropathy. *Journal of Lipid Research*, 55:561–572.

Herst, P. M. and Berridge, M. V. (2007). Cell surface oxygen consumption: A major contributor to cellular oxygen consumption in glycolytic cancer cell lines. *Biochimica et Biophysica Acta - Bioenergetics*, 1767.

Hilbrands, L. B. (2020). Latest developments in living kidney donation. *Current Opinion in Organ Transplantation*, 25:74–79.

Hiraiwa, H., Pan, C.-J., Lin, B., Akiyama, T. E., Gonzalez, F. J., and Chou, J. Y. (2001). A molecular link between the common phenotypes of type 1 glycogen storage disease and hnf1α-null mice. *Journal of Biological Chemistry*, 276:7963–7967.

Hiratsuka, K., Monkawa, T., Akiyama, T., Nakatake, Y., Oda, M., Goparaju, S. K., Kimura, H., Chikazawa-Nohtomi, N., Sato, S., Ishiguro, K., Yamaguchi, S., Suzuki, S., Morizane, R., Ko, S. B. H., Itoh, H., and Ko, M. S. H. (2019). Induction of human pluripotent stem cells into kidney tissues by synthetic mrnas encoding transcription factors. *Scientific Reports*, 9:913.

Hirst, J. A., Farmer, A. J., Ali, R., Roberts, N. W., and Stevens, R. J. (2012). Quantifying the effect of metformin treatment and dose on glycemic control. *Diabetes care*, 35:446–454.

Hoffmann, C., Hockele, S., Kappler, L., de Angelis, M. H., Häring, H.-U., and Weigert, C. (2018). The effect of differentiation and tgfβ on mitochondrial respiration and mitochondrial enzyme abundance in cultured primary human skeletal muscle cells. *Scientific Reports*, 8:737.

Holdaas, H., Fellstrom, B., Cole, E., Nyberg, G., Olsson, A., Pedersen, T., Madsen, S., Gronhagen-Riska, C., Neumayer, H.-H., Maes, B., Ambühl, P., Hartmann, A., Staffler, B., and Jardine, A. (2005). Long-term cardiac outcomes in renal transplant recipients receiving fluvastatin: The alert extension study. *American Journal of Transplantation*, 5:2929–2936.

Homan, K. A., Kolesky, D. B., Skylar-Scott, M. A., Herrmann, J., Obuobi, H., Moisan, A., and Lewis, J. A. (2016). Bioprinting of 3d convoluted renal proximal tubules on perfusable chips. *Scientific Reports*, 6:1–13.

Honegger, K. J., Capuano, P., Winter, C., Bacic, D., Stange, G., Wagner, C. A., Biber, J., Murer, H., and Hernando, N. (2006). Regulation of sodium-proton exchanger isoform 3 (nhe3) by pka and exchange protein directly activated by camp (epac). *Proceedings of the National Academy of Sciences*, 103:803–808.

Hoppensack, A., Kazanecki, C. C., Colter, D., Gosiewska, A., Schanz, J., Walles, H., and Schenke-Layland, K. (2014). A human ¡i¿in vitro¡/i¿ model that mimics the renal proximal tubule. *Tissue Engineering Part C: Methods*, 20:599–609.

Hsu, C.-Y., Chi, P.-L., Chen, H.-Y., Ou, S.-H., Chou, K.-J., Fang, H.-C., Chen, C.-L., Huang, C.-W., Ho, T.-Y., and Lee, P.-T. (2022). Kidney bioengineering by using decellularized kidney scaffold and renal progenitor cells. *Tissue and Cell*, 74:101699.

Humes, H. D., MacKay, S. M., Funke, A. J., and Buffington, D. A. (1999). Tissue engineering of a bioartificial renal tubule assist device: in vitro transport and metabolic characteristics. *Kidney international*, 55:2502–2514.

Hunter, K., Larsen, J. A., Love, H. D., Evans, R. C., Roy, S., Zent, R., Harris, R., Wilson, M. H., and Fissell, W. H. (2022). Inhibition of tgf-β improves primary renal tubule cell differentiation in long-term culture. *Tissue Engineering Part A*.

ichi Tsuchida, K., Zhu, Y., Siva, S., Dunn, S. R., and Sharma, K. (2003). Role of smad4 on tgf-beta-induced extracellular matrix stimulation in mesangial cells. *Kidney international*, 63:2000–2009.

Igarashi, P., Whyte, D. A., Li, K., and Nagami, G. T. (1996). Cloning and kidney cell-specific activity of the promoter of the murine renal na-k-cl cotransporter gene. *Journal of Biological Chemistry*, 271:9666–9674.

Jang, K.-J., Mehr, A. P., Hamilton, G. A., McPartlin, L. A., Chung, S., Suh, K.-Y., and Ingber, D. E. (2013). Human kidney proximal tubule-on-a-chip for drug transport and nephrotoxicity assessment. *Integrative Biology*, 5:1119.

Janzen, N. R., Whitfield, J., and Hoffman, N. J. (2018). Interactive roles for ampk and glycogen from cellular energy sensing to exercise metabolism. *International journal of molecular sciences*, 19:3344.

Jayagopal, A., Brakeman, P. R., Soler, P., Ferrell, N., Fissell, W., Kroetz, D. L., and Roy, S. (2019). Apical shear stress enhanced organic cation transport in human oct2/mate1-transfected madin-darby canine kidney cells involves ciliary sensing. *Journal of Pharmacology and Experimental Therapeutics*, 369:523–530.

Jenkinson, S. E., Chung, G. W., van Loon, E., Bakar, N. S., Dalzell, A. M., and Brown, C. D. A. (2012). The limitations of renal epithelial cell line hk-2 as a model of drug transporter expression and function in the proximal tubule. *Pflügers Archiv - European Journal of Physiology*, 464:601–611.

Jeon, S.-M. (2016). Regulation and function of ampk in physiology and diseases. *Experimental & molecular medicine*, 48:e245.

Ju, W., Ogawa, A., Heyer, J., Nierhof, D., Yu, L., Kucherlapati, R., Shafritz, D. A., and Bottinger, E. P. (2006). Deletion of smad2 in mouse liver reveals novel functions in hepatocyte growth and differentiation. *Molecular and Cellular Biology*, 26:654–667.

Kalantar-Zadeh, K., Jafar, T. H., Nitsch, D., Neuen, B. L., and Perkovic, V. (2021). Chronic kidney disease. *The Lancet*, 398:786–802.

Kanani, D. M., Fissell, W. H., Roy, S., Dubnisheva, A., Fleischman, A., and Zydney, A. L. (2010). Permeability–selectivity analysis for ultrafiltration: Effect of pore geometry. *Journal of Membrane Science*, 349:405–410.

Kang, H. M., Ahn, S. H., Choi, P., Ko, Y. A., Han, S. H., Chinga, F., Park, A. S. D., Tao, J., Sharma, K., Pullman, J., Bottinger, E. P., Goldberg, I. J., and Susztak, K. (2015). Defective fatty acid oxidation in renal tubular epithelial cells has a key role in kidney fibrosis development. *Nature Medicine*, 21.

Kaufhold, S. and Bonavida, B. (2014). Central role of snail1 in the regulation of emt and resistance in cancer: a target for therapeutic intervention. *Journal of Experimental & Clinical Cancer Research*, 33:62.

Khodo, S. N., Neelisetty, S., Woodbury, L., Green, E., Harris, R. C., Zent, R., and Gewin, L. (2016). Deleting the tgf-β receptor in proximal tubules impairs hgf signaling. *American Journal of Physiology-Renal Physiology*, 310:F499–F510.

Kiilerich, K., Adser, H., Jakobsen, A. H., Pedersen, P. A., Hardie, D. G., Wojtaszewski, J. F., and Pilegaard, H. (2010). Pgc-1α increases pdh content but does not change acute pdh regulation in mouse skeletal muscle. *American Journal of Physiology - Regulatory Integrative and Comparative Physiology*, 299.

Kim, Y. K., Refaeli, I., Brooks, C. R., Jing, P., Gulieva, R. E., Hughes, M. R., Cruz, N. M., Liu, Y., Churchill, A. J., Wang, Y., Fu, H., Pippin, J. W., Lin, L. Y., Shankland, S. J., Vogl, A. W., McNagny, K. M., and Freedman, B. S. (2017). Gene-edited human kidney organoids reveal mechanisms of disease in podocyte development. *Stem Cells*, 35:2366–2378.

Koo, S.-H., Flechner, L., Qi, L., Zhang, X., Screaton, R. A., Jeffries, S., Hedrick, S., Xu, W., Boussouar, F., Brindle, P., Takemori, H., and Montminy, M. (2005). The creb coactivator torc2 is a key regulator of fasting glucose metabolism. *Nature*, 437:1109–1111.

Krick, S., Shi, S., Ju, W., Faul, C., Tsai, S. Y., Mundel, P., and Bottinger, E. P. (2008). Mpv17l protects against mitochondrial oxidative stress and apoptosis by activation of omi/htra2 protease. *Proceedings of the National Academy of Sciences of the United States of America*, 105.

Kukat, A., Dogan, S. A., Edgar, D., Mourier, A., Jacoby, C., Maiti, P., Mauer, J., Becker, C., Senft, K., Wibom, R., Kudin, A. P., Hultenby, K., Flogel, U., Rosenkranz, S., Ricquier, D., Kunz, W. S., and Trifunovic, A. (2014). Loss of ucp2 attenuates mitochondrial dysfunction without altering ros production and uncoupling activity. *PLoS Genetics*, 10.

Lan, R., Geng, H., Polichnowski, A. J., Singha, P. K., Saikumar, P., McEwen, D. G., Griffin, K. A., Koesters, R., Weinberg, J. M., Bidani, A. K., Kriz, W., and Venkatachalam, M. A. (2012). Pten loss defines a tgf-β-induced tubule phenotype of failed differentiation and jnk signaling during renal fibrosis. *American Journal of Physiology-Renal Physiology*, 302:F1210–F1223.

Lazzaro, D., Simone, V. D., Magistris, L. D., Lehtonen, E., and Cortese, R. (1992). Lfb1 and lfb3 homeoproteins are sequentially expressed during kidney development. *Development*, 114:469–479.

Lee, J. W. (2015). Rna sequencing of the nephron transcriptome: A technical note. *Kidney Research and Clinical Practice*, 34:219–227.

Lee, M., Katerelos, M., Gleich, K., Galic, S., Kemp, B. E., Mount, P. F., and Power, D. A. (2018). Phosphorylation of acetyl-coa carboxylase by ampk reduces renal fibrosis and is essential for the anti-fibrotic effect of metformin. *Journal of the American Society of Nephrology*, 29:2326 LP – 2336.

Lentine, K. L. and Segev, D. L. (2017). Understanding and communicating medical risks for living kidney donors: A matter of perspective. *Journal of the American Society of Nephrology*, 28:12–24.

Leuning, D. G., Witjas, F. M. R., Maanaoui, M., de Graaf, A. M. A., Lievers, E., Geuens, T., Avramut, C. M., Wiersma, L. E., Berg, C. W., Sol, W. M. P. J., Boer, H., Wang, G., LaPointe, V. L. S., Vlag, J., Kooten, C., Berg, B. M., Little, M. H., Engelse, M. A., and Rabelink, T. J. (2019). Vascular bioengineering of scaffolds derived from human discarded transplant kidneys using human pluripotent stem cell–derived endothelium. *American Journal of Transplantation*, 19:1328–1343.

Li, B., Khanna, A., Sharma, V., Singh, T., Suthanthiran, M., and August, P. (1999). Tgf-β1 dna polymorphisms, protein levels, and blood pressure. *Hypertension*, 33.

Li, J., Qu, X., Yao, J., Caruana, G., Ricardo, S. D., Yamamoto, Y., Yamamoto, H., and Bertram, J. F. (2010). Blockade of endothelial-mesenchymal transition by a smad3 inhibitor delays the early development of streptozotocin-induced diabetic nephropathy. *Diabetes*, 59:2612–2624.

Li, N.-S., Zou, J.-R., Lin, H., Ke, R., He, X.-L., Xiao, L., Huang, D., Luo, L., Lv, N., and Luo, Z. (2016). Lkb1/ampk inhibits tgf-β1 production and the tgf-β signaling pathway in breast cancer cells. *Tumor Biology*, 37:8249–8258.

Li, Y., Kang, J., Fu, J., Luo, H., Liu, Y., Li, Y., and Sun, L. (2021). Pgc1α promotes cisplatin resistance in ovarian cancer by regulating the hsp70/hk2/vdac1 signaling pathway. *International Journal of Molecular Sciences*, 22:2537.

Lieberthal, W., Tang, M., Abate, M., Lusco, M., and Levine, J. S. (2019). Ampk-mediated activation of akt protects renal tubular cells from stress-induced apoptosis in vitro and ameliorates ischemic aki in vivo. *American Journal of Physiology-Renal Physiology*, 317:F1–F11.

Lin, N. Y. C., Homan, K. A., Robinson, S. S., Kolesky, D. B., Duarte, N., Moisan, A., and Lewis, J. A. (2019). Renal reabsorption in 3d vascularized proximal tubule models. *Proceedings of the National Academy of Sciences*, 116:5399–5404.

Lindgren, D., Eriksson, P., Krawczyk, K., Nilsson, H., Hansson, J., Veerla, S., Sjolund, J., Hoglund, M., Johansson, M. E., and Axelson, H. (2017). Cell-type-specific gene programs of the normal human nephron define kidney cancer subtypes. *Cell Reports*, 20:1476–1489.

Liu, H., Zhang, Z., Li, Y., Wang, X., Zhang, Y., Chu, Y., Yuan, X., and Wang, X. (2018). Preparation and evaluation of anti-renal fibrosis activity of novel truncated tgf-β receptor type ii. *Biotechnology and Applied Biochemistry*, 65:834–840.

Liu, L., Liu, X., Ren, X., Tian, Y., Chen, Z., Xu, X., Du, Y., Jiang, C., Fang, Y., Liu, Z., Fan, B., Zhang, Q., Jin, G., Yang, X., and Zhang, X. (2016). Smad2 and smad3 have differential sensitivity in relaying tgfβ signaling and inversely regulate early lineage specification. *Scientific Reports*, 6:21602.

Liyanage, T., Ninomiya, T., Jha, V., Neal, B., Patrice, H. M., Okpechi, I., hui Zhao, M., Lv, J., Garg, A. X., Knight, J., Rodgers, A., Gallagher, M., Kotwal, S., Cass, A., and Perkovic, V. (2015). Worldwide access to treatment for end-stage kidney disease: a systematic review. *The Lancet*, 385:1975–1982.

Lo, W. K. (2016). Metabolic syndrome and obesity in peritoneal dialysis. *Kidney Research and Clinical Practice*, 35:10–14.

Loeffler, I., Liebisch, M., Allert, S., Kunisch, E., Kinne, R. W., and Wolf, G. (2018). Fsp1-specific smad2 knockout in renal tubular, endothelial, and interstitial cells reduces fibrosis and epithelial-to-mesenchymal transition in murine stz-induced diabetic nephropathy. *Cell and Tissue Research*, 372:115–133.

Long, K. R., Shipman, K. E., Rbaibi, Y., Menshikova, E. V., Ritov, V. B., Eshbach, M. L., Jiang, Y., Jackson, E. K., Baty, C. J., and Weisz, O. A. (2017). Proximal tubule apical endocytosis is modulated by fluid shear stress via an mtor-dependent pathway. *Molecular Biology of the Cell*, 28:2508–2517.

Lonn, P., van der Heide, L. P., Dahl, M., Hellman, U., Heldin, C.-H., and Moustakas, A. (2010). Parp-1 attenuates smad-mediated transcription. *Molecular Cell*, 40:521–532.

Love, H., Evans, R., Humes, H. D., Roy, S., Zent, R., Harris, R., Wilson, M., and Fissell, W. H. (2020). Metformin and inhibition of transforming growth factor-beta stimulate in vitro transport in primary renal tubule cells. *Tissue Engineering Part A*, 26:1091–1098. doi: 10.1089/ten.tea.2019.0294.

Love, H. D., Ao, M., Jorgensen, S., Swearingen, L., Ferrell, N., Evans, R., Gewin, L., Harris, R. C., Zent, R., Roy, S., and Fissell, W. H. (2019). Substrate elasticity governs differentiation of renal tubule cells in prolonged culture. *Tissue Engineering Part A*, 25:1013–1022.

Low, J. H., Li, P., Chew, E. G. Y., Zhou, B., Suzuki, K., Zhang, T., Lian, M. M., Liu, M., Aizawa, E., Esteban, C. R., Yong, K. S. M., Chen, Q., Campistol, J. M., Fang, M., Khor, C. C., Foo, J. N., Belmonte, J. C. I., and Xia, Y. (2019). Generation of human psc-derived kidney organoids with patterned nephron segments and a de novo vascular network. *Cell Stem Cell*, 25:373–387.e9.

Luo, Z., Li, Y., Wang, H., Fleming, J., Li, M., Kang, Y., Zhang, R., and Li, D. (2015). Hepatocyte nuclear factor 1a (hnf1a) as a possible tumor suppressor in pancreatic cancer. *PLOS ONE*, 10:e0121082.

Mandel, L. J. and Balaban, R. S. (1981). Stoichiometry and coupling of active transport to oxidative metabolism in epithelial tissues. *American Journal of Physiology-Renal Physiology*, 240:F357–F371.

Marcelina, P., A, M. M., F, B. S., Amaya, P., Roser, C., Ramon, G., Francisca, R., and Jorge, F. (2001). Hepatic nuclear factor 1-α directs nucleosomal hyperacetylation to its tissue-specific transcriptional targets. *Molecular and Cellular Biology*, 21:3234–3243. doi: 10.1128/MCB.21.9.3234-3243.2001.

Markadieu, N. and Delpire, E. (2014). Physiology and pathophysiology of slc12a1/2 transporters. *Pflugers Archiv : European journal of physiology*, 466:91–105.

Markham, A. (2019). Tenapanor: First approval. *Drugs*, 79:1897–1903.

Martinez-Palomo, A., Meza, I., Beaty, G., and Cereijido, M. (1980). Experimental modulation of occluding junctions in a cultured transporting epithelium. *Journal of Cell Biology*, 87.

Martovetsky, G., Tee, J. B., and Nigam, S. K. (2013). Hepatocyte nuclear factors 4α and 1α regulate kidney developmental expression of drug-metabolizing enzymes and drug transporters. *Molecular pharmacology*, 84:808–823.

Martínez-Klimova, E., Aparicio-Trejo, O. E., Tapia, E., and Pedraza-Chaverri, J. (2019). Unilateral ureteral obstruction as a model to investigate fibrosis-attenuating treatments. *Biomolecules*, 9:141.

Massa, F., Garbay, S., Bouvier, R., Sugitani, Y., Noda, T., Gubler, M.-C., Heidet, L., Pontoglio, M., and Fischer, E. (2013). Hepatocyte nuclear factor 1β controls nephron tubular development. *Development*, 140:886–896.

Massague, J. (2000). New embo members review: Transcriptional control by the tgf-beta/smad signaling system. *The EMBO Journal*, 19:1745–1754.

Matsuki, K., Hathaway, C., Lawrence, M., Smithies, O., and Kakoki, M. (2015). The role of transforming growth factor in the regulation of blood pressure. *Current Hypertension Reviews*, 10.

Medici, D., Potenta, S., and Kalluri, R. (2011). Transforming growth factor-β2 promotes snail-mediated endothelial–mesenchymal transition through convergence of smad-dependent and smad-independent signalling. *Biochemical Journal*, 437:515–520.

Meng, X. M., Huang, X. R., Chung, A. C., Qin, W., Shao, X., Igarashi, P., Ju, W., Bottinger, E. P., and Lan, H. Y. (2010). Smad2 protects against tgf-β/smad3-mediated renal fibrosis. *Journal of the American Society of Nephrology*, 21:1477–1487.

Meng, X.-M., Tang, P. M.-K., Li, J., and Lan, H. Y. (2015). Tgf-β/smad signaling in renal fibrosis. *Frontiers in Physiology*, 6:82.

Merion, R. M., Goodrich, N. P., Johnson, R. J., McDonald, S. P., Russ, G. R., Gillespie, B. W., and Collett, D. (2018). Kidney transplant graft outcomes in 379 257 recipients on 3 continents. *American Journal of Transplantation*, 18:1914–1923.

Miguel, V., Tituaña, J., Herrero, J. I., Herrero, L., Serra, D., Cuevas, P., Barbas, C., Puyol, D. R., Márquez-Expósito, L., Ruiz-Ortega, M., Castillo, C., Sheng, X., Susztak, K., Ruiz-Canela, M., Salas-Salvadó, J., González, M. A. M., Ortega, S., Ramos, R., and Lamas, S. (2021). Renal tubule cpt1a overexpression protects from kidney fibrosis by restoring mitochondrial homeostasis. *Journal of Clinical Investigation*, 131.

Mihaylova, M. M., Vasquez, D. S., Ravnskjaer, K., Denechaud, P.-D., Yu, R. T., Alvarez, J. G., Downes, M., Evans, R. M., Montminy, M., and Shaw, R. J. (2011). Class iia histone deacetylases are hormone-activated regulators of foxo and mammalian glucose homeostasis. *Cell*, 145:607–621.

Mladinov, D., Liu, Y., Mattson, D. L., and Liang, M. (2013). Micrornas contribute to the maintenance of cell-type-specific physiological characteristics: mir-192 targets na+/k+-atpase β1. *Nucleic Acids Research*, 41:1273–1283.

Moe, O. W. (2012). *The Kidney: Physiology and Pathophysiology*. Academic Press, 5th edition.

Mookerjee, S. A. and Brand, M. D. (2015). Measurement and analysis of extracellular acid production to determine glycolytic rate. *Journal of Visualized Experiments*, 2015.

Morikawa, M., Koinuma, D., Miyazono, K., and Heldin, C. H. (2013). Genome-wide mechanisms of smad binding. *Oncogene*, 32.

Motoshima, H., Goldstein, B. J., Igata, M., and Araki, E. (2006). Ampk and cell proliferation–ampk as a therapeutic target for atherosclerosis and cancer. *The Journal of physiology*, 574:63–71.

Mráček, T., Drahota, Z., and Houštěk, J. (2013). The function and the role of the mitochondrial glycerol-3-phosphate dehydrogenase in mammalian tissues. *Biochimica et Biophysica Acta (BBA) - Bioenergetics*, 1827:401–410.

Mu, X., Zheng, W., Xiao, L., Zhang, W., and Jiang, X. (2013). Engineering a 3d vascular network in hydrogel for mimicking a nephron. *Lab on a Chip*, 13:1612.

Munagala, M. R. and Phancao, A. (2016). Managing cardiovascular risk in the post solid organ transplant recipient. *Medical Clinics of North America*, 100:519–533.

Musah, S., Mammoto, A., Ferrante, T. C., Jeanty, S. S. F., Hirano-Kobayashi, M., Mammoto, T., Roberts, K., Chung, S., Novak, R., Ingram, M., Fatanat-Didar, T., Koshy, S., Weaver, J. C., Church, G. M., and Ingber, D. E. (2017). Mature induced-pluripotent-stem-cell-derived human podocytes reconstitute kidney glomerular-capillary-wall function on a chip. *Nature Biomedical Engineering*, 1:0069.

Mutsaers, R., Trapasso, F., Hertig, A., and Simon, N. (2015). Alteration of fatty acid oxidation in tubular epithelial cells: from acute kidney injury to renal fibrogenesis. *Mini Reviews in Medicine*, 2.

Nieskens, T. T. G., Peters, J. G. P., Schreurs, M. J., Smits, N., Woestenenk, R., Jansen, K., van der Made, T. K., Roring, M., Hilgendorf, C., Wilmer, M. J., and Masereeuw, R. (2016). A human renal proximal tubule cell line with stable organic anion transporter 1 and 3 expression predictive for antiviral-induced toxicity. *The AAPS Journal*, 18:465–475.

Nishinakamura, R. (2019). Human kidney organoids: progress and remaining challenges. *Nature Reviews Nephrology*, 15:613–624.

Nlandu-Khodo, S., Neelisetty, S., Phillips, M., Manolopoulou, M., Bhave, G., May, L., Clark, P. E., Yang, H., Fogo, A. B., Harris, R. C., Taketo, M. M., Lee, E., and Gewin, L. S. (2017). Blocking tgf- ¡i¿β¡/i¿ and ¡i¿β¡/i¿ -catenin epithelial crosstalk exacerbates ckd. *Journal of the American Society of Nephrology*, 28:3490–3503.

Nowak, G. and Schnellmann, R. G. (1995). Improved culture conditions stimulate gluconeogenesis in primary cultures of renal proximal tubule cells. *American Journal of Physiology*, 268:1053–1061.

Orlando, G., Soker, S., and Stratta, R. J. (2013). Organ bioengineering and regeneration as the new holy grail for organ transplantation. *Annals of Surgery*, 258:221–232.

Owen, M. R., Doran, E., and Halestrap, A. P. (2000). Evidence that metformin exerts its anti-diabetic effects through inhibition of complex 1 of the mitochondrial respiratory chain. *The Biochemical journal*, 348 Pt 3:607–614.

Ozgen, N., Terashima, M., Aung, T., Sato, Y., Isoe, C., Kakuta, T., and Saito, A. (2004). Evaluation of long-term transport ability of a bioartificial renal tubule device using llc-pk1 cells. *Nephrology Dialysis Transplantation*, 19:2198–2207.

Palechor-Ceron, Krawczyk, Dakic, Simic, Yuan, Blancato, Wang, Hubbard, Zheng, Dan, Strome, Cullen, Davidson, Deeken, Choudhury, Ahn, Agarwal, Zhou, Schlegel, Furth, Pan, and Liu (2019). Conditional reprogramming for patient-derived cancer models and next-generation living biobanks. *Cells*, 8:1327.

Palmer, B. F. (2015). Regulation of potassium homeostasis. *Clinical journal of the American Society of Nephrology : CJASN*, 10:1050–1060.

Park, H. J., Fan, Z., Bai, Y., Ren, Q., Rbaibi, Y., Long, K. R., Gliozzi, M. L., Rittenhouse, N., Locker, J. D., Poholek, A. C., and Weisz, O. A. (2020). Transcriptional programs driving shear stress-induced differentiation of kidney proximal tubule cells in culture. *Frontiers in Physiology*, 11.

Patitucci, C., Couchy, G., Bagattin, A., Cañeque, T., de Reyniès, A., Scoazec, J.-Y., Rodriguez, R., Pontoglio, M., Zucman-Rossi, J., Pende, M., and Panasyuk, G. (2017). Hepatocyte nuclear factor 1α suppresses steatosis-associated liver cancer by inhibiting pparγ transcription. *Journal of Clinical Investigation*, 127:1873–1888.

Perl, J., Karaboyas, A., Morgenstern, H., Sen, A., Rayner, H. C., Vanholder, R. C., Combe, C., Hasegawa, T., Finkelstein, F. O., Lopes, A. A., Robinson, B. M., Pisoni, R. L., and Tentori, F. (2016). Association between changes in quality of life and mortality in hemodialysis patients: results from the dopps. *Nephrology Dialysis Transplantation*, page gfw233.

Poggio, E. D., McClelland, R. L., Blank, K. N., Hansen, S., Bansal, S., Bomback, A. S., Canetta, P. A., Khairallah, P., Kiryluk, K., Lecker, S. H., McMahon, G. M., Palevsky, P. M., Parikh, S., Rosas, S. E., Tuttle, K., Vazquez, M. A., Vijayan, A., and Rovin, B. H. (2020). Systematic review and meta-analysis of native kidney biopsy complications. *Clinical Journal of the American Society of Nephrology*, 15:1595–1602.

Polianskyte-Prause, Z., Tolvanen, T. A., Lindfors, S., Dumont, V., Van, M., Wang, H., Dash, S. N., Berg, M., Naams, J.-B., Hautala, L. C., Nisen, H., Mirtti, T., Groop, P.-H., Wähälä, K., Tienari, J., and Lehtonen, S. (2019). Metformin increases glucose uptake and acts renoprotectively by reducing ship2 activity.

FASEB journal : official publication of the Federation of American Societies for Experimental Biology, 33:2858–2869.

Ponticelli, C., Cucchiari, D., and Graziani, G. (2011). Hypertension in kidney transplant recipients. *Transplant International*, 24:523–533.

Pontoglio, M., Prié, D., Cheret, C., Doyen, A., Leroy, C., Froguel, P., Velho, G., Yaniv, M., and Friedlander, G. (2000). Hnf1α controls renal glucose reabsorption in mouse and man. *EMBO reports*, 1:359–365.

Qin, N., Cai, T., Ke, Q., Yuan, Q., Luo, J., Mao, X., Jiang, L., Cao, H., Wen, P., Zen, K., Zhou, Y., and Yang, J. (2019). Ucp2-dependent improvement of mitochondrial dynamics protects against acute kidney injury. *Journal of Pathology*, 247.

Rad, N. K., Aghdami, N., and Moghadasali, R. (2020). Cellular and molecular mechanisms of kidney development: From the embryo to the kidney organoid. *Frontiers in Cell and Developmental Biology*, 8.

Rangaswami, J., Bhalla, V., Blair, J. E., Chang, T. I., Costa, S., Lentine, K. L., Lerma, E. V., Mezue, K., Molitch, M., Mullens, W., Ronco, C., Tang, W. W., and McCullough, P. A. (2019). Cardiorenal syndrome: Classification, pathophysiology, diagnosis, and treatment strategies: A scientific statement from the american heart association. *Circulation*, 139.

Ren, Q., Gliozzi, M. L., Rittenhouse, N. L., Edmunds, L. R., Rbaibi, Y., Locker, J. D., Poholek, A. C., Jurczak, M. J., Baty, C. J., and Weisz, O. A. (2019). Shear stress and oxygen availability drive differential changes in opossum kidney proximal tubule cell metabolism and endocytosis. *Traffic*, 20:448–459.

Ross, S., Cheung, E., Petrakis, T. G., Howell, M., Kraus, W. L., and Hill, C. S. (2006). Smads orchestrate specific histone modifications and chromatin remodeling to activate transcription. *The EMBO Journal*, 25:4490–4502.

Ruan, H.-B., Singh, J. P., Li, M.-D., Wu, J., and Yang, X. (2013). Cracking the o-glcnac code in metabolism. *Trends in endocrinology and metabolism: TEM*, 24:301–309.

Saito, Y., Matsumoto, N., Yamanaka, S., Yokoo, T., and Kobayashi, E. (2022). Beneficial impact of interspecies chimeric renal organoids against a xenogeneic immune response. *Frontiers in Immunology*, 13.

Salani, M., Roy, S., and Fissell IV, W. H. (2018). Innovations in wearable and implantable artificial kidneys. *American Journal of Kidney Diseases*, 72(5):745–751.

Sanechika, N., Sawada, K., Usui, Y., Hanai, K., Kakuta, T., Suzuki, H., Kanai, G., Fujimura, S., Yokoyama, T. A., Fukagawa, M., Terachi, T., and Saito, A. (2011). Development of bioartificial renal tubule devices with lifespan-extended human renal proximal tubular epithelial cells. *Nephrology Dialysis Transplantation*, 26:2761–2769.

Sarah, D., Patrick, G., Jordan, L., Corina, F., Leyla, D., Marco, F., Florian, M., R, B. G., Daniela, T., Yannic, L., Alfred, Z., Anja, L., and Christoph, H. (2019). Tumor-derived tgf-β inhibits mitochondrial respiration to suppress ifn-γ production by human cd4+ t cells. *Science Signaling*, 12:eaav3334. doi: 10.1126/scisignal.aav3334.

Sawinski, D. and Poggio, E. D. (2021). Introduction to kidney transplantation: Long-term management challenges. *Clinical Journal of the American Society of Nephrology*, 16:1262–1263.

Schaffer, B. E., Levin, R. S., Hertz, N. T., Maures, T. J., Schoof, M. L., Hollstein, P. E., Benayoun, B. A., Banko, M. R., Shaw, R. J., Shokat, K. M., and Brunet, A. (2015). Identification of ampk phosphorylation sites reveals a network of proteins involved in cell invasion and facilitates large-scale substrate prediction. *Cell metabolism*, 22:907–921.

Schaub, J. A., Venkatachalam, M. A., and Weinberg, J. M. (2021). Proximal tubular oxidative metabolism in acute kidney injury and the transition to ckd. *Kidney360*, 2:355–364.

Schiffer, T. A. and Friederich-Persson, M. (2017). Mitochondrial reactive oxygen species and kidney hypoxia in the development of diabetic nephropathy. *Frontiers in Physiology*, 8.

Schutgens, F., Rookmaaker, M. B., Margaritis, T., Rios, A., Ammerlaan, C., Jansen, J., Gijzen, L., Vormann, M., Vonk, A., Viveen, M., Yengej, F. Y., Derakhshan, S., de Winter-de Groot, K. M., Artegiani, B., van Boxtel, R., Cuppen, E., Hendrickx, A. P. A., van den Heuvel-Eibrink, M. M., Heitzer, E., Lanz, H., Beekman, J., Murk, J.-L., Masereeuw, R., Holstege, F., Drost, J., Verhaar, M. C., and Clevers, H. (2019). Tubuloids derived from human adult kidney and urine for personalized disease modeling. *Nature Biotechnology*, 37:303–313.

Sciancalepore, A. G., Sallustio, F., Girardo, S., Passione, L. G., Camposeo, A., Mele, E., Lorenzo, M. D., Costantino, V., Schena, F. P., and Pisignano, D. (2014). A bioartificial renal tubule device embedding human renal stem/progenitor cells. *PLoS ONE*, 9.

Shankar, A. S., Du, Z., Mora, H. T., van den Bosch, T. P., Korevaar, S. S., den Berg-Garrelds, I. M. V., Bindels, E., Lopez-Iglesias, C., van Groningen, M. C. C., Gribnau, J., Baan, C. C., Danser, A. J., Hoorn, E. J., and Hoogduijn, M. J. (2021). Human kidney organoids produce functional renin. *Kidney International*, 99:134–147.

Shi, Y., Wang, Y.-F., Jayaraman, L., Yang, H., Massagué, J., and Pavletich, N. P. (1998). Crystal structure of a smad mh1 domain bound to dna. *Cell*, 94:585–594.

Simonsson, M., Kanduri, M., Gronroos, E., Heldin, C.-H., and Ericsson, J. (2006). The dna binding activities of smad2 and smad3 are regulated by coactivator-mediated acetylation. *Journal of Biological Chemistry*, 281:39870–39880.

Smith, E. R. and Hewitson, T. D. (2020). Tgf-β1 is a regulator of the pyruvate dehydrogenase complex in fibroblasts. *Scientific Reports*, 10.

Smith, E. R., Wigg, B., Holt, S. G., and Hewitson, T. D. (2019). Tgf-β1 modifies histone acetylation and acetyl-coenzyme a metabolism in renal myofibroblasts. *American Journal of Physiology - Renal Physiology*, 316.

Sohn, E. J., Kim, J., Hwang, Y., Im, S., Moon, Y., and Kang, D. M. (2012). Tgf-β suppresses the expression of genes related to mitochondrial function in lung a549 cells. *Cellular and molecular biology (Noisy-le-Grand, France)*, Suppl.58.

Soltoff, S. P. (1986). Atp and the regulation of renal cell function. *Annual review of physiology*, 48:9–31.

Song, J. J., Guyette, J. P., Gilpin, S. E., Gonzalez, G., Vacanti, J. P., and Ott, H. C. (2013). Regeneration and experimental orthotopic transplantation of a bioengineered kidney. *Nature Medicine*, 19:646–651.

Starkov, A. A. (2008). The role of mitochondria in reactive oxygen species metabolism and signaling. *Annals of the New York Academy of Sciences*, 1147.

Sureshbabu, A., Muhsin, S. A., and Choi, M. E. (2016). Tgf-beta signaling in the kidney: profibrotic and protective effects. *American journal of physiology. Renal physiology*, 310:F596–F606.

Takahashi-Iwanaga, H. (1992). Three-dimensional visualization of renal cells by naoh maceration. *Archives of Histology and Cytology*, 55.

Tang, J. X., Thompson, K., Taylor, R. W., and Oláhová, M. (2020). Mitochondrial oxphos biogenesis: Co-regulation of protein synthesis, import, and assembly pathways. *International Journal of Molecular Sciences*, 21.

Tennankore, K. K., Soroka, S. D., and Kiberd, B. A. (2012). The impact of an "acute dialysis start" on the mortality attributed to the use of central venous catheters: a retrospective cohort study. *BMC Nephrology*, 13:72.

Teruel, J. L., Vion, V. B., Couto, A. G., Gorrín, M. R., Fernández-Lucas, M., Mendiola, N. R., and Quereda, C. (2015). Choosing conservative therapy in chronic kidney disease. *Nefrologia*, 35.

Thurlow, J. S., Joshi, M., Yan, G., Norris, K. C., Agodoa, L. Y., Yuan, C. M., and Nee, R. (2021). Global epidemiology of end-stage kidney disease and disparities in kidney replacement therapy. *American Journal of Nephrology*, 52:98–107.

Tiong, H. Y., Huang, P., Xiong, S., Li, Y., Vathsala, A., and Zink, D. (2014). Drug-induced nephrotoxicity: Clinical impact and preclinical ¡i¿in vitro¡/i¿ models. *Molecular Pharmaceutics*, 11:1933–1948.

Tran, M., Tam, D., Bardia, A., Bhasin, M., Rowe, G. C., Kher, A., Zsengeller, Z. K., Akhavan-Sharif, M. R., Khankin, E. V., Saintgeniez, M., David, S., Burstein, D., Karumanchi, S. A., Stillman, I. E., Arany, Z., and Parikh, S. M. (2011). Pgc-1α promotes recovery after acute kidney injury during systemic inflammation in mice. *Journal of Clinical Investigation*, 121.

Tremblay, K., Hoodless, P., Bikoff, E., and Robertson, E. (2000). Formation of the definitive endoderm in mouse is a smad2-dependent process. *Development*, 127:3079–3090.

USRDS (2022). 2022 united states renal data system (usrds) annual data report: Epidemiology of kidney disease in the united states.

van Zonneveld, A. J., Au, Y. W., Stam, W., van Gelderen, S., Rotmans, J. I., Deen, P. M. T., Rabelink, T. J., and Bijkerk, R. (2020). Microrna-132 regulates salt-dependent steady-state renin levels in mice. *Communications Biology*, 3:238.

Vanholder, R., Glorieux, G., and Eloot, S. (2015). Once upon a time in dialysis: the last days of kt/v? *Kidney International*, 88:460–465.

Varughese, J. T., Buchanan, S. K., and Pitt, A. S. (2021). The role of voltage-dependent anion channel in mitochondrial dysfunction and human disease. *Cells*, 10.

Voelker, J., Berg, P. H., Sheetz, M., Duffin, K., Shen, T., Moser, B., Greene, T., Blumenthal, S. S., Rychlik, I., Yagil, Y., Zaoui, P., and Lewis, J. B. (2017). Anti–tgf- ¡i¿β¡/i¿ 1 antibody therapy in patients with diabetic nephropathy. *Journal of the American Society of Nephrology*, 28:953–962.

Wahdan-Alaswad, R., Harrell, J. C., Fan, Z., Edgerton, S. M., Liu, B., and Thor, A. D. (2016). Metformin attenuates transforming growth factor beta (tgf-β) mediated oncogenesis in mesenchymal stem-like/claudin-low triple negative breast cancer. *Cell Cycle*, 15:1046–1059.

Waldrip, W., Bikoff, E. K., Hoodless, P. A., Wrana, J. L., and Robertson, E. J. (1998). Smad2 signaling in extraembryonic tissues determines anterior-posterior polarity of the early mouse embryo. *Cell*, 92:797–808.

Walker, R. C., Morton, R. L., Tong, A., Marshall, M. R., Palmer, S., and Howard, K. (2015). Patient and caregiver preferences for home dialysis–the home first study: a protocol for qualitative interviews and discrete choice experiments. *BMJ Open*, 5:e007405–e007405.

Wang, W., Huang, X. R., Canlas, E., Oka, K., Truong, L. D., Deng, C., Bhowmick, N. A., Ju, W., Bottinger, E. P., and Lan, H. Y. (2006). Essential role of smad3 in angiotensin ii–induced vascular fibrosis. *Circulation Research*, 98:1032–1039.

Warburg, O. (1956). On the origin of cancer cells. *Science*, 123:309–314.

Warkad, M. S., Kim, C. H., Kang, B. G., Park, S. H., Jung, J. S., Feng, J. H., Inci, G., Kim, S. C., Suh, H. W., Lim, S. S., and Lee, J. Y. (2021). Metformin-induced ros upregulation as amplified by apigenin causes profound anticancer activity while sparing normal cells. *Scientific Reports*, 11.

Webster, A. C., Nagler, E. V., Morton, R. L., and Masson, P. (2017). Chronic kidney disease. *The Lancet*, 389:1238–1252.

Weinberg, E., Kaazempur-Mofrad, M., and Borenstein, J. (2008). Concept and computational design for a bioartificial nephron-on-a-chip. *The International Journal of Artificial Organs*, 31:508–514.

Welling, L. W. and Welling, D. J. (1988). Relationship between structure and function in renal proximal tubule. *Journal of Electron Microscopy Technique*, 9.

Wessels, B., Ciapaite, J., van den Broek, N. M. A., Nicolay, K., and Prompers, J. J. (2014). Metformin impairs mitochondrial function in skeletal muscle of both lean and diabetic rats in a dose-dependent manner. *PloS one*, 9:e100525.

Westover, A. J., Buffington, D. A., and Humes, H. D. (2012). Enhanced propagation of adult human renal epithelial progenitor cells to improve cell sourcing for tissue-engineered therapeutic devices for renal diseases. *Journal of Tissue Engineering and Regenerative Medicine*, 6:589–597.

Wills, L. P., Trager, R. E., Beeson, G. C., Lindsey, C. C., Peterson, Y. K., Beeson, C. C., and Schnellmann, R. G. (2012). The β ¡sub¿2¡/sub¿ -adrenoceptor agonist formoterol stimulates mitochondrial biogenesis. *Journal of Pharmacology and Experimental Therapeutics*, 342:106–118.

Wilmer, M. J., Ng, C. P., Lanz, H. L., Vulto, P., Suter-Dick, L., and Masereeuw, R. (2016). Kidney-on-a-chip technology for drug-induced nephrotoxicity screening. *Trends in Biotechnology*, 34:156–170.

Wilson, M. H., Veach, R. A., Luo, W., Welch, R. C., Roy, S., and Fissell, W. H. (2020). Genome engineering renal epithelial cells for enhanced volume transport function. *Cellular and Molecular Bioengineering*, 13:17–26.

Wu, H., Uchimura, K., Donnelly, E. L., Kirita, Y., Morris, S. A., and Humphreys, B. D. (2018). Comparative analysis and refinement of human psc-derived kidney organoid differentiation with single-cell transcriptomics. *Cell Stem Cell*, 23:869–881.e8.

Wu, L., Zhou, B., Oshiro-Rapley, N., Li, M., Paulo, J. A., Webster, C. M., Mou, F., Kacergis, M. C., Talkowski, M. E., Carr, C. E., Gygi, S. P., Zheng, B., and Soukas, A. A. (2016). An ancient, unified mechanism for metformin growth inhibition in c. elegans and cancer. *Cell*, 167:1705–1718.e13.

Wu, N., Zheng, B., Shaywitz, A., Dagon, Y., Tower, C., Bellinger, G., Shen, C.-H., Wen, J., Asara, J., McGraw, T. E., Kahn, B. B., and Cantley, L. C. (2013). Ampk-dependent degradation of txnip upon energy stress leads to enhanced glucose uptake via glut1. *Molecular cell*, 49:1167–1175.

Wu, S.-B. and Wei, Y.-H. (2012). Ampk-mediated increase of glycolysis as an adaptive response to oxidative stress in human cells: implication of the cell survival in mitochondrial diseases. *Biochimica et biophysica acta*, 1822:233–247.

Xinaris, C., Benedetti, V., Novelli, R., Abbate, M., Rizzo, P., Conti, S., Tomasoni, S., Corna, D., Pozzobon, M., Cavallotti, D., Yokoo, T., Morigi, M., Benigni, A., and Remuzzi, G. (2016). Functional human podocytes generated in organoids from amniotic fluid stem cells. *Journal of the American Society of Nephrology*, 27:1400–1411.

Yagi, K., Goto, D., Hamamoto, T., Takenoshita, S., Kato, M., and Miyazono, K. (1999). Alternatively spliced variant of smad2 lacking exon 3. *Journal of Biological Chemistry*, 274:703–709.

Yamagata, K., Oda, N., Kaisaki, P. J., Menzel, S., Furuta, H., Vaxillaire, M., Southam, L., Cox, R. D., Lathrop, G. M., Boriraj, V. V., Chen, X., Cox, N. J., Oda, Y., Yano, H., Beau, M. M. L., Yamada, S., Nishigori, H., Takeda, J., Fajans, S. S., Hattersley, A. T., Iwasaki, N., Hansen, T., Pedersen, O., Polonsky, K. S., Turner, R. C., Velho, G., Chèvre, J.-C., Froguel, P., and Bell, G. I. (1996). Mutations in the hepatocyte nuclear factor-1α gene in maturity-onset diabetes of the young (mody3). *Nature*, 384:455–458.

Yang, F., Griva, K., Lau, T., Vathsala, A., Lee, E., Ng, H. J., Mooppil, N., Foo, M., Newman, S. P., Chia, K. S., and Luo, N. (2015). Health-related quality of life of asian patients with end-stage renal disease (esrd) in singapore. *Quality of Life Research*, 24:2163–2171.

Yi, J. Y., Shin, I., and Arteaga, C. L. (2005). Type i transforming growth factor β receptor binds to and activates phosphatidylinositol 3-kinase. *Journal of Biological Chemistry*, 280:10870–10876. 10.1074/jbc.M413223200.

Yin, L., Du, G., Zhang, B., Zhang, H., Yin, R., Zhang, W., and Yang, S.-M. (2020). Efficient drug screening and nephrotoxicity assessment on co-culture microfluidic kidney chip. *Scientific Reports*, 10:6568.

Yoshizaki, Y., Mori, Y., Tsuzaki, Y., Mori, T., Nomura, N., Wakabayashi, M., Takahashi, D., Zeniya, M., Kikuchi, E., Araki, Y., Ando, F., Isobe, K., Nishida, H., Ohta, A., Susa, K., Inoue, Y., Chiga, M., Rai, T., Sasaki, S., Uchida, S., and Sohara, E. (2015). Impaired degradation of wnk by akt and pka phosphorylation of klhl3. *Biochemical and Biophysical Research Communications*, 467:229–234.

Yu, H., Shen, Y., Hong, J., Xia, Q., Zhou, F., and Liu, X. (2015a). The contribution of tgf-β in epithelial–mesenchymal transition (emt): Down-regulation of e-cadherin via snail. *Neoplasma*, 62:1–15.

Yu, J. S. L., Ramasamy, T. S., Murphy, N., Holt, M. K., Czapiewski, R., Wei, S.-K., and Cui, W. (2015b). Pi3k/mtorc2 regulates tgf-β/activin signalling by modulating smad2/3 activity via linker phosphorylation. *Nature Communications*, 6:7212.

Zeng, Z., Huang, B., Parvez, R. K., Li, Y., Chen, J., Vonk, A. C., Thornton, M. E., Patel, T., Rutledge, E. A., Kim, A. D., Yu, J., Grubbs, B. H., McMahon, J. A., Pastor-Soler, N. M., Hallows, K. R., McMahon, A. P., and Li, Z. (2021). Generation of patterned kidney organoids that recapitulate the adult kidney collecting duct system from expandable ureteric bud progenitors. *Nature Communications*, 12:3641.

Zhang, C. Y., Yin, H. M., Wang, H., Su, D., Xia, Y., Yan, L. F., Fang, B., Liu, W., Wang, Y. M., Gu, A. H., and Zhou, Y. (2018). Transforming growth factor-β1 regulates the nascent hematopoietic stem cell niche by promoting gluconeogenesis. *Leukemia*, 32.

Zhang, Y., Wang, S., Liu, S., Li, C., and Wang, J. (2015). Role of smad signaling in kidney disease. *International Urology and Nephrology*, 47:1965–1975.

Zhang, Y. E. (2009). Non-smad pathways in tgf-beta signaling. *Cell research*, 19:128–139.

Zhu, Y., Richardson, J. A., Parada, L. F., and Graff, J. M. (1998). Smad3 mutant mice develop metastatic colorectal cancer. *Cell*, 94:703–714.

Zhuo, J. L. and Li, X. C. (2013). Proximal nephron. *Comprehensive Physiology*, 3:1079–1123.

Zi, F., Zi, H., Li, Y., He, J., Shi, Q., and Cai, Z. (2018). Metformin and cancer: An existing drug for cancer prevention and therapy. *Oncology letters*, 15:683–690.